THE UNIVERSITY OF ADELAIDE

School of Electrical and Electronic Engineering

Digital Signal Processing Techniques for Improving the Automatic Classification of Power Quality Events

Ameen M. Gargoom

A Thesis presented for the degree of
Doctor of Philosophy

December 2006

Dedicated to my parents

Digital Signal Processing Techniques for Improving the Automatic Classification of Power Quality Events

Ameen M Gargoom

Submitted for the degree of Doctor of Philosophy

December 2006

Abstract

Electric power quality problems have become an important issue due to their technical and financial consequences on industry. Several solutions have been provided for addressing these problems such as the use of custom power solutions. These solutions, however, could themselves be a source of power quality distortions. On the other hand, existing power quality monitors provide sufficient information on power quality distortions, which require individual inspection of the events. However, with the growing number of monitors installed in power systems, the amount of data collected continues to grow, which makes individual inspection of events impossible. Therefore, it is desirable to have automatic analysis tools integrated with the monitoring systems, that can be applied to large existing databases for automating the classification process. This makes the clustering of similar events more visible which is necessary for analysing and identifying the source of the distortion in a particular power system.

The work presented in this thesis investigates the application of digital signal processing techniques in the power quality automatic classification field, and thus, proposes an optimized automatic monitoring system with an improved accuracy. The proposed monitoring system involves three main sections: detection of the power quality events, extraction of the distinctive features that characterise each event, and automatic classification of the similar events under pre-defined categories. The thesis proposes new power quality processing techniques for detection and feature extraction sections, including the Hilbert and Clarke transforms. The former proposed technique was used for analysing single phase signals, while the later technique was proposed for the simultaneous analysis of three phase signals.

In the classification section of the monitoring system, the k-Nearest Neighbour pattern recognition technique was used as a decision-making technique. The main advantage of the k-Nearest Neighbour technique is that it is nonparametric technique which is simple, yet, effective in many cases, as no prior statistical knowledge about the data is required. Although the k-Nearest Neighbour technique requires a large capacity of memory to store the training data, the ever development the memory size technology makes it a good candidate in the automatic recognition of power quality events.

The k-Nearest Neighbour technique was used in this thesis with two feature extraction techniques (the Hilbert and the Clarke transforms) to construct two new classifiers for single-phase systems and three-phase systems. As the number of neighbors affects the accuracy of the decision-making in the technique, this research also determines the optimum number of neighbors in each classifier.

On the basis of the classification tests performed on nine power quality classes, (including specified classes such as, sags due to starting motors and sags with harmonics), it was demonstrated that the proposed classifiers are very effective. The performance of the proposed classifiers was compared with the k-Nearest Neighbour classifier based on the up-to-date feature extraction techniques; S Transform and Wavelet Packet transform. By considering identical test data set, the over all accuracy of the k-Nearest Neighbour classifier with Clarke transform was around 88.5% and the k-Nearest Neighbour with Hilbert transform was about 89.2%, whereas the accuracies of the k-Nearest Neighbour with the S Transform and Wavelet Packet transform were 82.2% and 74.4% respectively. It should be noted that the above accuracy figures are calculated based on all nine studied power quality classes, which can be increased significantly if the classes with similar characteristics, (such as sags due to starting motors and sags with harmonics), were excluded from the calculations. A number of real time measured events based on laboratory experiments and on-site measurements was also provided in this study for testing the proposed feature extraction techniques and classifiers.

Declaration

This work contains no material which has been accepted for the award of any other degree or diploma in any university or other tertiary institution and, to the the best of my knowledge and belief, contains no material previously published or written by another person, except where due reference has been made in the text.

I give consent to this copy of my thesis, when deposited in the University Library, being made available for loan and photocopying, subject to the provisions of the Copyright Act 1968.

Signed: Date: 08/01/2007

Acknowledgements

First and foremost, I would like to thank and praise Allah almighty for enlightening my way and directing me through each and every success I have or may reach.

I am especially grateful to my supervisor Dr. Nesimi Ertugrul for his guidance, insightful conversations and endless encouragement throughout the duration of this research. It has been very stimulating and enjoyable to work with him. I am also sincerely grateful to my co-supervisor Dr. Wen L Soong for his consistent support and invaluable advices for finishing this work.

I am also grateful to the Libyan Ministry of Education for the financial support of this work. My thanks go also to all the members in the School of Electrical and Electronic Engineering of The University of Adelaide. My appreciation goes also to the team at Pelican Point power station, South Australia, Australia.

Last, but not least, the constant and many-sided support of my parents and family has been very important to me.

Ameen Gargoom

Contents

List of Figures

List of Tables

Chapter 1

Introduction

1.1 An Overview of Power Quality

THIS introductory chapter provides the context and motivation for the study of power quality.

An ideal three-phase AC supply consists of three phase voltages that are 120 degrees out of phase and have identical magnitudes. Above all, these voltages should have sinusoidal waveform characteristic and should be available continuously. Any diversion from these requirements to the level that has an adverse effect on the electric consumers is considered as poor quality of power.

As a general statement, power quality can be referred to as the degree to which voltages and currents in a power system represent sinusoidal waveforms. *Clean power* refers to voltage and current waveforms that represent pure sine waves and are free from any distortion, while *polluted power* refers to voltage and current waveforms that are distorted and can not be represented by pure sine waves. Voltage *dips* (*sags*), *swells*, *interruptions*, *switching transients*, or *harmonics* are examples of the most frequent disturbances in power system networks (see Figure 1.1).

In the industrialized world, electric power systems have become more polluted than ever before. This issue is primarily related to ever increasing sources of disturbances that occur in interconnected power grids, which accommodates a large

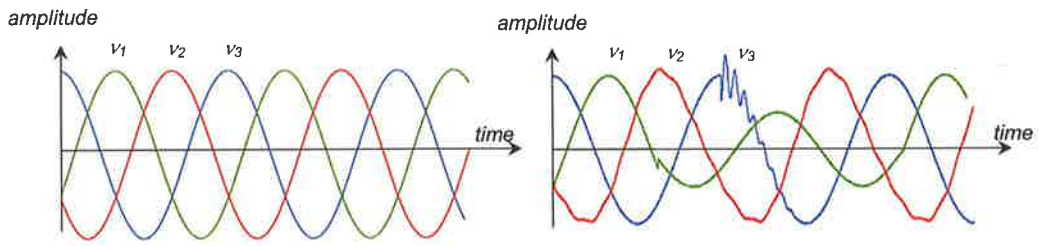

Figure 1.1: Left: Ideal, 'clean', three-phase waveform represented by sine functions having identical amplitudes, frequency, and 120° apart. Right: Hypothetical polluted sample, phase v_1 with voltage sag, phase v_2 with harmonics, and phase v_3 with transients.

number of power sources, transmission systems, transformers and interconnected loads. In addition, such systems are exposed to environmental disturbances like lighting strokes. Furthermore, non-linear power electronic loads, such as converter-driven equipment (from consumer electronics and computers, up to adjustable-speed drives), have become increasingly common in power systems. Although these converter-driven equipments are manufactured according to the associated standards, the wide utilization of such devices pollutes the power systems. If these unwanted variations in the voltage and current signals are not mitigated properly, they can lead to failures or malfunctions of the many sensitive loads connected to the same systems, which may be very costly for the end users.

It is not easy to estimate accurately the exact cost of the pollution in the quality of the power. However, some reports, (e.g. [1] and [2]), estimated that, poor power quality in the United States of America causes about US$13.3 billion in damage per year. As examples of these costs, one glass plant estimates that a five cycle interruption can cost about US$200,000, and a major computer center reports that a two second outage can cost about US$600,000 [3].

Numerous studies have attempted to address and reduce the impact of the power quality aspects. The previous research studies can be categorized into two groups: *the custom power solutions* and *the power quality monitoring solutions*. The research areas in these two groups are shown in Figure 1.2.

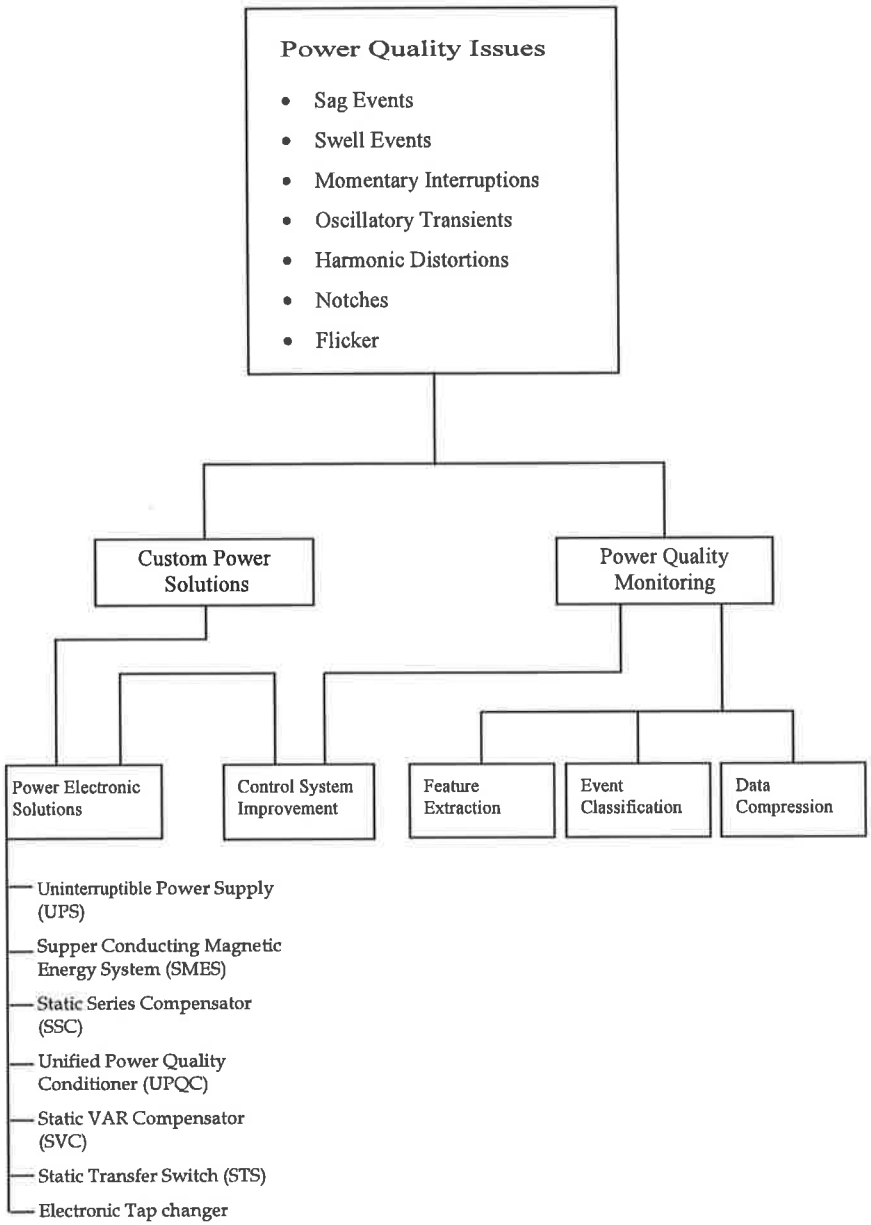

Figure 1.2: Research groups on power quality.

In the first research group, (the custom power solutions), the emphasis is given to how to protect the electrical loads from seeing any disturbances in the supplied AC power [4] – [10]. These solutions are available and effective for low voltage level systems. However, thanks to continual improvement in the rating of power electronic devices, which provided solutions at the medium voltage level. Examples of these solutions are shown in Figure 1.2. However, for medium voltage systems, these solutions are still not yet economically viable at high power ratings (MVA order), as they are energy inefficient, and require additional maintenance [11]. Moreover, power electronic-based solutions themselves can be the source of the power quality related problems such as harmonics and notches.

In the second research group, the research is focusing on power quality monitoring. The utilization of these monitoring systems gives detailed information on the characteristics of the events that cause the power quality related problems. The analysis of this information by expert power quality engineers can identify the characteristics and origin of such events and so suggest possible improvements based on custom power solutions. For example, in [12], two cases of utilizing power quality monitoring systems are described. In the first case, monitoring revealed that a pump control system was exposed to voltage sags and, as a solution, a constant voltage transformer was installed to support the voltage. In the second case, monitoring showed that plants in the same geographical area were experiencing voltage sags of relatively long duration. These long voltage sags were affecting the operation of a number of apparatuses. The problem was solved by shorting the protection clearance times at certain points in the power system within the zone of influence of the plants. In addition, the information about the monitored events like sag magnitude and duration are usually used to compare with the voltage tolerance curves of the loads (see section 2.2.1) to evaluate the influence of these events.

1.2 Project Motivation and Objectives

Due to the advanced developments in this industrial world, electricity is no longer viewed as a "*load*" which may the disturbances be part of it, instead it is now viewed as a "*product*" with certain characteristics have to be met. In addition, because of privatisation of the power system structures, starting from the generation up to the end users, it is not clear who is responsible for the quality and the reliability of this *product*. For example, if there is any power quality failure, it is important to specify the source of this failure and identify who is responsible for the improvement, (i.e. generation authorities, the distributors, or the customers). Due to the above ambiguity, monitoring instruments have become an integral part for assessing and improving the power quality. However, due to the extensive number of different types of disturbances, the analysis of the captured disturbances manually is no longer a practical option. Therefore, it is desirable to have automatic analysis tools, integrated with the monitoring systems, that can be applied to large disturbance databases to cluster them automatically based on some predefined criteria.

Although, due to the advances in the signal processing field, many techniques have been exploited for extending the ability of the monitoring systems to be automated, a reliable systems for the automatic classification of a full range of disturbances is yet to be formalised. Therefore the objective of this thesis is to investigate the implementation of different signal processing techniques in order to develop and propose an accurate automatic power quality monitoring system. The principle of this system as it is illustrated in in Figure 1.3 will include three major steps described as follows:

1. **Triggering**

   Because the power quality disturbances usually affect the voltage and/or current signals in different ways, different disturbances may require different triggering mechanisms. As a result, the existing triggering techniques may not capture every type of the disturbances. Therefore, this study will offer an appropriate triggering mechanism that can be implemented in a custom developed monitoring program, to capture a wider range of disturbances.

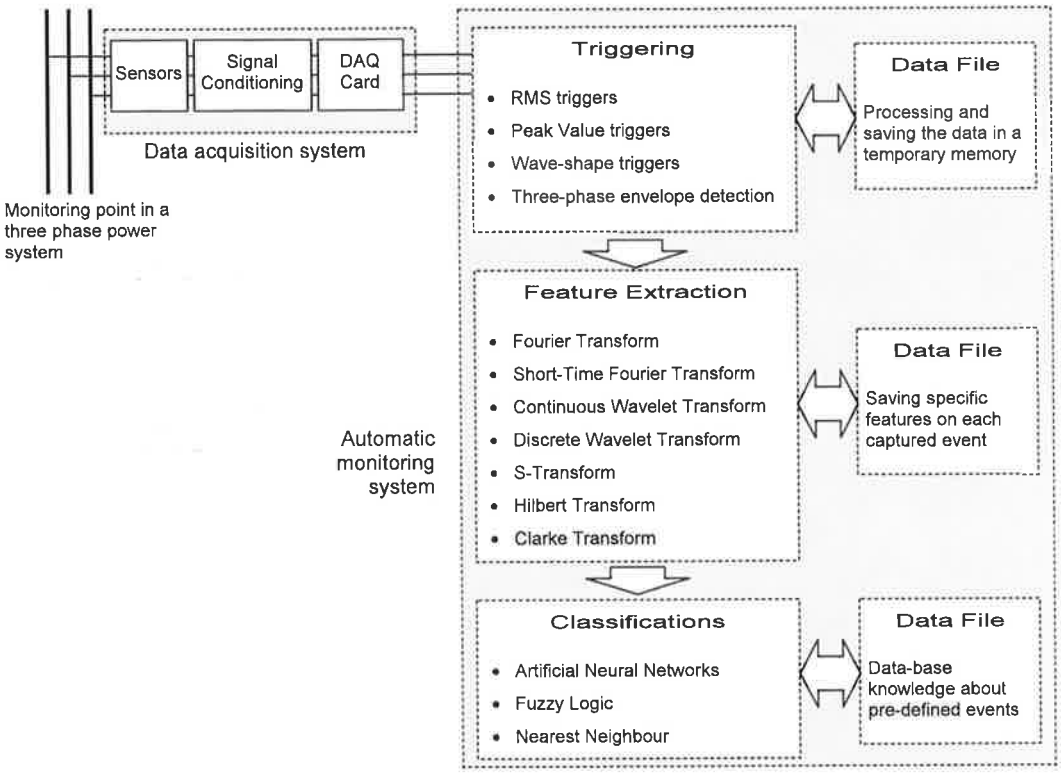

Figure 1.3: A block diagram highlights the main three steps of automatic monitoring process.

2. **Feature Extraction**

   This study will also investigate different signal processing tools that are able to extract the distinctive characteristics (features) of the disturbances. Different features from different techniques (or different features from the same technique) will be proposed and examined to show their capability to distinguish different power quality disturbances. In addition, in case of three-phase systems, processing the three-phase signals simultaneously will be considered instead of the traditional methods of processing each phase separately.

3. **Classification**

   Finally this study will implement a decision-making technique based on the extracted features to automatically classify a wide range of power quality disturbance classes accurately.

1.3 Literature Review

In order to classify different categories of power quality disturbances automatically, it is necessary to extract the distinctive features of each category using an appropriate signal processing technique. The accuracy of the automatic classification systems depends mainly on how distinctive the extracted features are. Different studies have been reported on the literature considering the feature extraction and decision-making techniques. These research can be divided into two sections as follows.

1.3.1 Power Quality Feature Extractions

In order to obtain distinctive features for the classification, a number of studies on signal processing techniques were reported in the literature. Among these techniques the Fourier Transform (FT) technique was the most commonly used technique in practice to provide harmonic information about the signals monitored. However, as reported in [14] – [17], the FT alone is not sufficient for analysing power quality signals as these signals are generally non stationary in nature and the FT ignores the time information which is required for effective analysis.

As an improvement to the FT technique, the Short Time Fourier Transform (STFT) technique was implemented in [18] and [19]. In [18], the STFT was used to ascertain the frequency content of a non-stationary signal at different time intervals. Hamming windows were used of lengths of 16, 32, 64, and 128 points. For an oscillatory transient event, the technique provided more accurate time information (e.g. start time, end time, rise time, fall time, and duration). For a sag event, the STFT technique was used for extracting the fundamental components of the signals with respect to time.

In [19], the voltage disturbances were analyzed in the time-frequency domain using the STFT technique. The signal studied was split into a set of output signals, which were obtained using band-pass filters centered at the harmonic frequencies. The paper also provided a comparison between the STFT and Wavelet multi-resolution analysis. It was shown that, once the center of the window function is

selected, the center frequencies of the band-pass filters associated with the STFT can be chosen freely. However, it was found that the proposed technique requires a significant amount of computational resources. This is due to the fact that the proposed STFT based approach needs the implementation of the FT technique $(N-L)$ times, where N is the length of the signal and L is the window function length.

In addition, although the STFT technique offered a partial solution for the absence of time information in the FFT, it has also limitations due to its fixed window length, which has to be chosen prior to the analysis. This drawback is reflected by the achievable frequency resolution when analysing non-stationary signals with low- and high-frequency components, as will be explained in Chapter 4.

The Wavelet Transform (WT), has been shown to be suitable for power quality analysis, specifically for non-stationary signals. Due to the varying window function of the WT at different frequency levels, it has been explored extensively in various studies as an alternative to the STFT technique ([20] – [39]). These studies examined both the Continuous Wavelet Transform (CWT) and the Discrete Wavelet transform (DWT) (also known as Multi-Resolution Analysis, MRA).

Most of the previous work on the CWT was based on visual detection of power quality events in the time-scale plane (e.g. [20] – [25]). In [20] – [22], a method was discussed in which the CWT technique was used to extract the superimposed disturbances in the signal from the fundamental component in order to be able to analyse the disturbance. By this method, the disturbance time duration is estimated by evaluating the local maximum at different scales. In [23], the CWT technique was applied on four power quality events, (voltage sag, transient, harmonic distortion, and flicker). It was shown that the magnitude of the fundamental component in the signal can be accurately extracted. However, poor extracting of the harmonic magnitudes due to the poor frequency localisation at high frequencies. In [24], an algorithm based on computing a recursive continuous wavelet transform was used for detecting the sag and transient events in the signals. A what called "clean" time-frequency plane is presented by computing the magnitudes of the CWT coefficients taking only a few steps (i.e. the fundamental and higher frequencies). This presented

plane demonstrates the main signal characteristics change in the fundamental and higher frequencies. In [25], the detection of harmonic distortions due to adjustable speed drive and oscillatory transient events using the CWT technique with a dyadic Daubechies wavelet as a Mother Wavelet, was discussed and compared with the STFT technique.

Although it was shown that the CWT technique has the capability of handling the noisy signals, the main disadvantage of the CWT is its redundancy of using a large number of scales resulting in a significant computational overhead.

In order to avoid the redundancy in the CWT, the MRA was adapted by many researchers. In [26], the Wavelet MRA technique was used to expand the distorted signals in terms of five detailed coefficients and the approximation coefficient. These coefficients were used to form six feature vectors which were used to represent three groups of power quality disturbances based on their harmonic contents and the frequency ranges in each decomposition level. However, in some cases the coefficients of the high-frequency decomposition levels are small enough to be affected by the noise and hence the feature of some disturbances may not be identified. In [27] – [29], the Wavelet MRA was applied on three types of power quality events (transformer energizing, converter operation, and capacitor energizing). The features of these events were extracted using the statistics of the squared wavelet coefficient at four decomposition scales. The reason for squaring the wavelet coefficient was to reduce the effect of noise in the signals. In [30] – [35], the standard deviation of the wavelet coefficient at different resolution levels based on the MRA was calculated to construct a feature vector for charcterising different types of power quality events.

Another algorithm explored widely in [36] – [39] using the MRA and Parseval's Theorem to extract the features of the power quality signals in terms of their energies at different resolution levels. In this algorithm, it was shown that the energy values of the decomposed signals at different levels are sensitive to the type of the disturbances. However, non of these studies did investigate the effect of phase shift of the signals, which has a significant effect on the energy values of the decomposed signals even if the signals are pure.

From the above studies on the WT technique, it can be considered as a powerful signal processing technique. However, it has limitations in detecting and extracting the features of some power quality signals which have small changes in the slope of the signal, such as sags or swells that start at the beginning of the half periods of the measured signal. In other word, the WT technique can be considered as an analysis tool for the first derivative of the target signal and not the amplitude of the target signal. This is why the WT technique is sensitive to signal irregularities but insensitive to regular-like behavior of the signals [40].

The S-Transform (ST) was also introduced recently in as a new power quality signal processing technique, [42] – [47]. In [42], the amplitude contours of four simulated events, (sag, swell, momentary interruption, and oscillatory transient), using the ST technique were shown to be suitable for power quality classification by simple visual inspection. In addition, an attempt was shown to classify three of the studied events, (i.e. voltage sag, swell, and momentary interruption), by calculating the standard deviation of the time frequency representation of the signal. In [43] – [47], the ST technique was used to construct a feature vector comprising the standard deviation of the lowest ST contour that is above the fundamental frequency, the minima and maxima of the ST absolute matrix, and the standard deviation of the instantaneous frequency above twice the fundamental frequency.

Similar to the STFT, the ST also requires significant amount of computational resources. This is due to the fact that the ST matrix is calculated by performing the inverse Fourier transforms for a number of iterations depending on the frequency resolution.

1.3.2 Power Quality Classifications

Power quality events classification is often troublesome because it involves a broad range of disturbance categories or classes where the decision boundaries of the disturbance features may overlap. One of the oldest and most extensively applied for the classification purposes is the Artificial Neural Networks (ANN) technique, ([40], [41],

and [48] – [52]). The advantage of this technique is its capability to handle easily the noisy data that is present in real-time measurements. However, the main drawback of the ANN technique is the need for large numbers of training cycles and the requirement of re-training the entire neural networks for every new power quality event [53]. In addition, the ANN technique suffers from the computation overhead in some cases [26].

The Fuzzy Logic (FL) technique was also reported in [38], [44], and [53] – [57] for automatic classification of power quality events. Although the FL technique does not require a training process for automatic recognition, as it uses simple "IF-THEN" relations, the technique has limitations for events (such as transients and flicker) that cannot be described easily.

Another technique which has not been explored widely in the power quality classification is the k-Nearest Neighbor (k-NN) pattern recognition technique research. In [35] and [58], the k-NNtechnique was applied to classify the disturbances online. The proposed k-NNclassifier demonstrated 88% accuracy for a set of simulated data with a 3.5% noise level, without examining the effect of the number of neighbors.

The techniques studied so far are based on single-phase measurements. If three-phase system monitoring is required, it is necessary to monitor each phase separately, which results in more computational resources and poor accuracy. Therefore, this study considers a new power quality monitoring technique that is introduced for monitoring three-phase systems. In addition, for single-phase systems, the Hilbert Transform (HT) technique is also examined as an alternative technique, and compared to the previous single-phase monitoring techniques.

1.4 Outline of the Thesis

The thesis is divided into seven chapters which can be summarized as follows. Chapter 2 provides the characteristics of several power quality issues belonging to different categories based on the IEEE standard, [59]. The main causes of power quality issues is also discussed in the chapter.

In chapter 3, the most widely used power quality detection techniques are reviewed. In addition, an alternative proposed detection technique which is based on monitoring all of the three-phase signals in power systems simultaneously is described and tested. A monitoring system which was developed to accommodate the proposed detection technique is also described in this chapter.

Chapter 4 discusses the proposed power quality feature extraction techniques. The application of various signal-processing techniques on real-time power quality waveforms are investigated and their performance in extracting the relevant features are studied. In each technique, the effect of the use of different parameter settings on the performance of the technique is also investigated.

Chapter 5 investigates the capability of the feature extraction techniques to distinguish different power quality events. Unlike the previous studies which were based on examining a single signal processing technique, in this chapter, combinations of different features from different techniques (or different features from the same technique) are investigated to show their capability in distinguishing between different power quality events.

Chapter 6 examines automatic power quality event classification algorithms based on the k-Nearest Neighbour technique. The optimum selection of number of neighbors is also investigated to minimize the classification errors.

Finally, chapter 7 presents the main conclusions of this work, and provides insights for the possible future research.

Chapter 2

Power Quality Events and their Causes

2.1 Introduction

POWER quality is an issue of ever-increasing concern for many power users whose day to day operations rely on sensitive electronic technologies. The emergence of this issue, as discussed in the previous chapter, is attributed to a variety of reasons of which a major one is the increasing utilization of power electronic loads. Such loads are sensitive to the disturbances in power systems and also cause power quality issues.

This issue of power quality involves a wide variety of electromagnetic phenomena that characterise the voltage and current signals at a given time and at a given location on the power system. The Institute of Electrical and Electronic Engineers (IEEE) Standard, [59], categorised these phenomena (which are usually referred to as power quality events) into different categories as shown in Table 2.1. This categorisation is done in terms of the frequency components (spectral content) that appear in the voltage signals during the phenomenon, the duration of the phenomenon, and the typical voltage magnitude. For the classification purposes, most of the primary categories are further expanded into subcategories that provide additional specifications on the event. For example, the sag event can be further categorised based on

the cause of the event (e.g. motor starting sag, sag due to faults, etc.). In addition, a combination of events may occur. For example sag events are usually contaminated with harmonics. More details on the characteristics of the most common events will be described in this chapter.

2.2 Classes of Power Quality Events

In power systems, different actions may cause different power quality events having specific characteristics. In this section the most common power quality events will be described. This will include: sags, swells, interruptions, harmonics, oscillatory transients, and flicker.

2.2.1 Sag (Dip) Events

The sag event is the most common event in power systems. It is defined by a reduction in the amplitude of the nominal voltage signals. According to the IEEE standards, as shown in Table 2.1, the depth of the sag varies from 0.1 to 0.9 pu of the signal. Figure 2.1 shows a sample of a typical sag event of 0.5 pu, which continues for eight cycles.

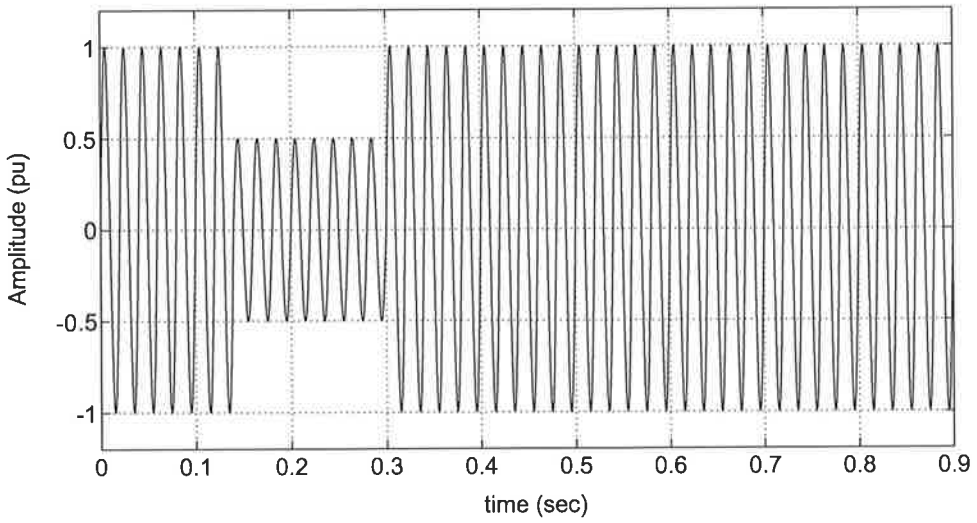

Figure 2.1: A sample sag event of 0.5 pu.

Table 2.1: Categorisation of power quality events [59].

Categories	Spectral content	Typical duration	Voltage magnitude
1.0 Transients			
1.1 Impulsive			
1.1.1 Nanosecond	5ns rise	< 50ns	
1.1.2 Microsecond	1μs rise	50ns – 1ms	
1.1.3 Millisecond	0.1ms rise	> 1ms	
1.2 Oscillatory			
1.2.1 Low frequency	< 5kHz	0.3 – 50ms	0 – 4pu
1.2.2 Medium frequency	5 – 500kHz	20μs	0 – 8pu
1.2.3 High frequency	0.5 – 5MHz	5μs	0 – 4pu
2.0 Short duration variations			
2.1 Instantaneous			
2.1.1 Sag		0.5 – 30cyc.	0.1 – 0.9pu
2.1.2 Swell		0.5 – 30cyc.	1.1 – 1.8pu
2.2 Momentary			
2.2.1 Interruptions		0.5cyc. – 3s	<0.1pu
2.2.2 Sag		30cyc. – 3s	0.1 – 0.9pu
2.2.3 Swell		30cyc. – 3s	1.1 – 1.2pu
2.3 Temporary			
2.3.1 Interruptions		3s – 1min	<0.1pu
2.3.2 Sag		3s – 1min	0.1 – 0.9pu
2.3.3 Swell		3s – 1min	1.1 – 1.2pu
3.0 Long duration variations			
3.1 Interruption, sustained		> 1min	0.0pu
3.2 Undervoltage		> 1min	0.8 – 0.9p
3.3 Overvoltage		> 1min	1.1 – 1.2pu
4.0 Voltage Imbalance		steady state	0.5 – 2%
5.0 Waveform distortion			
5.1 DC offset		steady state	0 – 0.1%
5.2 Harmonics	0 – 100th H	steady state	0 – 20%
5.3 Interharmonics	0 – 6 kHz	steady state	0 – 2%
5.4 Notching		steady state	
5.5 Noise	broad-band	steady state	0 – 1%
6.0 Voltage fluctuations	< 25Hz	Intermittent	0.1 – 7%
7.0 Power frequency variations		< 10s	

The major cause of experiencing the sags on the customer sides is usually the faults in power systems. Other sources are the starting of large loads (especially common in industrial systems), starting of induction motors, or energizing transformers. The difference between the sags due to faults and the sags due to starting motors or energizing transformers is in the way the affected signals recover from the event. The sags due to faults usually recover as soon as the fault causing it is cleared, while the sags due to starting induction motors or energizing transformers recover gradually. Figure 2.2 shows an example of a simulated voltage sag due to starting an induction motor. In this sample figure, the magnitude of the voltage decreases and gradually recovers within about 0.4 seconds.

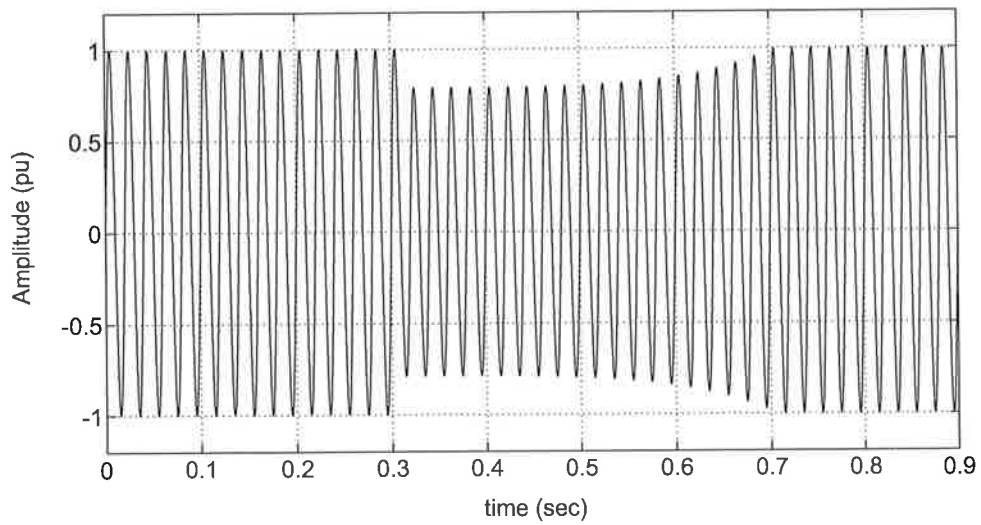

Figure 2.2: A sample of sag event due to starting of motors.

The magnitude and duration of the sag events are often compared against tolerance envelopes to identify the severity of the event. The most widely used curve for this purpose was proposed by the Computer Business Equipment Manufacturer's Association (CBEMA), which was intended to specify the ability of mainframe computers to sustain voltage sags, as shown in Figure 2.3 (top) [77]. The "CBEMA Curves" has been updated and renamed the "ITIC Curve" (for Information Technology Industry Council), and adopted by IEEE Std. 446-1995 [60]. The ITIC Curves is presented in Figure 2.3 (bottom).

In both curves, the vertical axis represents the percentage voltage magnitude change with respect to its nominal value, and the horizontal axis represents the time duration of the event. Upper and lower curves indicates the maximum and minimum limits. In the center of the plot is the acceptable area. Outside this area is the region where the equipment may be damaged or may not function correct. The overvoltage zone at the top involves the tolerance of equipment to excessive voltage levels, while the zone at the bottom describes the tolerance of equipment to a loss or reduction in applied voltage for a certain period of time.

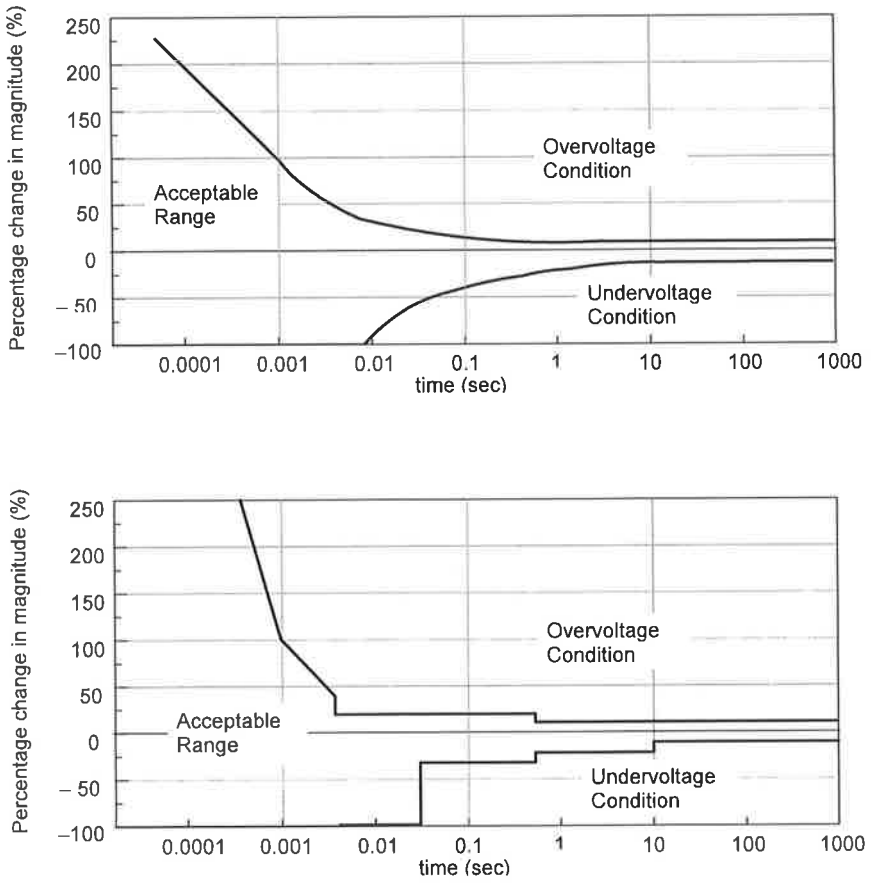

Figure 2.3: (Top), Computer Business Equipment Manufacturer's Association Curves (CBEMA Curves). (Bottom), Information Technology Industry Council Curves (ITIC Curve) [77].

2.2.2 Swell Events

Swell events are defined by an increase in the amplitude of the signal starts from 1.1 pu and up to 1.8 pu for a duration more than 0.5 cycle according to the IEEE Std. 1159. Figure 2.4 shows a typical swell event of 1.3 pu.

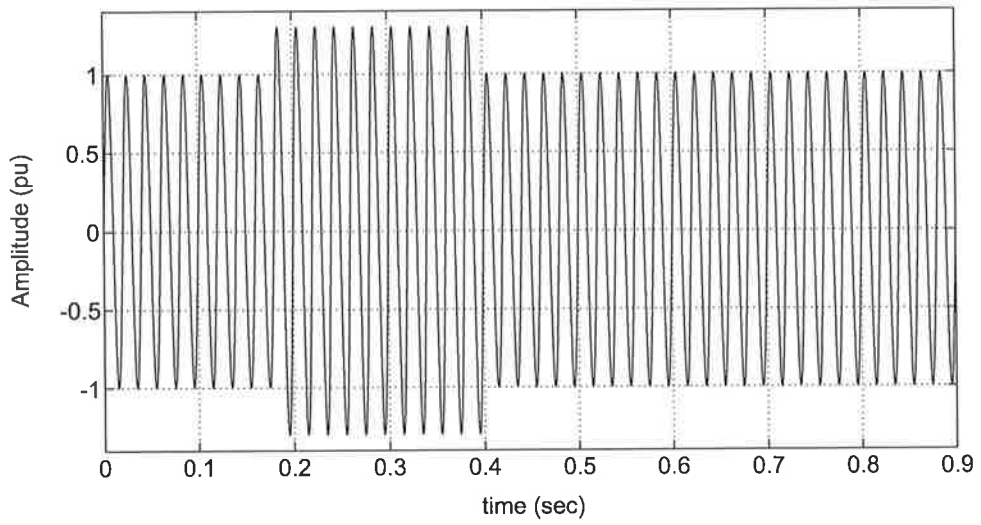

Figure 2.4: A sample of swell event of 1.3 pu.

Swell events are commonly caused by the de-energizing of large loads or by asymmetrical faults (e.g. a line to ground fault will cause a voltage rise in the other two phases). Swells can cause insulation breakdown in sensitive electronic equipment if voltage increases are high enough for a sufficient period of time. Equipment tolerance to swells, like sags, is described by voltage tolerance envelopes described by the ITIC Curves in a similar way to the sag events (see Figure 2.3).

2.2.3 Interruption Events

An interruption event is a complete loss of electric power or a more than 90% reduction in the signal nominal amplitude for more than half a cycle as shown in Figure 2.5. The major cause of interruptions is faults in power systems or the malfunction of protection systems.

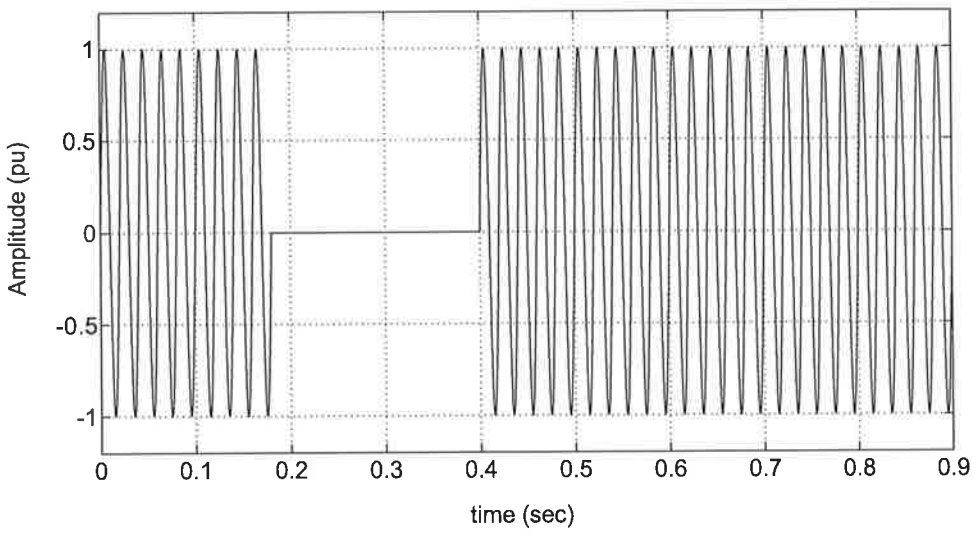

Figure 2.5: A sample of an interruption event.

2.2.4 Harmonic Distortion

Harmonics are sinusoidal components superimposed onto the voltage or current signals having frequencies that are integer multiple of the fundamental frequency in the power system. An example of a signal distorted by harmonic components is shown in Figure 2.6(top). The frequency spectrum of this signal which shows the harmonic content is illustrated in Figure 2.6(bottom).

Harmonic distortion is normally attributed to the application of nonlinear loads (i.e. loads that when supplied by a sinusoidal voltage do not draw a sinusoidal current). The current in these loads can be heavily distorted compared to a sine wave, and usually containing the odd harmonics, 3, 5, 7, 9, etc. For example in an extreme case, the third harmonic may be 80% of the fundamental, and the fifth may be 60% of the fundamental. These nonlinear loads not only have the potential to create problems within the facility that contains the nonlinear loads but also can adversely affect neighboring facilities [63].

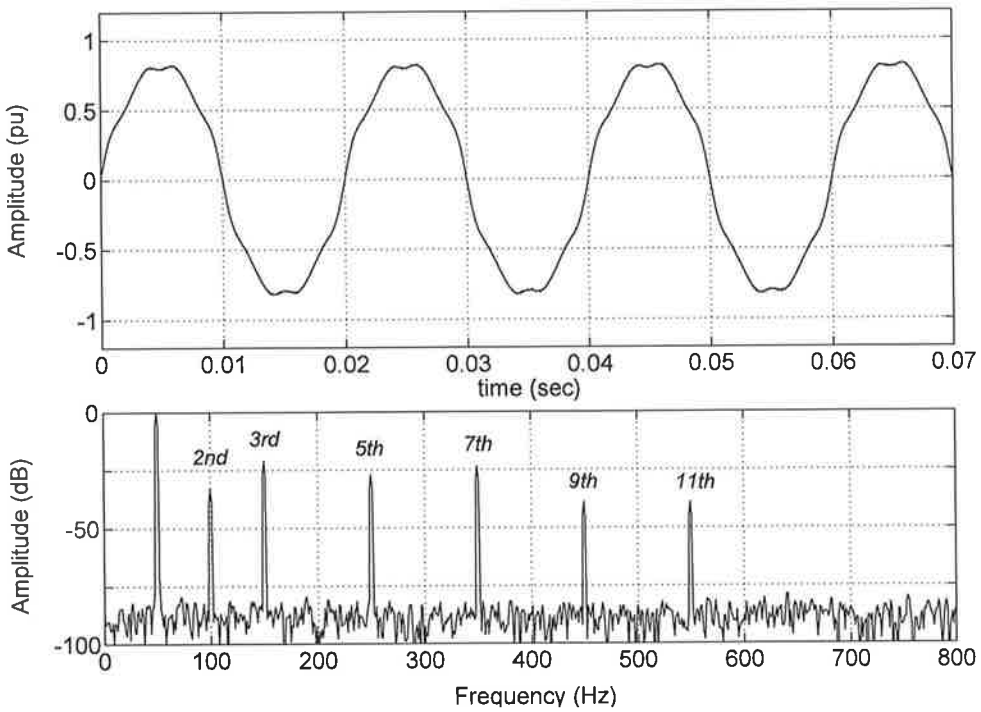

Figure 2.6: A sample of harmonic distortion event (top), and its frequency spectrum (bottom).

Examples of common nonlinear loads are adjustable-speed drives and dc power supplies. These devices rectify the incoming three-phase AC supply. In doing this, the current is distorted with harmonics of order 5, 7, 11, 13, etc. (i.e. all of the odd harmonics except multiples of three). In theory, the amplitude of the fifth harmonic is one-fifth of the fundamental, the seventh harmonic is one-seventh of the fundamental, and so forth.

Other harmonic-producing loads include arc furnaces, arc welders, fluorescent lights (with magnetic and especially with electronic ballasts), battery chargers, and cycloconverters.

The harmonic currents drawn by loads distort supply voltage waveforms due to finite supply impedance of the power system, and hence produce voltage harmonics. The effect of the resulting supply voltage harmonics is determined by the susceptibility of the load to them. The least susceptible loads to the harmonics are the

resistive loads whose main function is heating, such as in the electric ovens. The most susceptible loads, in the other hand, are that require a (nearly) perfect sinusoidal fundamental input. Communications or data processing equipment often fall into this category of loads. Even in the case of the least susceptible loads, harmonics still can have some harmful effects. In the case of an oven, for example, they can cause dielectric thermal or voltage stress, which causes a premature aging of the electrical insulation.

A type of load that normally falls between these two extremes of susceptibility are motor/generator loads. These loads are relatively tolerant to harmonics. The major effect of harmonic voltages and currents in rotating machinery is increased heating due to iron and copper losses at the harmonic frequencies. The harmonic components thus affect the machine efficiency and can also reduce the output torque [61].

A common measure of the severity of harmonics in power systems is what known as the Total Harmonic Distortion,(THD), which is the square-root of the sum of the squares of each individual harmonic expressed as a ratio with the fundamental component. Thus, for voltage signals the total harmonic distortion, (V_{THD}), is calculated as:

$$V_{THD} = \frac{\left(\sum_{h=2}^{\infty} V_h^2\right)^{1/2}}{V_1} \tag{2.2.1}$$

where,
V_1 is the RMS magnitude of the fundamental component in the voltage signal, and
V_h is the RMS magnitude of the harmonic component h.

The IEEE provides a recommended practice for harmonics, IEEE Std. 519-1992 [61], which sets voltage harmonic limits for utilities and for end users. As shown in Table 2.2, for suppliers at 69 kV and below, the IEEE voltage limits are 3% on each individual harmonic and 5% on the total harmonic distortion. Both of these percentages are referenced to the nominal voltage [61].

For the current distortion, the IEEE Std. 519-1992 also provided current har-

monic limits, (illustrated in Table 2.3) which are designed to be consistent with the voltage distortion limits. That means, if users limit their current injections according to the guidelines, the voltage limits will remain under the guidelines imposed on the utility. In the table, the harmonic current limits are based on the size of the load which respect to the size of the power system to which the load is connected. The ratio I_{sh}/I_L is the ratio of the short-circuit current available at the point of common coupling (PCC), to the maximum fundamental load current. The individual harmonics and the total harmonics (total demand distortion, TDD) are referenced to the maximum demand at that point. The TDD is calculated as [63]:

$$I_{TDD} = \frac{\left(\sum_{h=2}^{\infty} I_h^2\right)^{1/2}}{I_L} \times 100\% \tag{2.2.2}$$

where,

I_{TDD} is the total demand distortion in percentage,

I_h is the RMS magnitude of the harmonic component h, and

I_L is the maximum fundamental load current(rated current).

Table 2.2: Voltage Distortion Limits for Distribution Systems [61].

	Voltage Distortion Limits
Individual Harmonics	3%
Total Harmonic Distortion (THD)	5%

2.2.5 Oscillatory Transients

Transients are high frequency components that occur in the voltage or current signals for a short time. As stated in Table 2.1, based on the spectral content, the oscillatory transients are considered as *Low-*, *Medium-*, or *High- frequency oscillatory transients* with primary frequency component is less than 5 kHz, between 5 kHz and 500 kHz, or, between 500 kHz and 5 MHz respectively.

Table 2.3: Current Distortion Limits for Distribution Systems [61].

I_{sh}/I_L	$h < 11$	$11 \leq h < 17$	$17 \leq h < 23$	$23 \leq h < 35$	$35 \leq h$	TDD
< 20	4.0	2.0	1.5	0.6	0.3	5.0
$20 - 50$	7.0	3.5	2.5	1.0	0.5	8.0
$50 - 100$	10.0	4.5	4.0	1.5	0.7	12.0
$100 - 1000$	12.0	5.5	5.0	2.0	1.0	15.0
> 1000	15.0	7.0	6.0	2.5	1.4	20.0

Note: Even harmonics are limited to 25% of the odd harmonic limits above. Current distortion that result in a dc offset are not allowed.

The main cause of transients is switching of capacitors in power systems, where once the capacitor is switched, it momentarily pulls the system voltage down (as a large current flows into the capacitor to charge it up). As the system is normally under damped, rebounds and the voltage overshoots and oscillates about the fundamental frequency [64]. This transient normally decays quickly. The oscillation occurs at the natural resonance frequency between the capacitor being and the inductance of the power system, which can be calculated as [64]:

$$f_c = \frac{1}{2\pi\sqrt{L_s C}} \tag{2.2.3}$$

where,

f_c is the frequency of the oscillatory transient,

C is the capacitance of the capacitor, and

L_s is the system inductance.

Figure 2.7 shows a simulated example of an oscillatory transient having a 1kHz resonant frequency.

In power systems, the switching of capacitors is often an unavoidable action, where it has several purposes. Two different cases are [29]:

1. *Normal Energizing of Utility Capacitors*: As part of normal operation in the utility system for anticipating a load increase at customer side, or to correct the power factor, capacitors are switched in on a daily basis.

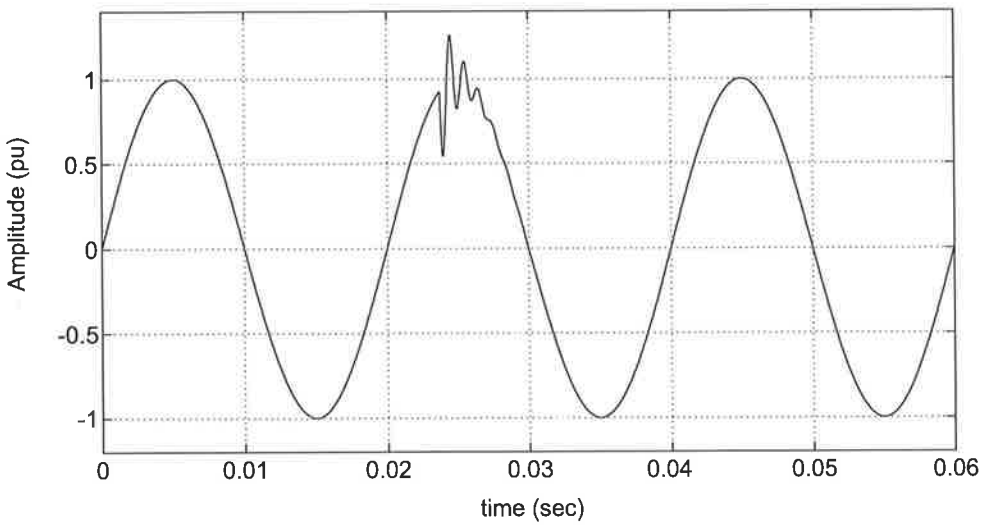

Figure 2.7: A sample of an oscillatory transient event having a 1kHz resonant frequency.

2. *Back-to-Back Capacitor Energizing*: Back-to-Back energizing transient involve two capacitors in close vicinity. One of them is fully energized (local), when the other is switching in. The resulting step voltage in this case is not as large as if the fully energized capacitor did not exist. However, the oscillation frequency in this case is higher than that in normal energizing case, due to the much smaller effective system inductance.

   The overvoltage in this scenario depends on the rating values of the two capacitors as it was shown by a study done by [65]. The results of the study is shown in Figure 2.8, which shows the effect of switching three capacitors, (1.2 MVar, 1.8 MVar, and 3 MVar), on the peak voltage for a range of different sizes of local energized capacitors. One can see from the figure that for each size of the capacitor being switched, there is a specific value of local capacitor that generates the maximum peak voltage. For example, for switching 1.2 MVar capacitor, the maximum voltage peak, (2.4 pu), occurs when the energized capacitor size is 100 kVar.

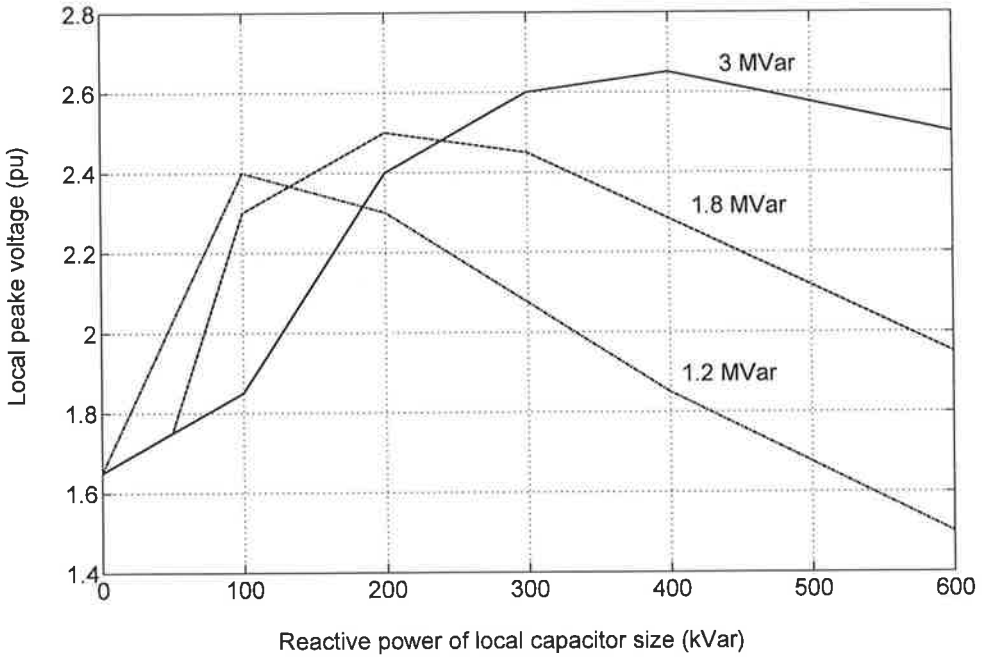

Figure 2.8: Transient magnitude for various sizes of switched and local capacitors [65].

2.2.6 Voltage fluctuations (Flicker Event)

Voltage fluctuation is a low-frequency phenomenon in which the magnitude of the voltage signal changes periodically. If these changes are at such a rate as to be perceptible to the human eye, it is called flicker. A sample of a flicker event is shown in Figure 2.9. Although the flicker does not normally have a serious impact on electrical equipment, flickering lights, televisions, or computer monitors can disturb end users.

The most common causes of voltage fluctuations on the transmission and distribution system are the Arc furnaces and periodical starting of motors. The flicker is usually expressed in percentage as:

$$V_F = \frac{V_{\max} - V_{\min}}{V_r} \times 100\% \tag{2.2.4}$$

where,

V_F is the percentage of the flicker,

$V_{\max}$ and $V_{\min}$ are the maximum and minimum changes in the RMS voltage respectively, and V_r is the rated RMS voltage.

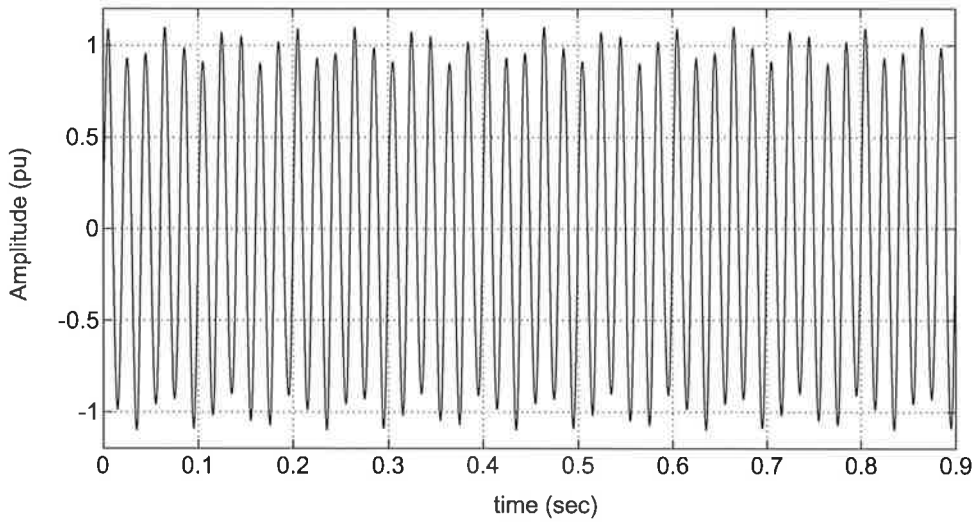

Figure 2.9: A sample of a flicker event.

The IEEE standards [62] provided "Flicker curves" shown in Figure 2.10 which are derived from controlled experiments to offer thresholds of acceptable voltage flicker for incandescent lights used by a large number of utilities. In this figure, the two curves show how the acceptable voltage flicker magnitude depends on the frequency of dips in the flicker. The lower curve shows a borderline where people begin to detect flicker. The upper curve is the borderline where some people will find the flicker objectionable. For example, at 10 dips per hour, people begin to detect incandescent lamp flicker for voltage fluctuations larger than 1% and begin to object when the magnitude exceeds 3%.

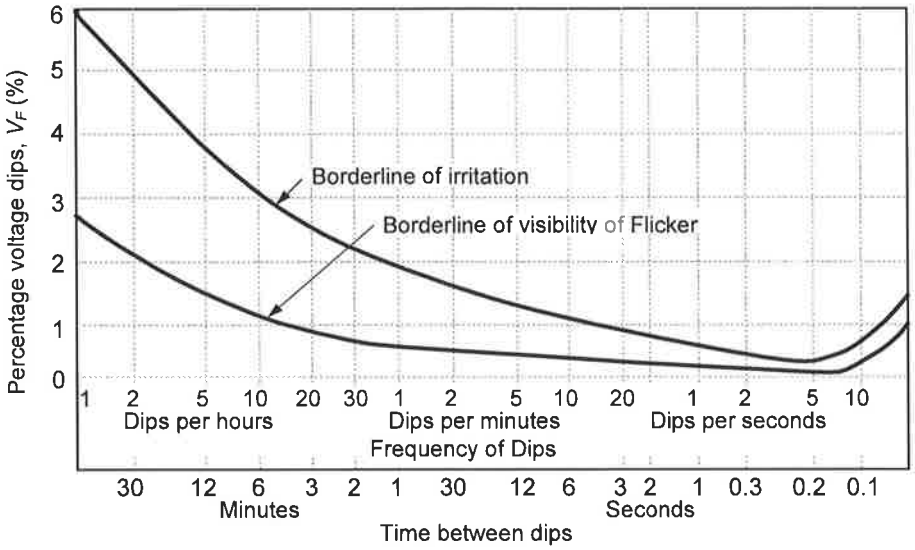

Figure 2.10: The perceptibility threshold of voltage flicker verse time [62].

2.3 Conclusion

A wide variety of electromagnetic phenomena are becoming an every day issue in power systems. These phenomena have different characteristics that affect the voltage and/or current signals at a given time and given location on power systems.

This chapter described the characteristics of the most frequent phenomena in the power systems including sags due to faults, sags due to starting of motors, swells, interruptions, harmonic distortions, transients, and flicker. The main causes of these phenomena are also discussed. In addition, the acceptable limits of some phenomena (i.e. sags, swells, harmonics, and flicker) based on the available relevant standards are also explored. The phenomena explained in this chapter will be the main categories in the automatic classification system explained in the forth coming chapters.

Chapter 3

Detection Techniques for Power Quality Events

3.1 Introduction

DIFFERENT monitoring devices are currently available that can capture and collect large amounts of power quality disturbance data. The techniques used for capturing these disturbance are usually based on detecting when a certain threshold level is exceeded. The limits or threshold levels are primarily defined by the standards that define the acceptable level of disturbances in AC power systems seen by the end users.

It is imperative that the detection mechanism of the monitoring devices be fast enough to process any acquired sequences of the monitored signal before the acquisition of the new sequences starts. Delayed detection of distorted signals may result in missing the second of two closest spaced events or overlapping of two successive sequences of the same signal which may lead to errors in processing the signal.

The sensitivity of the monitoring devices depends on the selected threshold level. A high threshold results in missing disturbances which should have been recorded, while a low threshold results in capturing large number of waveforms. Practical monitoring systems, however, have a limited size of memory to store the disturbance data. Therefore, an important task in power quality monitoring is to set the

triggering to capture only the desired power quality events to make the best use of available memory [79].

Commonly used thresholds for power quality monitoring are the changes in the root mean square or the peak value of the signal (RMS or Peak thresholds), or cycle-by-cycle signal comparison threshold. In this technique, the monitored waveforms are broken down into user-defined windows of time that represent a percentage of the overall waveform. Each window is compared to the same window of time in the previous waveform and if the difference exceeds the user's limits an event is recorded. The technique has a drawback of not being able to capture disturbances that appear periodically in many cycles of the waveform, like flat-top and phase controlled load (repeated notch) waveforms [80].

This chapter, therefore, discusses the performance of two widely used detection techniques in power quality monitoring systems (the root mean square and the peak values of signals). In addition, monitoring the signal envelope using the Clarke transform is introduced as an alternative detection technique for monitoring all phases of three-phase systems simultaneously with high sensitivity to short duration events.

3.2 Point-by-Point Root Mean Square Technique

The main advantage of the Root Mean Square (RMS) technique as a triggering threshold for power quality events is its speed and simplicity in terms of the calculations involved. The general formula for calculating the RMS value of a sinusoidal signal is given by:

$$V_{rms} = \sqrt{\frac{1}{T}\int_0^T v(t)^2 \cdot dt} \tag{3.2.1}$$

where,

$v(t)$ is the continuous function of voltage (or current) signal in the time domain,

T is the time period of the signal, and

V_{rms} is the RMS value of the signal.

In real time applications, however, the power quality signals are captured in a discrete sequence of samples. Therefore, for monitoring purposes, the RMS values of power quality signals have to be calculated at each point of the sampled signal. This can be performed as described by the following equation:

$$V_{rms}[n_k + i] = \left[\frac{1}{n_k}\sum_{k=i}^{n_k+i} v[k]^2\right]^{1/2}, \quad i = 1, 2, \ldots, N - n_k \tag{3.2.2}$$

where,

$v[k]$ is the sampled voltage (or current) signal,

n_k is the number of samples in a half cycle or one full cycle (window size),

$V_{rms}[n_k + i]$ is the RMS value at the sample point $n_k + i$,

N is the total number of samples in the signal, and

k is the discrete time index.

In order to investigate the performance of the RMS algorithm, it has been applied on two common real power quality signals; sag, and oscillation transient events. The results are shown in Figures 3.1 and 3.2.

In Figure 3.1, the RMS value of a three-phase voltage sag followed by an interruption is calculated over a window of one cycle length, (Figure 3.1 middle), and half cycle length, (Figure 3.1 bottom). It should be noted that the exact frequency of the signal should be known *a priori* in order to be able to calculate the one cycle window length. For the signal in Figure 3.1, the number of points in each cycle is 50. Note that, in the case of the one cycle calculation, because the RMS calculation described in Equation 3.2.2 starts at the 50^{th} point, the RMS value is only available from the 50^{th} point onwards. Similarly, in the case of the half-cycle calculation, the RMS value is only available from the 25^{th} point.

From Figure 3.1 one can see that when using the half-cycle window, the RMS values tracks the distortions in the signals more rapidly. This can be observed from the curves of the half-cycle RMS values which drop more quickly to the lowest value of the disturbance, while the response of the one-cycle RMS curves are delayed by about half a cycle.

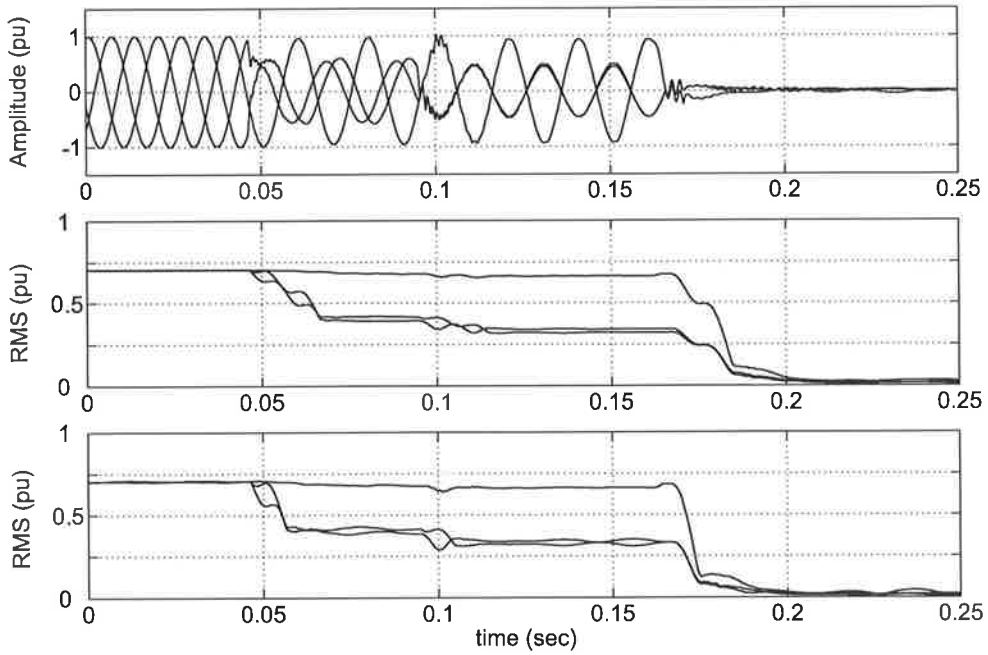

Figure 3.1: Three-phase distorted signal (top), and its point-by-point one-cycle RMS value (middle) and half-cycle RMS value (bottom).

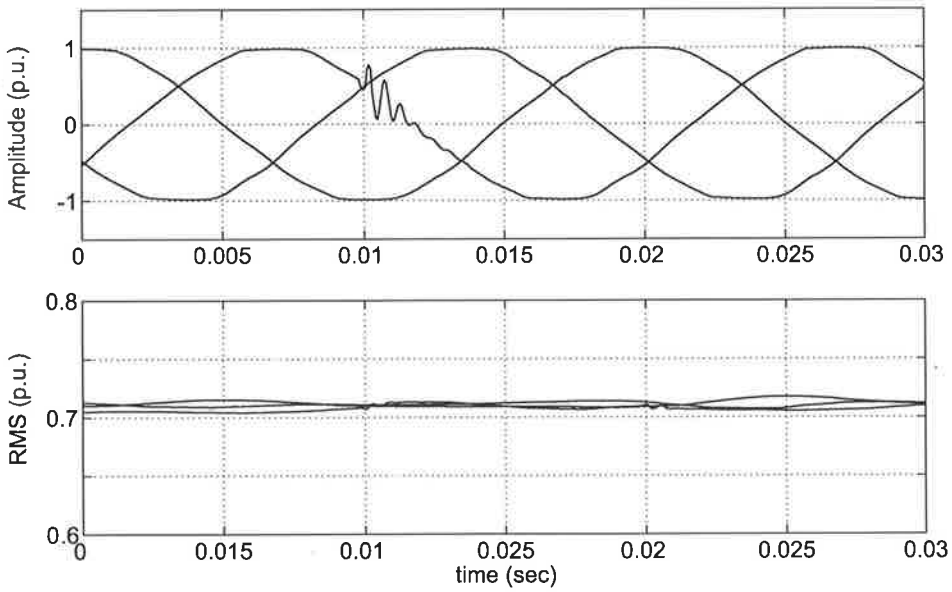

Figure 3.2: Oscillatory transient on a single phase of a three-phase signal (top) and its point-by-point half-cycle RMS value (bottom).

Although the RMS technique is shown to be sensitive to low frequency disturbances like sags and swells, it fails to detect disturbances that have high frequency components and occur for only a short time, as in the case of transient events. Figure 3.2 shows an oscillatory transient event that occurs on one phase of a three phase signal. The point-by-point RMS values are calculated over a window of half a cycle. From the figure, one can see that, because the event has a high frequency component which lasts for less than a quarter cycle, this event will not be detected with the RMS technique. This limitation make the RMS technique not suitable for detecting transient events.

3.3 Point-by-Point Peak Value

Another common technique used for monitoring and detecting signals is the Point-by-Point peak value of the signal. This technique is obtained by tracking the maximum of the absolute value of the signal over a preselected window length. The window length is selected to be a multiple of one half-cycle of the signal. Therefore, for a discrete time signal $v[k]$, its point-by-point peak values is calculated as [13]:

$$V_{peak}[k+n_k] = \max \left| v[k-n_k] \right| \qquad \forall \qquad 0 < n_k < T \tag{3.3.3}$$

where,

$v[k-n_k]$ is the segment of the signal of length n_k,

$V_{peak}[k+n_k]$ is the peak value of the signal at point $k+n_k$,

T is the period time of the signal, and

k is the discrete time index.

It should be noted that the above equation gives the point-by-point peak value starting at the end of the first cycle (or half a cycle). Therefore, similar to the RMS technique, the first cycle (or half a cycle) peak value is set to the same value of the last point in the cycle (or half a cycle).

The application of this technique on the real sag events is shown in Figure 3.3.

In Figure 3.3 (middle), one cycle is used for the calculations, while in Figure 3.3 (bottom), half a cycle is used for the calculations. Similarly to the RMS performance, the calculation with a half a cycle window is shown to have faster response than using a one cycle length. This is obvious from the quicker response of the calculation with half a cycle at the start and end of the event.

In Figure 3.4, the technique is tested with the short transient event. In the figure, the peak values of an oscillatory transient event when using half a cycle window for the calculations is shown. As it can be seen from the figure, the transient was not detected by the technique which indicates the unsuitability of this technique for monitoring such short duration events.

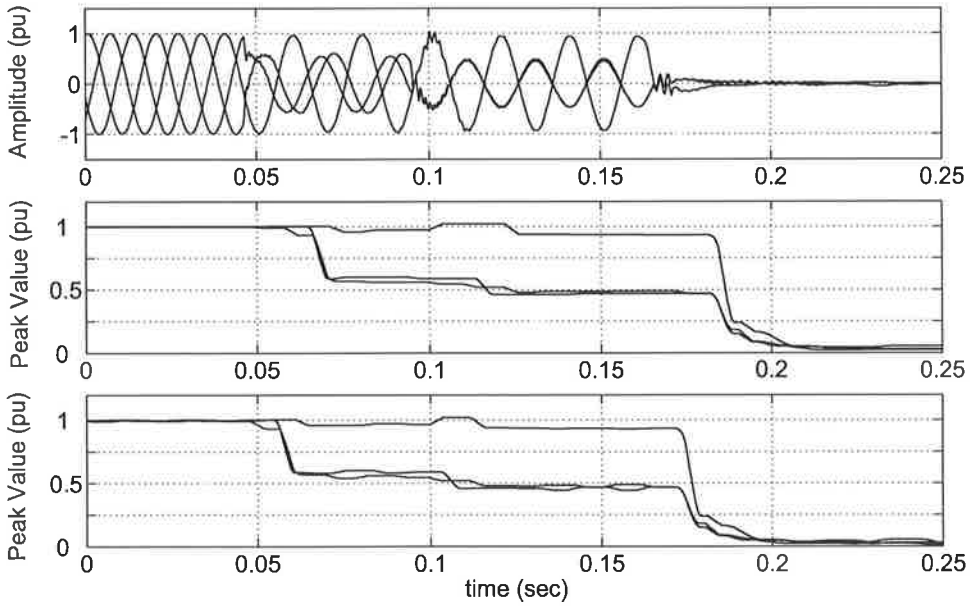

Figure 3.3: Three-phase distorted signal (top), and its point-by-point one-cycle peak value (middle) and half-cycle peak value (bottom).

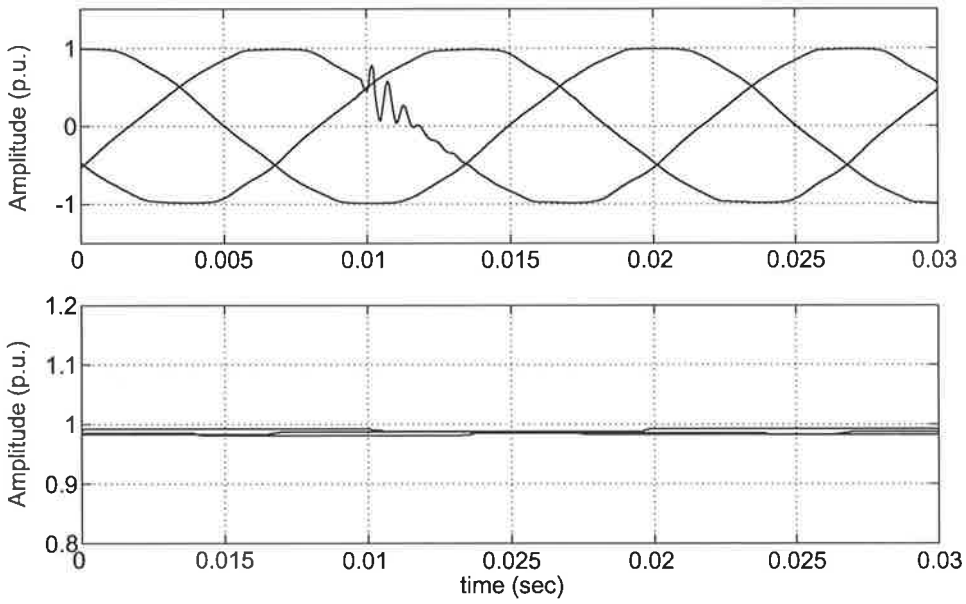

Figure 3.4: Oscillatory transient on a single phase of a three-phase signal (top) and its point-by-point half-cycle peak value (bottom).

3.4 Point-by-Point Three-Phase Envelope

In order to overcome the limitations mentioned above in the point-by-point RMS and Peak value monitoring approaches, this section presents a new triggering method for a more reliable monitoring system. In this triggering method, the three-phase signal envelope approach is used. The principle idea in this approach is based on the characteristic of a balanced three-phase system, in which the magnitude of the instantaneous vector sum of the three phases at any time is constant. As it will be discussed in more detail in Chapter 4, the Point-by-Point three-phase envelope of a three-phase signal can be calculated from sampled data as:

$$V_E[k] = v_1 \angle \phi[k] + v_2 \angle (\phi[k] - 2\pi/3) + v_3 \angle (\phi[k] + 2\pi/3) \qquad (3.4.4)$$

where,

$V_E[k]$ is the three-phase envelope at point k,

v_1, v_2, and v_3 are the three-phase system signals, and

ϕ is the phase shift of phase v_1.

In order to examine the sensitivity of the proposed approach, it was applied to the sag followed by interruption event (shown in Figures 3.5 (top)) and to the oscillatory transient event (shown in Figure 3.6 (top)). The three-phase envelope of these events are shown in Figures 3.5 (bottom) and 3.6 (bottom) respectively. As can be seen in the figures, this approach has the ability to track the changes in the three-phase signals simultaneously. The changes are superimposed on a constant value of 1.5 pu.

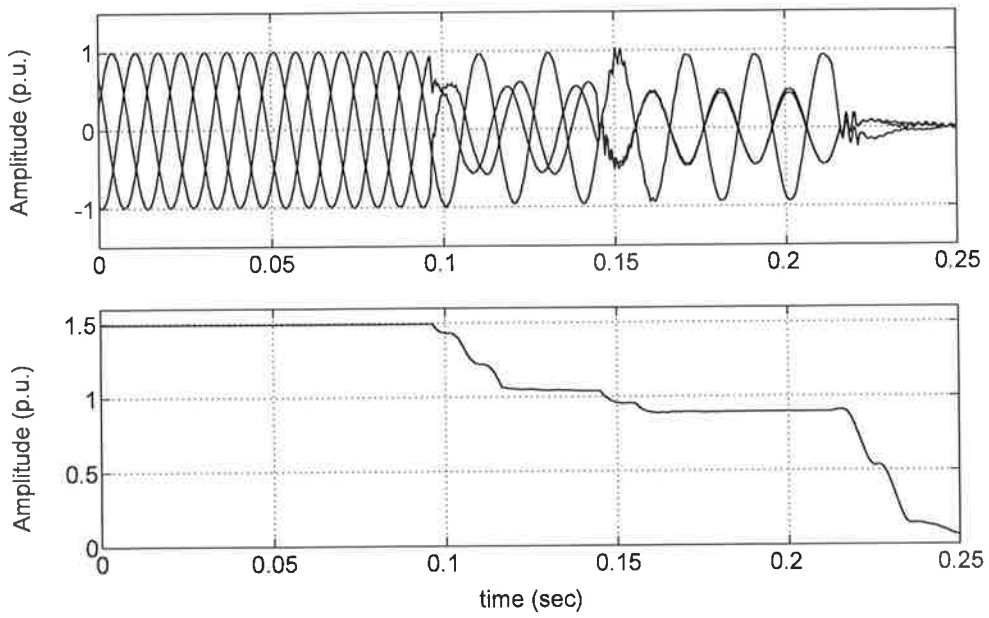

Figure 3.5: Three-phase distorted signal (top), and its point-by-point three-phase envelope (bottom).

It should be noted in Figure 3.6 that the steady-state ripple in the envelope around the average value of 1.5 pu is attributed to the distortion on the three-phase

voltages. The steady-state ripple amplitude is about 0.03 pu, which is much less than the capacitor switching transient in the signal (about 0.2 pu). Therefore, setting the triggering index in this approach above the ripple value will be sensitive enough for detecting short transient events.

Therefore, as compared with the previous results, these results demonstrate that the point-by-point three-phase envelope approach is a useful method to detect short duration transient events as well as voltage sags that may be present in any of the three phases of a power system.

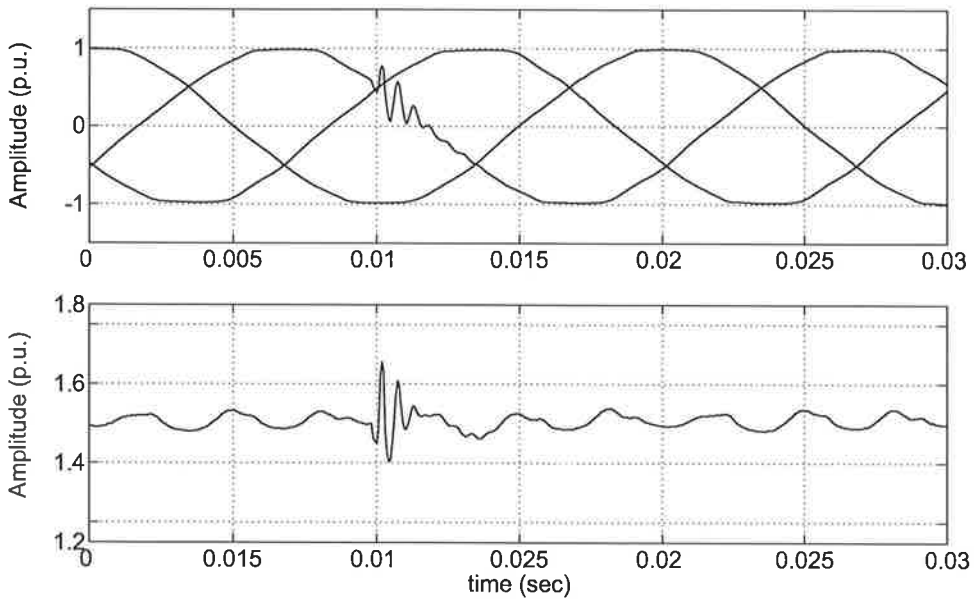

Figure 3.6: Oscillatory transient on a single phase of a three-phase signal (top) and its point-by-point three-phase envelope (bottom).

3.5 Custom Developed Monitoring System

This section describes a power quality monitoring system that was developed as a part of this project, for capturing real time power quality signals. The monitoring system has been tested in the laboratory for capturing a number of experimentally simulated power quality signals. In addition, it was also used to perform monitoring at a power station, the Pelican Point Generation Station in South Australia, as will be shown in Chapter 6. The monitoring systems includes two sections: the software section and the hardware section.

3.5.1 The Software Architecture

In the software section, a custom monitoring program for tracking real-time distortions in voltage and current signals was developed based on the point-by-point three-phase signal envelope. The program was written using a graphical programming language, LabVIEW, (Laboratory Virtual Instrument Engineering Workbench), developed by National Instruments® company. This language was chosen for writing the program, because its capability to communicate easily with the hardware system.

The program consists of a number of subprograms called VI's, (Virtual Instruments) each of which executes a specific function. The hierarchal structure of the main sub VI's in the program are shown in Figure 3.7. As demonstrated in the figure, the main VI communicate with other five sub-VI's. In the "Configuration VI", the specifications of the hardware are configured and defined. The "File setup VI" specifies the type of each data from the I/O file and adjusts the gain of the acquired data. The "Read Data VI" allows the system to start acquiring the data from the DAQ card. In the "Data Processing VI", the data is diagnosed for any out-of-tolerance condition. Finally, in the "Save Data VI", the information about any distorted signal is saved in a specific memory.

Each of these sub-VI's consists of a block diagram, which represents the structure of the program, and a front panel interface. The main VI block diagram and its front panel interface which allows the monitoring parameters and limits to be set

are shown in Figures 3.8 and 3.9 respectively. Therefore, in the program, the voltage or current signals are continuously monitored for any out-of-tolerance in signals. If a predefined limit of the three-phase envelope is exceeded, the program saves the signal in a temporary memory for further analysis.

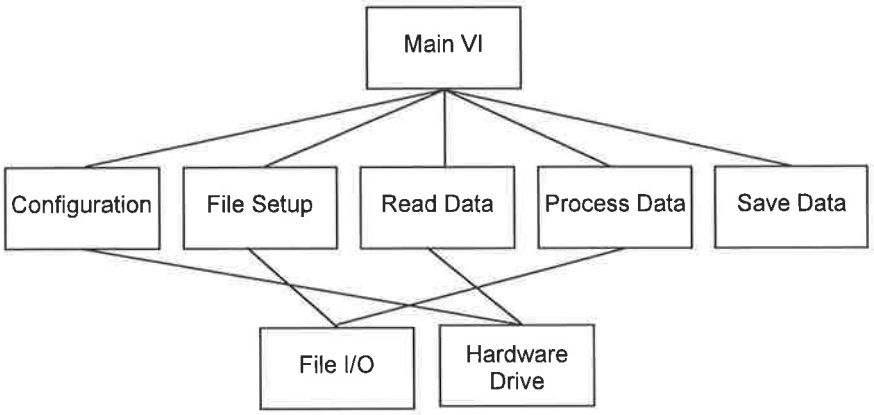

Figure 3.7: Block diagram of the monitoring system software.

3.5.2 The Hardware Architecture

The hardware section includes the data acquisition card (DAQ), which is hosted by a personal computer, and the voltage or current sensors. The specifications of the voltage and current sensors are presented in Tables 3.1 and 3.2 . The DAQ card used in the system is from National Instruments® which has the following specifications:

- 4 analog inputs; dedicated 12 bit A/D converter per channel
- Up to 10 MS/s per channel sample rate
- Analog and digital triggering
- AC or DC coupling
- 8 input ranges from ±200 mV to ±42 V

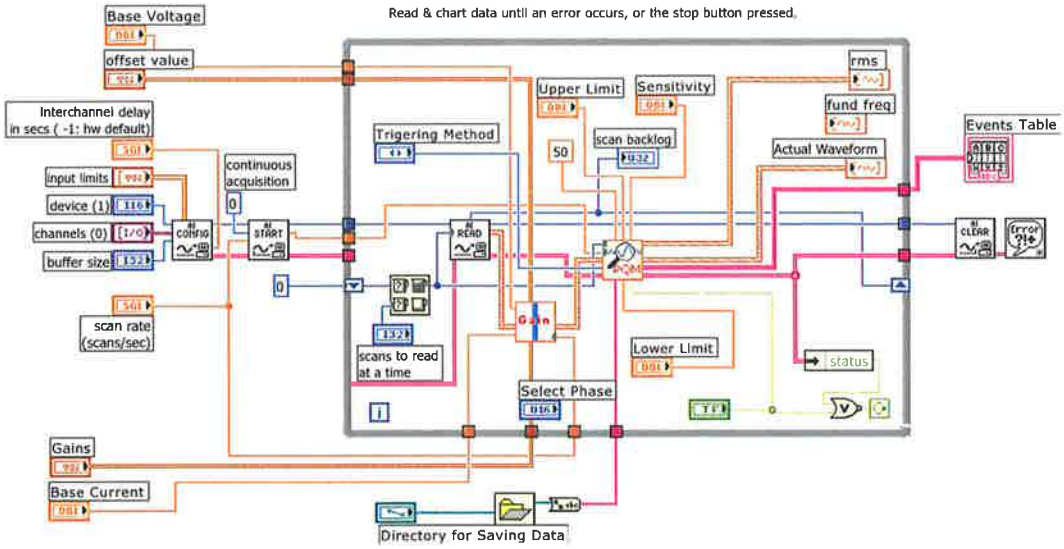

Figure 3.8: Block diagram of the main VI in the monitoring system software.

- 2 analog outputs at 4 MS/s single channel or 2.5 MS/s dual channel
- 8 digital I/O lines (5 V TTL/CMOS)
- Two 24-bit counter/timers.

Table 3.1: Voltage sensor specifications

Bandwidth	DC to 15 MHz (−3 dB)
Input attenuation ratio	Between 1/10, 1/100
Maximum allowed differential voltage	±500V (DC + AC_{peak}) or 350 Vrms (1/100)
Maximum common mode input voltage	±500V (DC + AC_{peak}) or 350 Vrms (1/10, 1/100)

The general schematic diagram of the developed monitoring system is depicted in Figure 3.10. The PCC in the figure denotes the Point of Common Connection which is the point of connection of the monitoring system.

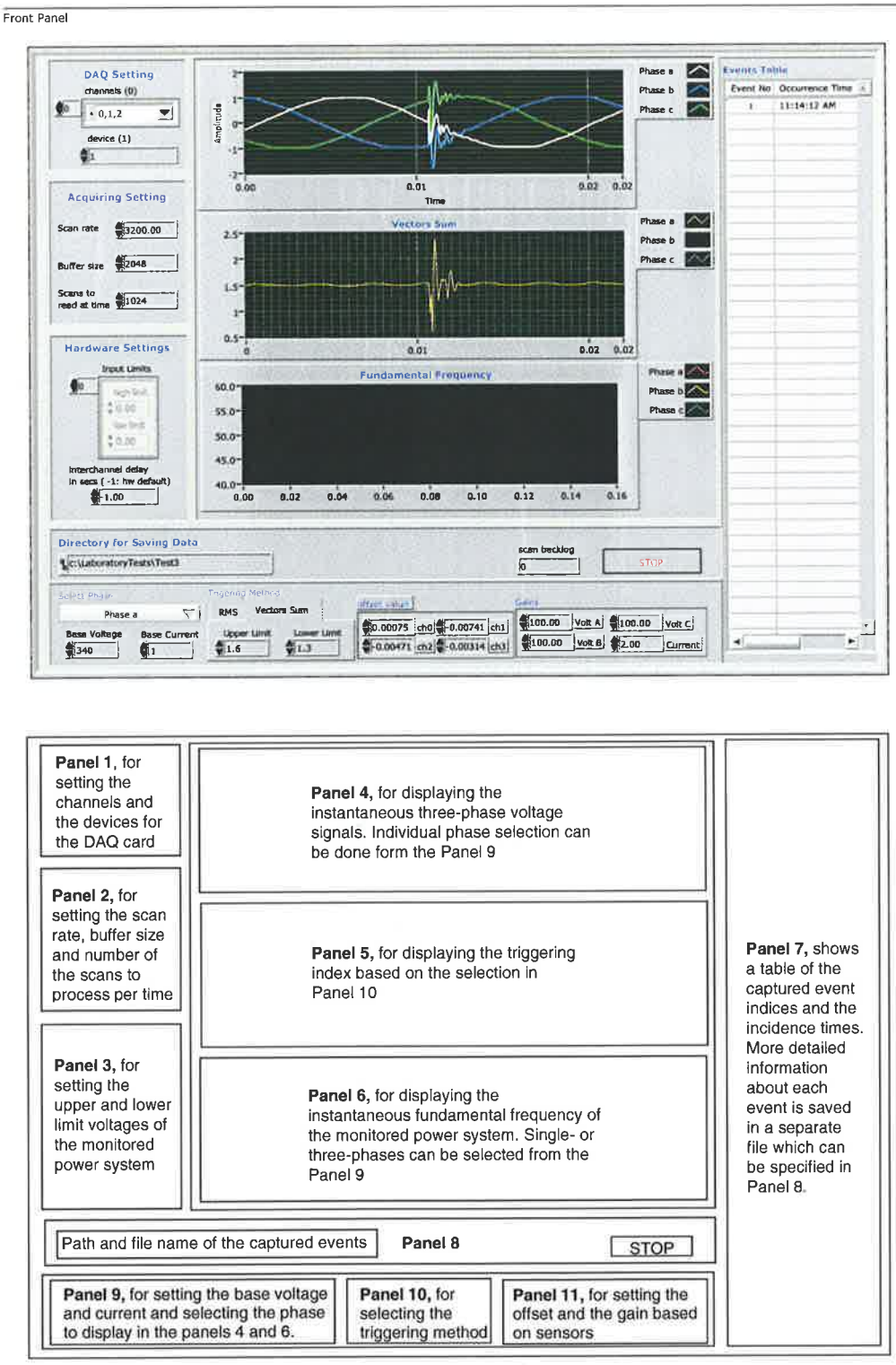

Figure 3.9: Front panel of the monitoring system (top), and an explanation of the function of each the sub-panels (bottom).

Table 3.2: Current sensor specifications

Current range	20A DC / 30A AC
Accuracy	±1% 2mA
Dielectric strength	3.7kV, 50Hz, 1min
Output sensitivity	100mV/A
Frequency range	DC – 100kHz
Resolution	±1mA
Load impedance	> 100kΩ

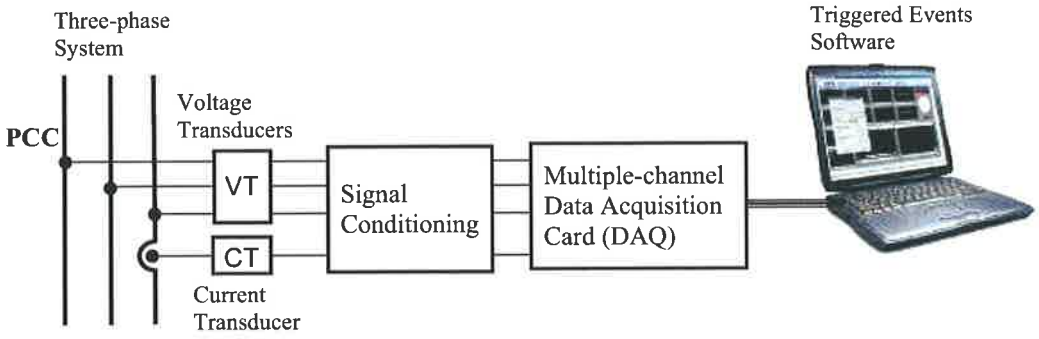

Figure 3.10: General block diagram of the monitoring system.

As stated earlier, the developed monitoring system has been tested in the laboratory by monitoring a number of power quality signals. In order to generate various disturbances, different power system configurations have been arranged in the laboratory as shown in Figure 3.11. In these configurations, a 415 V three-phase power source is connected to different loads, such as resistors, induction motors, capacitors, and transformers, to investigate the effect of switching and resulting power disturbances at the PCC point. It can be noted here that the components in the test setup were chosen to introduce a degree of power quality events at PCC.

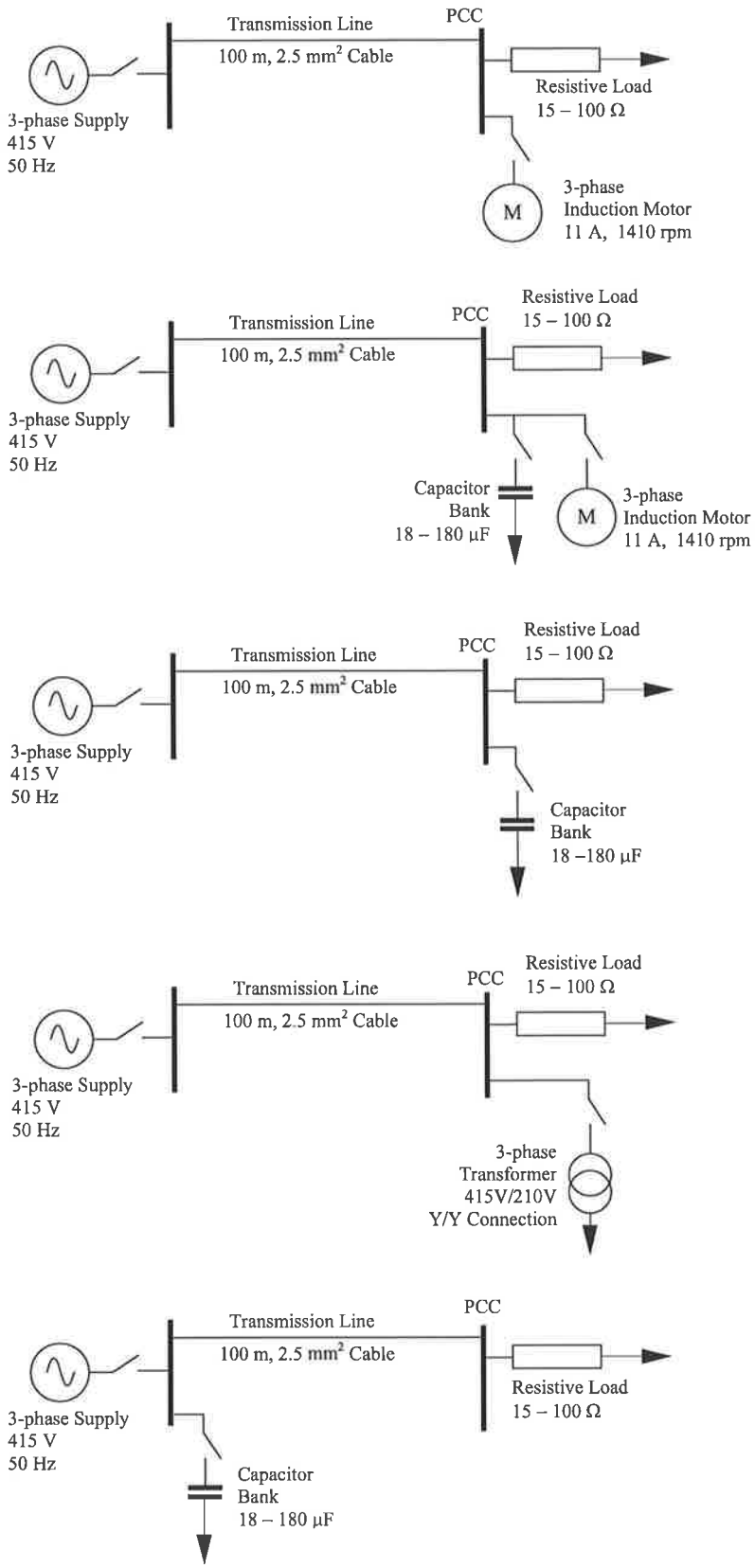

Figure 3.11: Different setup configurations used to experimentally simulate the power quality events.

3.6 Conclusion

In this chapter the performance of two widely used detection techniques in power quality monitoring systems (the root mean square and the peak values of signals) on different power quality events was discussed. It was shown that, because power quality disturbances can affect the voltage signals in power systems in different ways, the existing detection strategies are not suitable for monitoring all power quality events. Therefore, in this study, an alternative detection technique is proposed based on monitoring all three phase voltage simultaneously. This was shown to have high sensitivity to both short and long duration events. The main advantage of the proposed technique is its ability to monitor three phase systems and detect a wide range of power quality events.

In order to test the proposed detection mechanism, a power quality monitoring system has been developed for capturing real time power quality signals. The monitoring system have been tested in the laboratory and in a real power system for capturing power quality signals.

Chapter 4

Feature Extraction Techniques

4.1 Introduction

GENERALLY, feature extraction can be defined as a unique process that transforms the raw signals from its original form to a new form so that suitable information can be extracted. The feature extraction step is crucial in an automatic classification system. This is because a classifier can only operate reliably if the features of each event are selected properly.

Therefore, to be able to distinguish and classify the different types of disturbances in power systems, it is necessary to perform further processing on the original waveforms. However, due to the large number of events and disturbances that may be present in modern AC power systems, it is important to study the unique features of each event and determine the effectiveness of a selected technique in extracting the unique features. This chapter aims to address these issues and provides comprehensive discussions about the features extraction techniques considered.

In the following sections of the chapter, the application of various signal-processing techniques on real-time power quality waveforms were investigated and their performances in extracting the features of power quality signals were studied visually. In each technique, the effect of different parameters on the performance of the technique were also investigated. The feature extraction techniques considered in this research are:

- The Short Time Fourier Transform
- The Wavelet Transform Technique
- The S-Transform Technique
- The Hilbert Transform Technique
- The Clarke Transform Technique

The performance of the above techniques will be presented using a number of experimental power quality waveforms obtained using the setup described in the pervious chapter. In addition, a set of test power quality waveforms which are available at [70] will also be utilized in the tests. All the analysis have been done in MATLAB® environment.

4.2 Short-Time Fourier Transform

The Short-Time Fourier transform (STFT) has been implemented in power quality analysis due to its applicability to analyze the non-stationary signals, as it is the case of most power quality signals [25]. The main advantage of the STFT technique is its ability to provide the harmonic content of a given signal at every time period that is specified by a pre-defined window. Therefore, since the frequency contents of the analyzed power quality signals usually vary in only short period of time, it is useful to utilize the time-frequency information.

4.2.1 Theoretical Background of the STFT

The STFT of a time varying signal, $v(t)$, is obtained by multiplying the signal with a window function, $w(t-\tau)$ localized around the delay parameter, τ, as shown in Figure 4.1, and then taking the Fourier Transform of the product as follows:

$$V(\omega,t) = \int_{-\infty}^{+\infty} v(t) \cdot w(t-\tau) \cdot e^{-j\omega t} dt \tag{4.2.1}$$

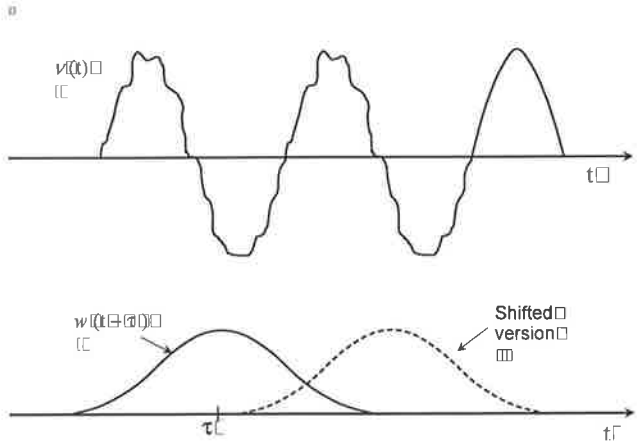

Figure 4.1: A time varying signal $v(t)$, (top) and the sliding window function $w(t-\tau)$, (bottom).

where,

$V(\omega, t)$ is the STFT of $v(t)$, and $\omega = 2\pi f$, where f is the frequency of the signal.

In practical applications, where the analyzed signal is in a discrete form $v[k]$, (where $k = 1, \ldots N$, and N is the total number of samples of the signal), the STFT of the discrete signals can be given by [19]:

$$V[n\omega_s, kT_s] = \sum_{k=1}^{N} v[k] \cdot w[k - kT_s] \cdot e^{-jn\omega_s k} \tag{4.2.2}$$

where,

$\omega_s = 2\pi n f / f_s$,

f_s is sampling frequency,

T_s is the time between colliquative samples, and

k and $n = 1, \ldots N$.

Equation (4.2.2), therefore, is used to transfer the one-dimension signal, $v[k]$, into two-dimensions signal, $V[n\omega_s, kT_s]$, which reserves the time and frequency information by multiplying $v[k]$ by a window function and taking the Fourier transform of the results. By shifting the window function along the the signal, $v[k]$, and repeating the above process, further time-frequency information is obtained. The whole process is repeated for the entire length of $v[k]$.

4.2.2 Experimental Results of the STFT

The STFT has been investigated using two categories of power quality events according to the IEEE standard [59], transients and short duration events (Table 2.1). The signals selected to study the above events using the STFT include a capacitor switching event (Figure 4.2 bottom) and voltage sag due to induction motor starting event (Figure 4.2 top). As stated previously, the test signals were captured using the test setup arrangements shown in Figure (3.11) at sampling rates of 16.4 kHz for the transient event, and 6.4 kHz for the short duration event. The results of the tests using the captured signals are given in Figures 4.3 and 4.4.

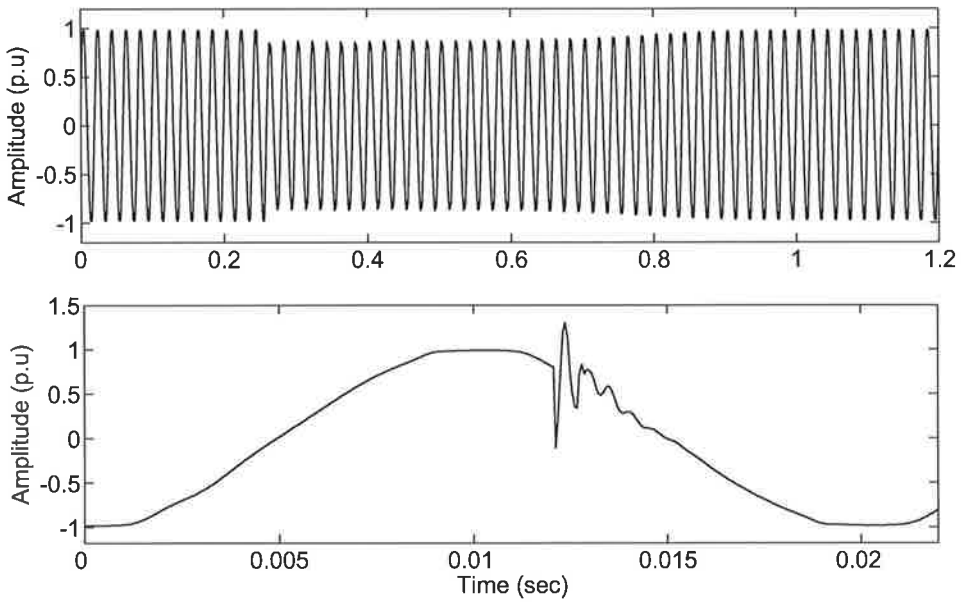

Figure 4.2: Voltage waveforms of the events studied: Short duration event due to an induction motor starting (top), and Transient event due to a capacitor switching (bottom).

The effect of the window function length of the STFT (the Hanning window) is investigated for the two categories studied. The results are presented in Figures 4.3 and 4.4. Figure 4.3 shows the STFT of the voltage sag signal using three different window lengths, 5 ms (1/4 cycle), 10 ms (1/2 cycle), and 20 ms (1 cycle). In each plot in the figure, the corresponding spectrogram of the window size is given, which also include the original signal at the bottom of the corresponding tests.

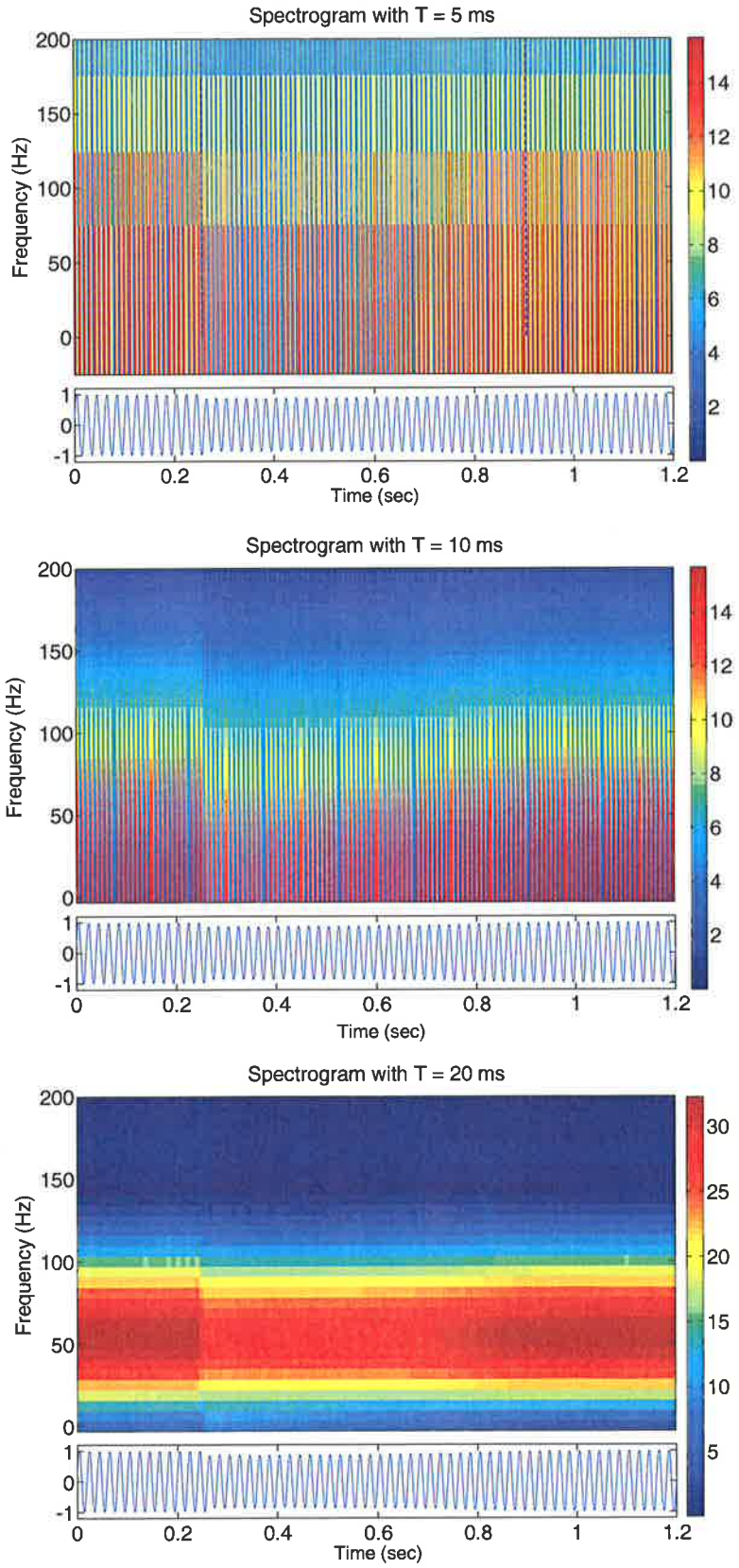

Figure 4.3: The STFT of a voltage sag event using different lengths of Hanning windows: 5 ms (top), 10 ms (middle), and 20 ms (bottom).

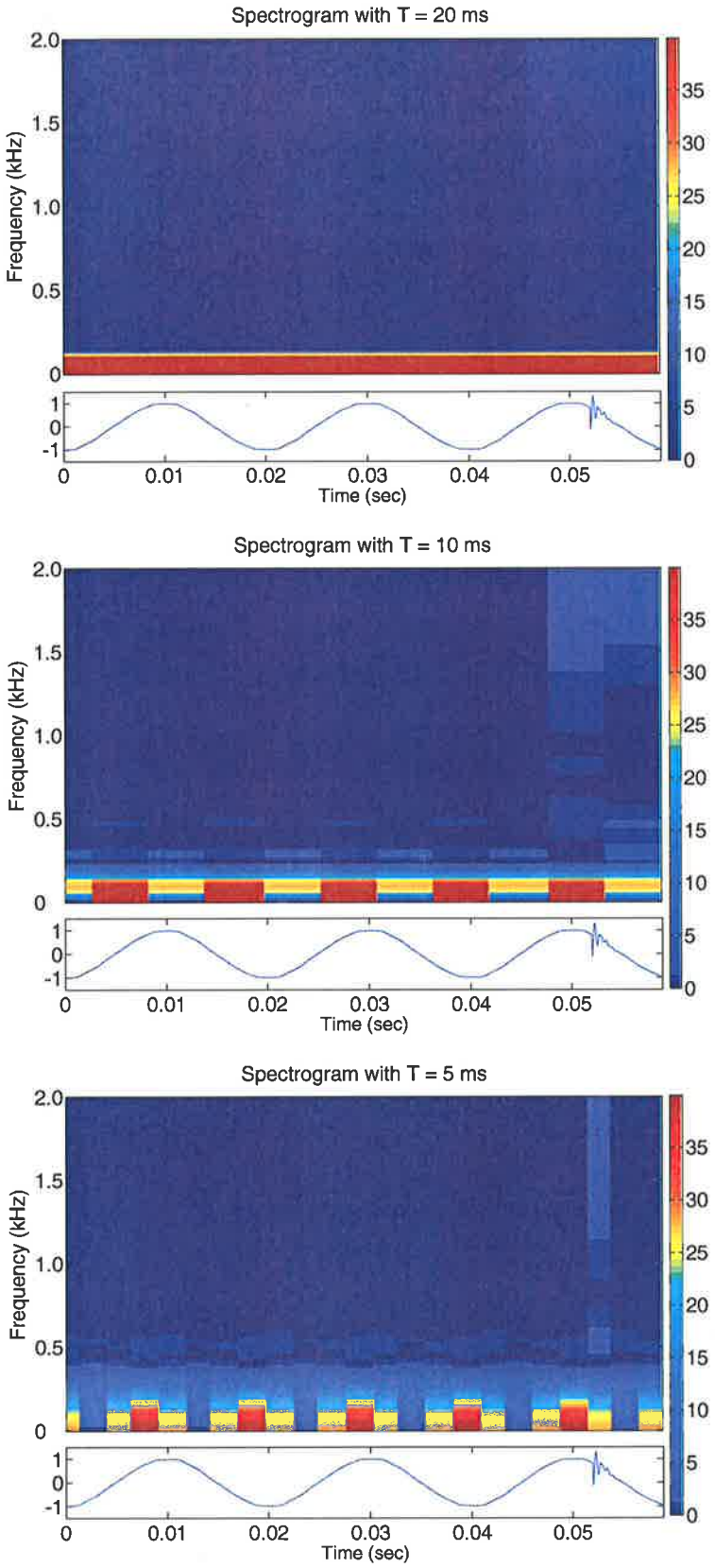

Figure 4.4: The STFT of a capacitor switching transient event using different lengths of Hanning windows: 5 ms (top), 10 ms (middle), and 20 ms (bottom).

These results clearly reveals that the selection of a small window length is not suitable for a relatively long duration events. Although, the small window length gives a high time resolution (Figure 4.3 top), the fundamental frequency and harmonics overlap. It can be also concluded that the most suitable window length in this case is 1-cycle as shown in Figure 4.3 (bottom), where the values of fundamental and harmonics can be distinguished clearly.

However, when performing the test on the transient event with high frequency components (transient oscillations), the STFT with a 1-cycle window failed in detecting the transient (Figure 4.4 top). It was found that it is required to reduce the window size to a 1/4 cycle to be able to detect the transient in the waveform. As can be seen in Figure 4.4 (bottom), the result reveal that the switching transient has a frequency between 1.0 kHz and 2.0 kHz, which occurred after about 0.05 second. It should be noted here that, the range of the detected frequency is large due to the low frequency resolution in this case.

It can be concluded that the selection of the window length is a trade off between the high time resolution which is better for the short duration events, and the high frequency resolution which is better for the long duration events.

4.3 Wavelet Transform

In power systems applications, the Wavelet Transform (WT) has been first suggested by Ribeiro in 1994 for analyzing harmonic distortion in power systems [66]. Since then, the Wavelet technique has been exploited in many fields in power systems, and in particular, in the area of power quality, as shown in Figure 4.5 [67].

In the previous studies, the WT has been shown to be a powerful signal processing technique in various fields of research. The advantage of the Wavelet transform is its ability to preserve the time and frequency information more efficiently than other methods such as the Fourier transform. Therefore, the main drawback of the fixed window in the STFT is solved in the WT technique which uses a variable length window. This makes the WT more suitable for non-stationary signals.

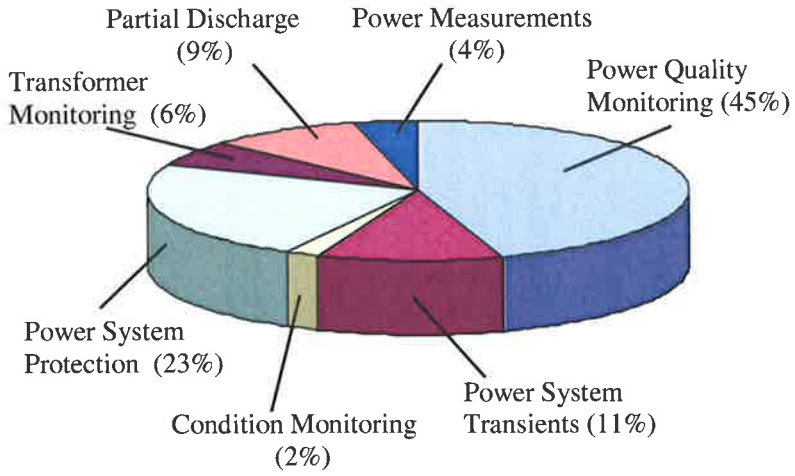

Figure 4.5: Application areas of the Wavelet transform in power systems.

Generally speaking, there are two algorithms of the Wavelet transform: the Continuous Wavelet transform (CWT) and the Discrete Wavelet transform (DWT). In the CWT, the raw signal is transferred from a time domain into a continuous time-scale domain which is similar to the time-frequency domain in the STFT. The scales in the WT correspond to the frequency contents of the signal. However, each scale does not have a fixed relation with each individual frequency in the signal.

The DWT, in the other hand, decomposes the raw signals in terms of a specific number of scales (discrete), providing that sufficient information can be obtained from its analysis. In the following sections, these techniques and their applications will be explained using a set of power quality events.

4.3.1 Continuous Wavelet Transform (CWT)

Unlike the Fourier transform, which expands the signals in terms of trigonometric polynomials (sine and cosine waveforms), the Wavelet transform is based on the decomposition of the signals in terms of small waves (daughter Wavelets) derived from translation (shifting in time) and dilation (scaling) of a fixed Wavelet function called a "Mother Wavelet". This Wavelet family, (the mother and the daughters), represents the bases functions of the Wavelet transform.

The general formula of the Wavelet transform of a signal $v(t)$ is given by:

$$V_{CWT}(a,\tau) = \frac{1}{\sqrt{a}} \int_{-\infty}^{+\infty} v(t) \cdot \psi^*_{a,\tau} \left(\frac{t-\tau}{a} \right) dt \tag{4.3.3}$$

where,

$V_{CWT}(a,\tau)$ is the Continuous Wavelet transform of $v(t)$

$\psi_{a,\tau}$ is the mother Wavelet function (or bases function),

a, and τ are the scaling and the translation respectively, and the asterisk in the equation denotes a complex conjugate of the function.

There are, however, few conditions that must be met for the bases functions to be considered as Wavelets [68]. These conditions are: must be orthogonal, must be oscillatory, and must have amplitudes that quickly decay to zero. It can be noted here that there are a number of functions that can meet such conditions. Some examples of the Mother Wavelets used in this study are illustrated in Figure 4.6.

The main advantage of the CWT is the variable length of its window function, $\psi_{a,\tau}$, which is controlled by the scale parameter, a. That is, the window function at small scales will be more compressed than at large scales. Thus, the window function will have a smaller length at small scales, whereas large scales will stretch the length of the window.

In order to investigate the practical performances of the CWT as compared to the STFT, identical real power quality events those studied in the pervious section have been implemented here. The performance of the CWT on these events is given in Figure. 4.7. In the figure, Daubechies-4, (db4), has been chosen as a Mother Wavelet in the analysis. The choice of db4 Wavelet is based on the analysis that will be discussed later in section 4.3.5.

From these results it was observed that, the drawback of the window length, as mentioned in section 4.2.2, on detecting the disturbances that have different frequency components has been overcome in the CWT technique. This can be seen in Figure 4.7, where both disturbances (with low-frequency and high-frequency components) are detected by this technique. However, the technique does not show a high

sensitivity to the smooth variations in the signals as can be seen in Figure 4.7 (top), as compared to its response to the transient event which is more visible, as shown in Figure 4.7 (bottom). In addition, although in the practical calculation of the CWT the scales are discretised, the larger number of scales used, the more accurate results are achieved. This makes this technique redundant and more difficult to interpret its results for the automatic classifications.

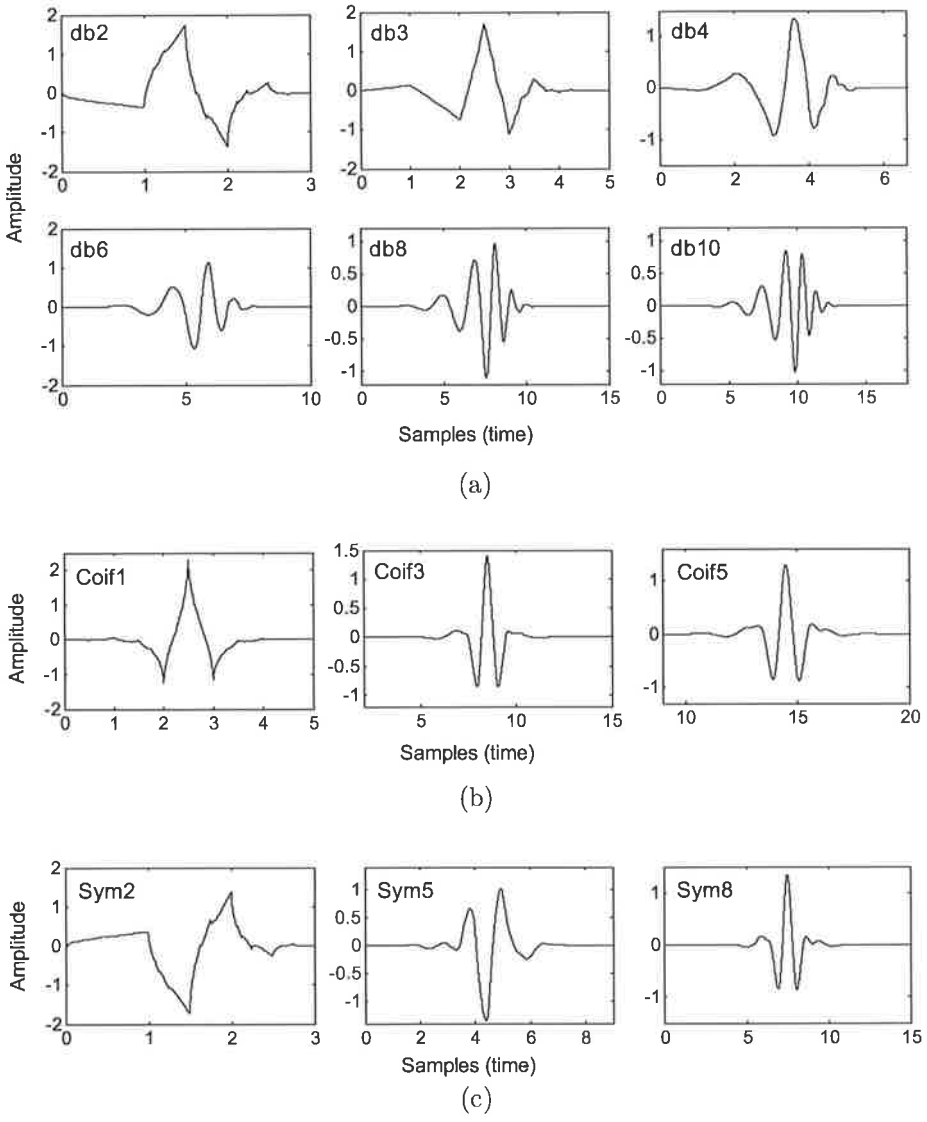

Figure 4.6: Examples of some Mother Wavelets: (a) Daubechies family (b) Coiflets family (c) Symlet family.

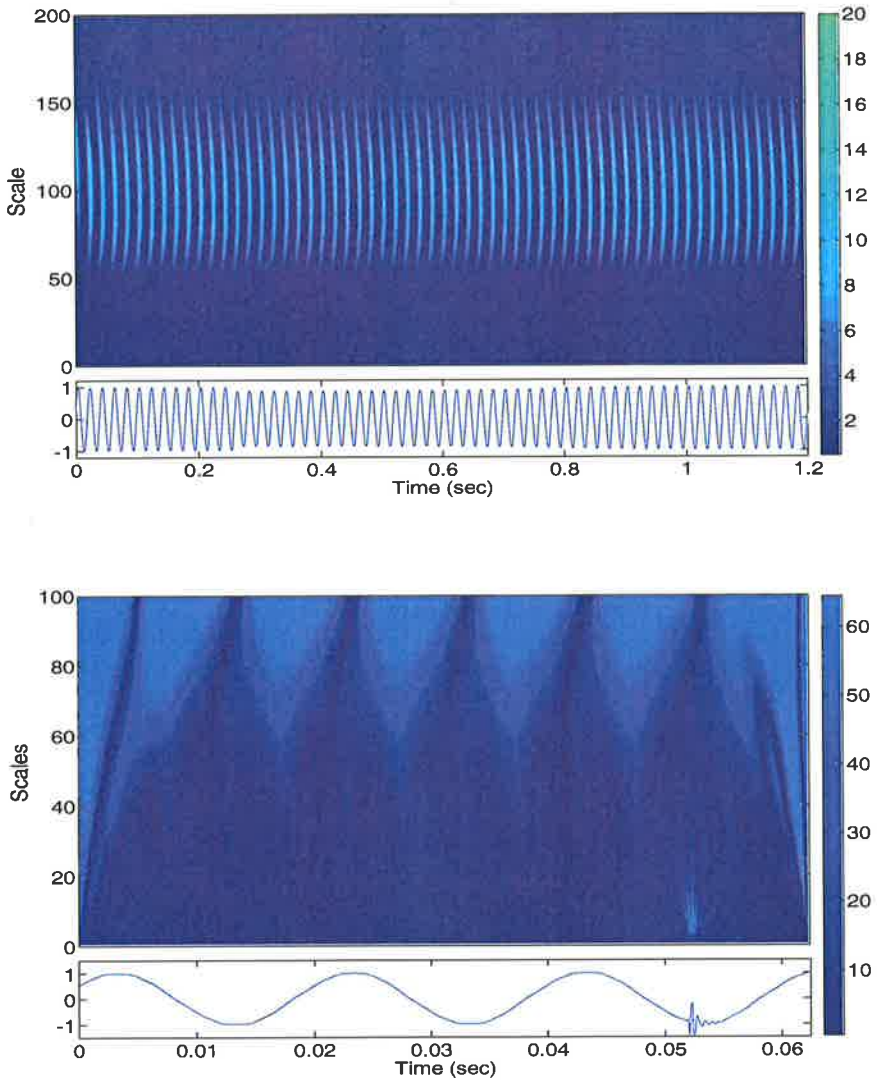

Figure 4.7: The CWT of two events: sag event due to the motor starting (top), and transient event due to capacitor switching (bottom).

4.3.2 Discrete Wavelet Transform (DWT)

Instead of continuously dilation (scaling) and translation the Mother Wavelet function as in the CWT algorithm, which generates substantial redundant information, in the DWT the parameters a and τ in Equation (4.3.3) are discretised as follows [69]:

$$a = a_o^m \tag{4.3.4a}$$

$$\tau = n\ \tau_o\ a_o^m \tag{4.3.4b}$$

where, a_o and τ_o are the sampling intervals and m, and n are integer numbers. Therefore, from Equations (4.3.3) and (4.3.4), the DWT is calculated as:

$$V_{DWT}(m,n) = a_0^{-m/2} \int_{-\infty}^{+\infty} v(t) \cdot \psi(\frac{t - n\tau_o a_o^m}{a_o^m}) \tag{4.3.5}$$

In the above equation, the selection of a_0, and τ_o requires special intention so that the family of the dilated Mother Wavelets constitutes orthonormal bases. The simplest choice of a_0, and τ_o, which fulfill the orthonormality condition is 2 and 1 respectively. Thus, in case of a discrete-time signal $v[k]$, the calculation of the DWT is performed as:

$$V_{DWT}(m,n) = 2^{-m/2} \sum_k v[k] \cdot \psi(2^{-m}k - n) \tag{4.3.6}$$

As it can be observed in this equation, the redundant computations due to the continuous scales can be avoided when only the scales 2^m are used, where m is called the level of the decomposition.

In Equation (4.3.6), the Wavelet coefficients at different decomposition levels are used to reconstruct different versions of the raw signal at different frequency bands (resolutions). This algorithm is named the Wavelet Multiresolution Analysis, which will be explained in the following subsection.

4.3.3 Wavelet Multiresolution Analysis (MRA)

The MRA algorithm is mainly based on the reconstruction of the analysed signal using the details (high frequencies) and approximation (low frequencies) coefficients of the DWT. However, instead of reconstructing the original raw signal, different versions of the raw signal at different resolution levels can be reconstructed by

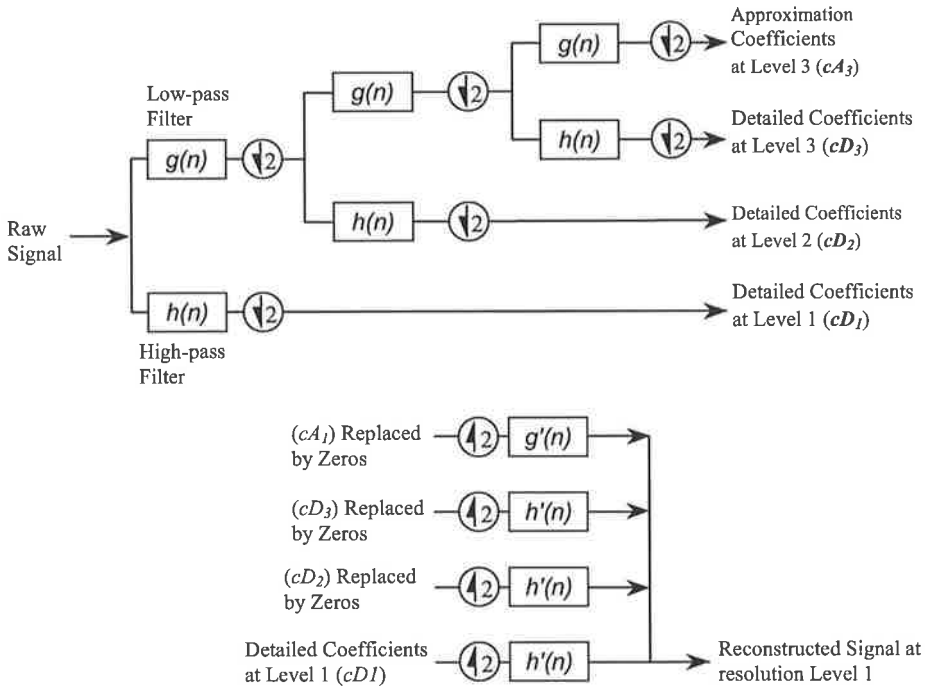

Figure 4.8: Three levels decomposing of signal using MRA (top), and the reconstruction process of the the first detailed version of the signal, (bottom).

considering the coefficients at one decomposition level and setting the remaining coefficients of other levels to zero. This can be explained in Figure 4.8 as follows.

The figure shows the block diagram of the reconstruction process of a version of a raw signal at the first resolution level. As can be seen in the figure, two sets of coefficients (approximation coefficients, cA, and detail coefficients, cD) are generated by convolving the raw signal with a low-pass filter, $g(n)$, and a high-pass filter, $h(n)$, respectively. Then the coefficients are down-sampled by 2 (shown by a downward arrow in a circle). These coefficients are defined by:

$$cD_m = \sum_k h(k-2n)cA_{m-1} \tag{4.3.7a}$$

$$cA_m = \sum_k g(k-2n)cA_{m-1} \tag{4.3.7b}$$

where,
cD_m and cA_m are the detail and the approximation Wavelet coefficients at the decomposing level m respectively, and h and g are the high- and low- pass filter coefficients.

As seen in Figure 4.8, if a raw signal contains of N samples of data, then the resultant signals of the low- and high- pass filters will each have N samples, and a total of $2N$ samples. Therefore, the purpose of the down-sampling process is to reduce the number of samples generated from the high- and low- filters. The filtering and down-sampling process can be repeated multiple times. In this process, the successive approximations are decomposed further in order to obtain more detailed versions of the raw signal at higher decomposition levels.

In order to reconstruct a specific version of the raw signal at a specified resolution level, a reverse process can be performed by using Inverse Wavelet Transform. In this process, as shown in Figure 4.8 (bottom), all the coefficients are up-sampled and replaced by zeros except the coefficient vector at the required level. As stated above, the purpose of the up-sampling process is to restore back the original number of samples. Generally, this process can be defined as:

$$cA_m = \sum_k cA_{m+1}h(n-2k) + cD_{m+1}g(n-2k) \tag{4.3.8}$$

Thus, if a raw signal is sampled at a sampling rate of f_s, which means the maximum frequency in the signal will be $f_s/2$ (Nyquist criterion), then at the first level of decomposition process, the raw signal can be expressed in terms of pair of signals having low frequency band ranged from $(0 \backsim f_s/4)$ and high frequency band of $(f_s/4 \backsim f_s/2)$. The former decomposed signal, with the low frequency components, can be further processed in order to narrow the frequency bands in the decomposed signals. However, in this process, the decomposed signals with the high frequency components are always not further processed.

4.3.4 Wavelet Packet Transform (WPT)

As illustrated in Figure 4.8, the decomposed signals in the MRA algorithm will always have unequal frequency bands. This is because the reconstructed signals from the detail coefficients are not decomposed further, while the approximations are. However, in the WPT technique, which is in fact a generalization of the Wavelet MRA, the details and the approximations both are decomposed further as shown in Figure 4.9. The advantage of this technique is that the decomposed signals that utilized the raw signals have a narrower and equal frequency bands.

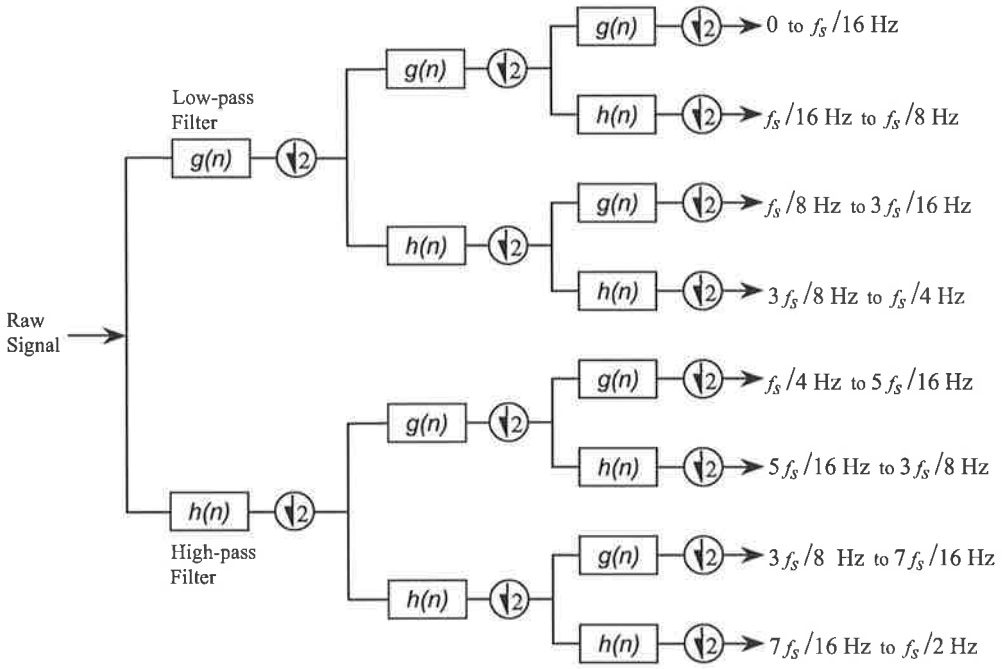

Figure 4.9: Three levels decomposing of a raw signal using WPT technique.

4.3.5 Appropriate Choice of Mother Wavelet for Power Quality Analysis

As described previously, the Wavelet transformation process is based on window functions having specific characteristics, known as "Mother Wavelets". Therefore, to

analyse a signal with Wavelet technique, different Mother Wavelets may be selected. Some examples of typical Mother Wavelets were illustrated in Figure 4.6. It can be noted here that, in power quality analysis, the selection of a Mother Wavelet has different impacts on the detection and analysis of the power quality events.

For example, the results given in Figure 4.10 show the effects of two different Mother Wavelets, (Daubechies- 2 and 6), as they are applied to a real voltage sag signal that is obtained from the test waveforms available at [70].

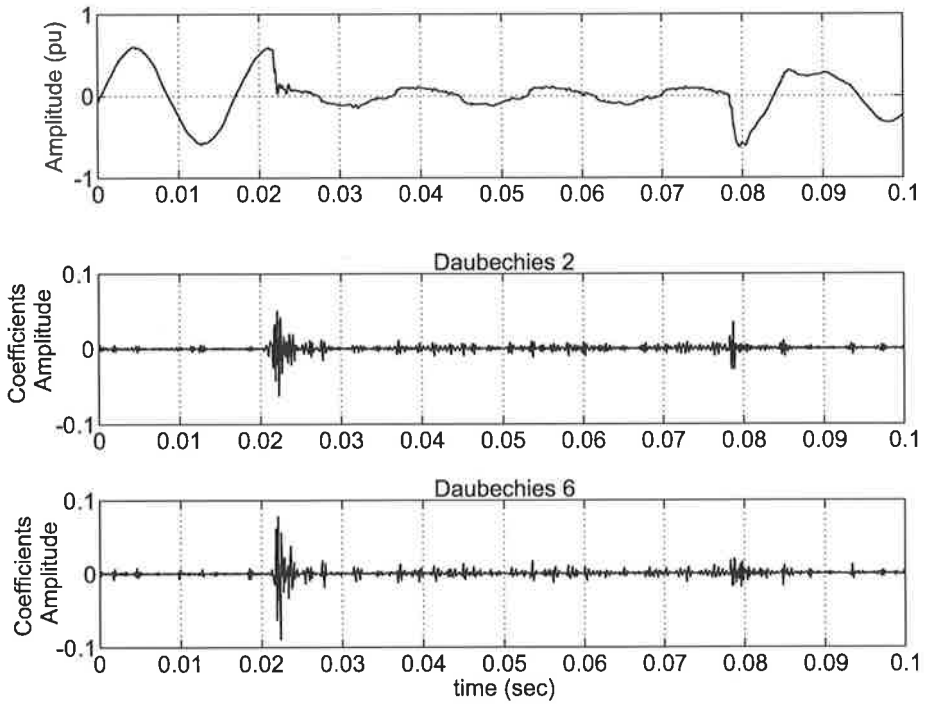

Figure 4.10: The Wavelet MRA of voltage sag using two different Mother Wavelets.

The Figure shows the detailed versions signals of the analysed signal at the second decomposition level using Wavelet MRA with both Daubechies-2 (middle) and Daubechies-6 (bottom) as Mother Wavelets. One can see from the results that there is a clear visual differences between the two Mother Wavelets. Specifically, the detailed version when using Daubechies-6 has a more obvious detection of the

starting of the sag event, while the end of the event is more obvious when using Daubechies-2 as a Mother Wavelet.

Therefore, it is important to investigate the proper choice of the Mother Wavelets in order to study the performance of the Wavelet technique more accurately in power quality signals analysis. In this thesis, the following Wavelet families have been used to compare their performance.

- **Daubechies** with 2, 4, 6, 8, 10, 12 and 40 vanishing moments.
- **Coiflet** with 1 and 5 vanishing moments.
- **Symlet** with 2 and 8 vanishing moments.

4.3.5.1 Comparison Criterion for Mother Wavelets Selection

To be able to compare the above Wavelet families, it is necessary to interpret the results of Wavelet transforms accurately by using a measurable index which can be used for the comparison. This is important since the visual inspection does not give a precise comparison index. Therefore, for the comparison purposes, the energies of the reconstructed signals from the Wavelet coefficients at different levels have been calculated and compared for each Mother Wavelets.

The idea of calculating the energies of the decomposed signals is based on Parseval's theorem, which states that the energy of a signal is equal to the energies of their transformation coefficients. Therefore, the energy of a distorted signal (E_{signal}) can be partitioned mathematically in term of the Wavelet expansion coefficients as follows:

$$E_{signal} = \sum_{k} |u[k]|^2 + \sum_{m} \sum_{k} |w_m[k]|^2 \tag{4.3.9}$$

where $u[k]$ and $w_m[k]$ are the approximated and detailed versions of the original signal at level m respectively.

The above approach has been chosen for comparison purpose, because the energies values of the reconstructed signals from the Wavelet coefficients are sensitive to

any changes in the original signal, as reported in [3]. This is demonstrated in Figure 4.11 for two different disturbances (sag and swell events) and the energies values of their decomposed signals at 10 decomposition levels. As shown in the figure, it is clear that how the energies values are affected by the type of the disturbances.

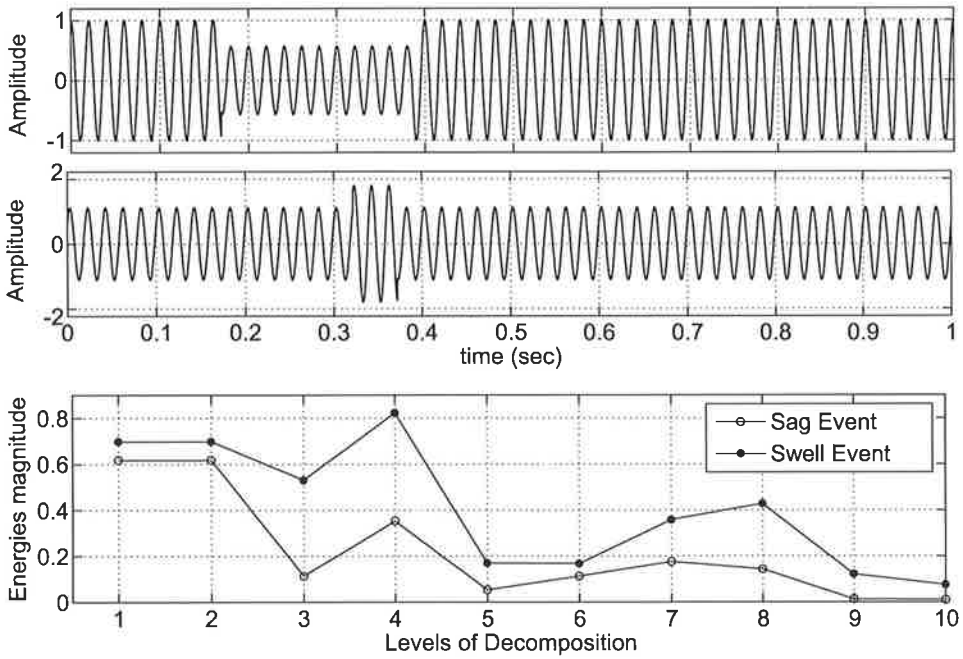

Figure 4.11: Energy values of decomposed signals from the sag and swell events at 10 decomposition levels.

However, in this research two modifications were introduced to improve the method described in [3], as follows.

1. In [3], the energies of the decomposed signals from a fixed pure sine-wave (with zero phase-shift) were used as references for all the other disturbed signals. However, it was found in this study that the phase shift of the reference signal have a significant effect on the results as demonstrated in Figure 4.12. In the figure, the magnitudes of the decomposed signals energies of two pure signals, having different phase shifts, are plotted at 10 decomposition levels. It can be concluded from the figure that the energies of the decomposed signals at

levels 9 and 10 are clearly affected by the phase shift of the reference signal. Therefore, in this study a proposed method in which the energies of each distorted signal are compared with a reference signal that should be *in-phase* with the disturbance.

2. In [3], the decomposition of the signals was based on the Wavelet MRA, where the reconstructed signals have different frequency bands. However, in this study, the WPT has been used instead of the Wavelet MRA, where the reconstructed all output signals will all have the same and narrower frequency bands as stated in section 4.3.4.

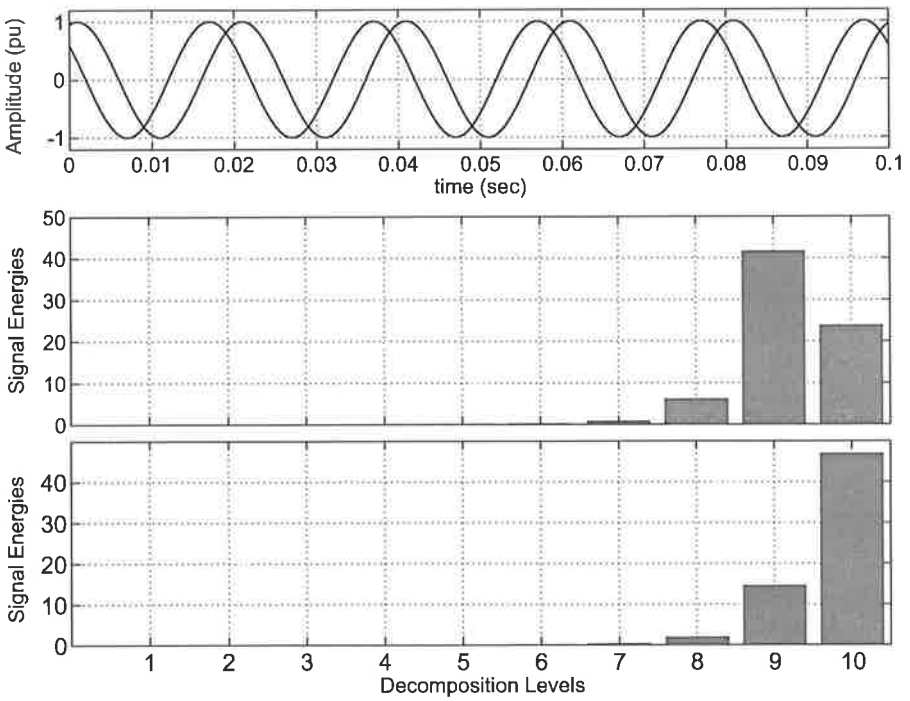

Figure 4.12: The effect of the phase shift on the energies of the decomposed signals.

Therefore, the comparison criterion used in this study is based on Mother Wavelet that give a clear difference between the energies of a distorted signal and in-phase of a pure signal at different decomposition levels using the WPT technique.

4.3.5.2 The Tested Waveforms

Four test signals belong to different power quality classes have been chosen to investigate the performance of different Mother Wavelets on different classes of real power quality events. In this section, two of the tested classes are obtained from [59], and two remaining events were generated in the laboratory using the set-up explained in Chapter 3.

The first class of test signal represents a sag (dip) and is shown in Figure 4.13 (top) together with its simulated in-phase reference signal, which named as Signal A. The second class of test signal is shown in Figure 4.13 (bottom) which represents a harmonic distortion event together with its in phase reference. This signal is referred as Signal B. The sampling rate of the both signals are 15.36 kHz.

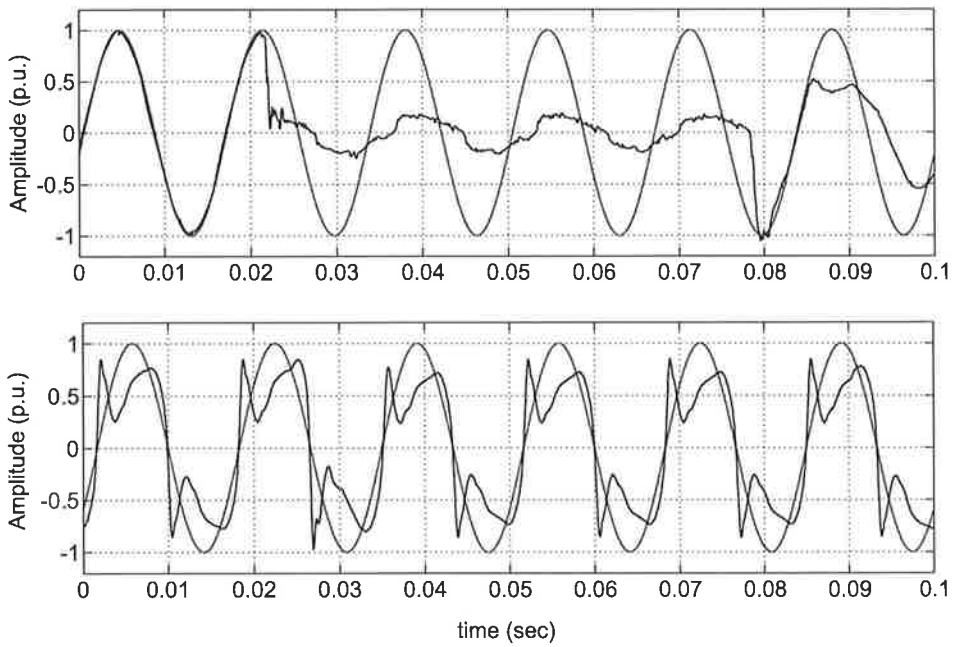

Figure 4.13: The test waveforms together with corresponding in phase references: Top, Signal A (sag), Bottom, Signal B (harmonics).

The third tested event represent a motor starting event as shown in Figure 4.14 (top). The depth of the sag was about 20% of the signal amplitude, and it lasted

for about 0.6 second. This signal was captured at a 6.4 kHz sampling rate, and the signal is labelled as Signal C.

A capacitor switching transient was also tested. Since the superimposed frequency in this event is expected to be high, the sampling frequency in this test was increased to 16.4 kHz. This signal is labelled as Signal D and given in Figure 4.14 (bottom).

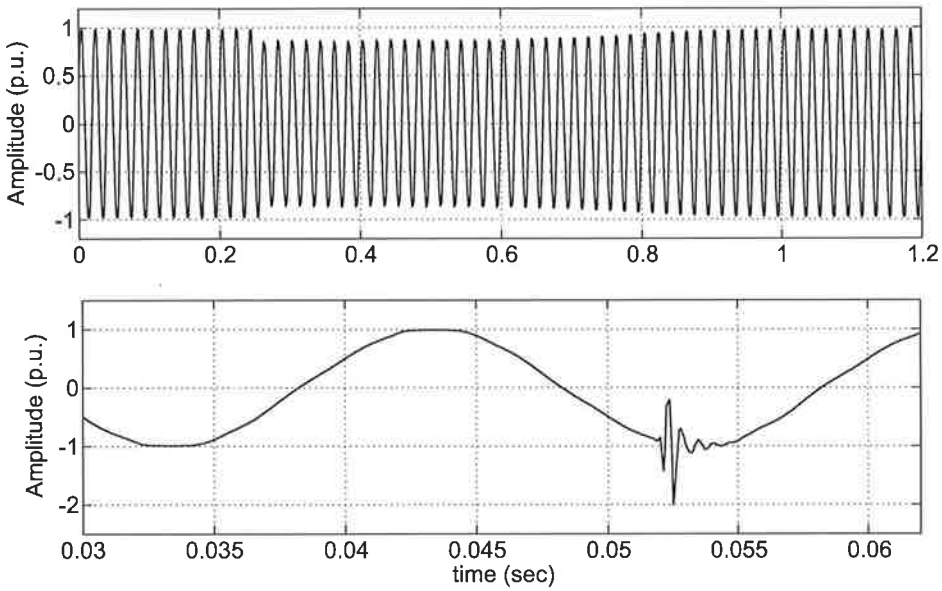

Figure 4.14: The test waveforms: Top, Signal C (motor starting), Bottom, Signal D (capacitor switching)

4.3.5.3 Comparison of the test results

To analyse the test resuslts, the test signals and their relative references signals were decomposed into 5 levels using the WPT. Therefore, as explained previously, the studied signals were split into 32 frequency bands. The frequency range of these bands are depending on the sampling frequency of the signals, which is given by:

$$\text{Frequency Range of Decomposed signals} = \frac{f_s}{2^{m+1}} \tag{4.3.10}$$

where, f_s is the sampling frequency and m is the level of decomposition.

From the above equation, it can be noted that for Signals A, and B, each decomposed signal at the fifth level has a 240 Hz range, while for Signals C and D it is a 100 Hz range and 256 Hz range respectively.

The reconstructed signals at the first five bands resulted from the decomposition of studied signals using Daubechies-4 (db4) as a Mother Wavelet are shown in Figures 4.15 and 4.16.

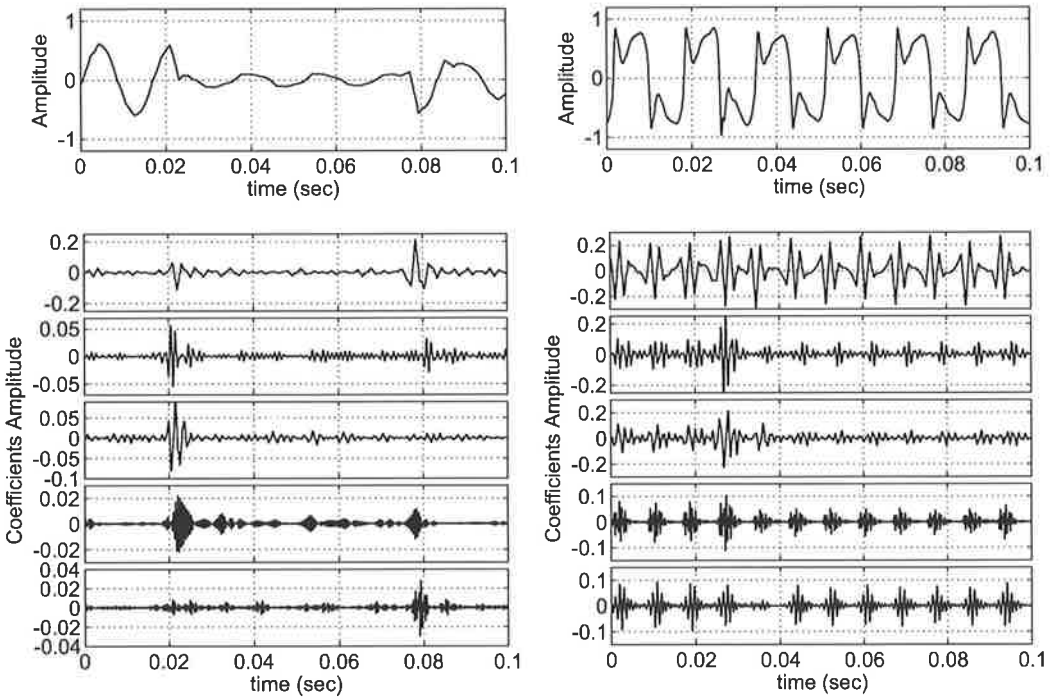

Figure 4.15: The first five bands of the reconstructed signals from Signal A (left column), and Signal B (right column), using WPT technique.

As explained in section 2.3.5.1, for each Mother Wavelets studied, the energies of the 32 decomposed signals from the test signals were calculated and compared with the energies of the decomposed signals from their relative pure reference signals. The percentage of the differences between the calculated energies at each decomposition levels have been used as an indicator on how the Mother Wavelets can distinguish between the pure and the distorted signals. The energies values of the reconstructed

signals are given in Figures 4.17 to 4.20 for each of the test signals using three types of Mother Wavelets. The complete calculation tables of all the studied Wavelets are presented in Appendix A. It should be noted here that the high values of the percentage ratio of the energy at bands 17 and higher are attributed to the small values of energy contribution of the pure signals (reference signals) at the subject bands compared to the contribution of the distorted signals. In addition, it can be noted that, although the calculation of the average energy over all the bands may give a general overview of energy of signal, the energy contribution of each band will be lost.

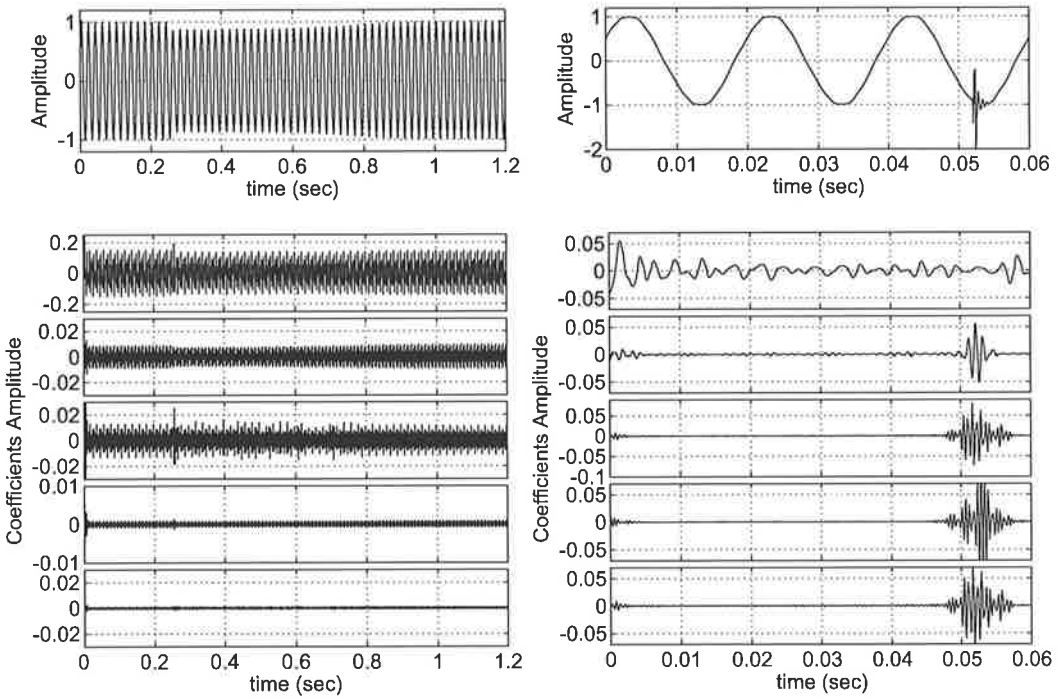

Figure 4.16: The first five bands of the reconstructed signals from Signal C (left column), and Signal D (right column), using WPT technique.

The results in Figures 4.17 to 4.20 in conjunction with the information provided in Appendix A reveal that, different types of Mother Wavelets response differently at different levels of the decompositions. However, some Mother Wavelets have much clear respond at more decomposition levels than others.

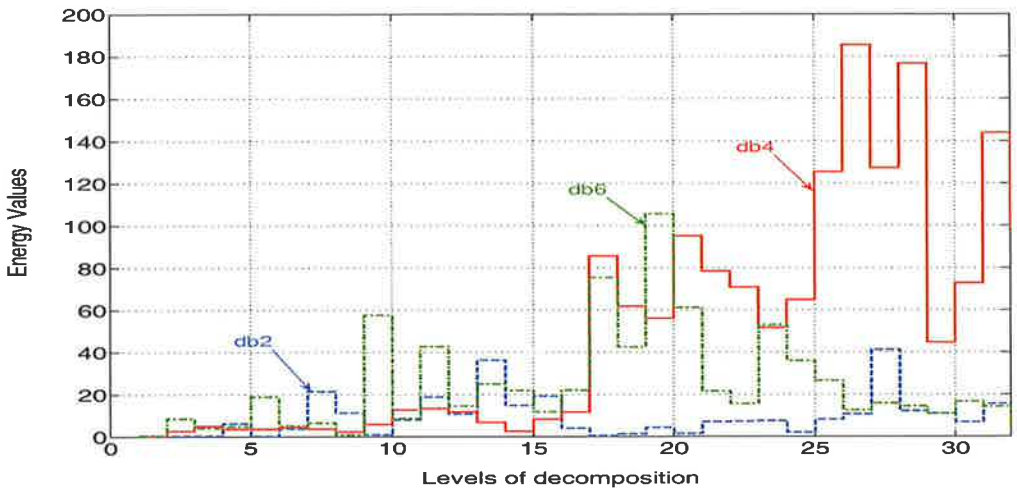

Figure 4.17: Energy values of 32 reconstructed signals form Signal A using WPT with db2, db4, and db6 as a Mother Wavelets.

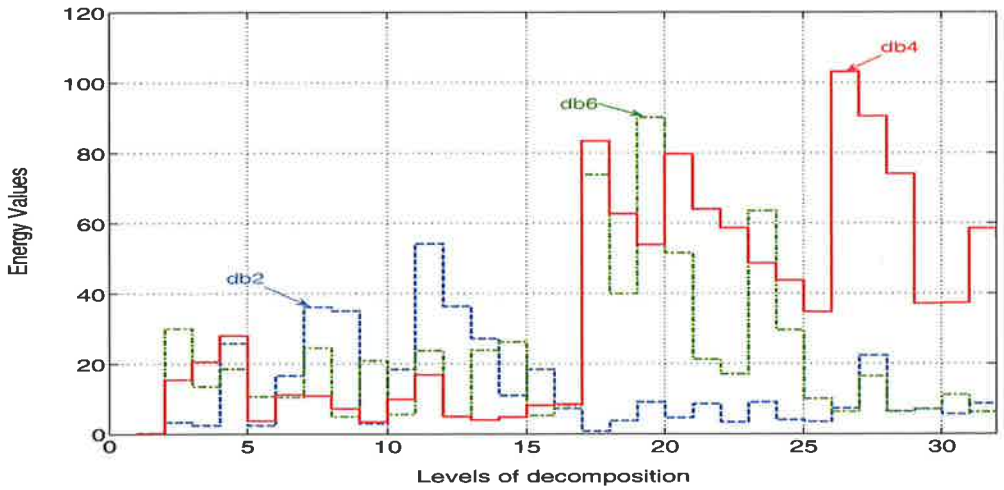

Figure 4.18: Energy values of 32 reconstructed signals form Signal B using WPT with db2, db4, and db6 as a Mother Wavelets.

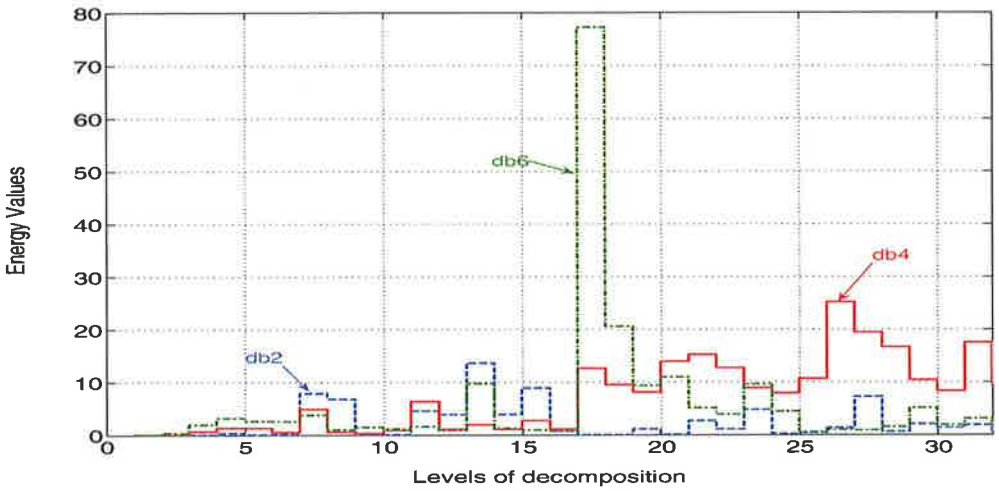

Figure 4.19: Energy values of 32 reconstructed signals form Signal C using WPT with db2, db4, and db6 as a Mother Wavelets.

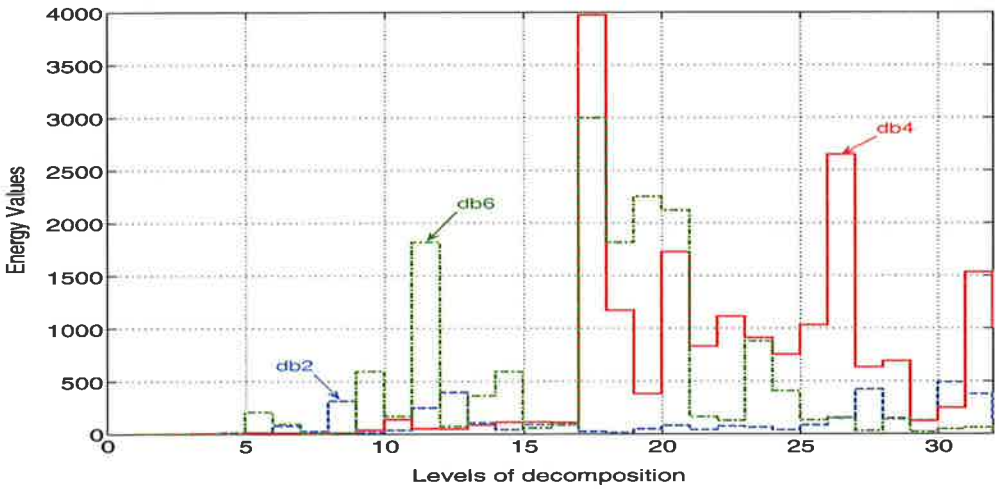

Figure 4.20: Energy values of 32 reconstructed signals form Signal D using WPT with db2, db4, and db6 as a Mother Wavelets.

The summary of the Mother Wavelets that have generated the maximum percentage ratio at different bands is given in Table 4.1. It can be concluded from the table that Daubechies family, in general, has the most clear detection of changes in the energy of the distorted signals over the majority of the decomposition bands. However, Coiflet and Symlet families were identified as the least suitable Mother Wavelets for the power quality analysis. In addition, among the Daubechies family, the db4 Wavelet has generated the maximum energy ratio in the most number of bands, hence, it can be considered the most appropriate Mother Wavelet in the power quality analysis.

Table 4.1: The summary of the Mother Wavelets that generated the maximum percentage ratio at different bands

Mother Wavelets Type	Number of maximum percentage ratio bands between the distorted and the pure signals			
	Signal A	Signal B	Signal C	Signal D
db2	4	7	3	6
db4	9	10	11	6
db6	6	4	6	4
db8	4	3	5	9
db10	3	4	3	2
db12	0	1	0	1
db40	2	0	1	0
Coif1	2	2	0	0
Coif5	2	1	3	2
Sym2	0	0	0	0
Sym8	0	0	0	2

4.4 The S-Transform

The S-transform (ST) technique is introduced by Stockwell, [71] as an alternative to the STFT technique for time-frequency spectral localization. This technique can be considered conceptually as a hybrid of the STFT and CWT techniques where it provides time and frequency information similar to the STFT but at different resolutions using variable window length as in the CWT [72].

4.4.1 Theoretical Background of ST

The ST technique is derived from the CWT by modifying phase of the Mother Wavelet function in the CWT. Therefore, for a time series, $v(t)$, the ST is calculated by multiplying Equation (4.3.3) and a phase correction function, $\mathbf{exp}(j2\pi f\tau)$ as follows [71]:

$$V_{ST}(\tau, a, f) = \int_{-\infty}^{+\infty} v(t) \cdot \psi\left(t - \tau, a\right) \cdot e^{j2\pi f\tau} \cdot dt \tag{4.4.11}$$

where,

V_{ST} is the ST of $v(t)$,

ψ is the Mother Wavelet function,

j is $\sqrt{-1}$, and

f is frequency.

Unlike the WT technique, the Mother Wavelet (the window function) for this transform is chosen to be a function of the frequency contents in the signal instead of the scale a. This is given below:

$$\psi(t, \sigma, f) = \frac{1}{\sigma\sqrt{2\pi}}\, e^{-t^2/2\sigma^2} \cdot e^{-j2\pi ft} \tag{4.4.12}$$

where σ controls the length of window function, and it is chosen to be proportional to the inverse of the frequency in the signal.

The plot of this Wavelet function, ψ, at three different frequencies is shown in Figure 4.21. This function does not satisfy the conditions of the Mother Wavelets in

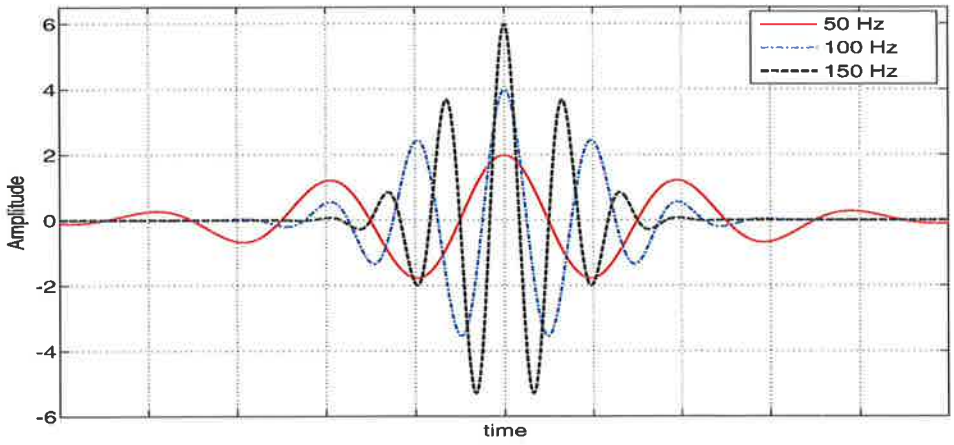

Figure 4.21: Gaussian window function for ST at three different frequencies.

the WT technique, which makes this transform different than the CWT technique. Thus, if Equations (4.4.12) is substituted in Equation (4.4.11), the ST of $v(t)$ can be given as:

$$V_{ST}(\tau, \sigma, f) = \int_{-\infty}^{+\infty} v(t) \cdot \frac{1}{\sigma\sqrt{2\pi}} e^{-(t-\tau)^2/2\sigma} \cdot e^{-j2\pi f(t-\tau)} \cdot e^{j2\pi f\tau} \cdot dt \qquad (4.4.13)$$

Then, the above equation can be simplified as:

$$V_{ST}(\tau, \sigma, f) = \int_{-\infty}^{+\infty} v(t) \cdot \frac{1}{\sigma\sqrt{2\pi}} e^{-(t-\tau)^2/2\sigma} \cdot e^{-j2\pi ft} \cdot dt \qquad (4.4.14)$$

The σ function in the above equation is proportional to the inverse of the frequency contents of the signal, f, and is defined as:

$$\sigma(f) = \frac{1}{c + b|f|} \qquad (4.4.15)$$

where, b and c are constants, and $b \neq 0$. Note that, setting b to zero, transforms the window function as that used in the STFT technique.

For simplicity, c is set to zero. Thus, the ST is rewritten as:

$$V_{ST}(\tau, f) = \int_{-\infty}^{+\infty} v(t) \cdot \frac{|f|}{b\sqrt{2\pi}} \, e^{-(t-\tau)^2 f^2/2b^2} \cdot e^{-j2\pi ft} \cdot dt \tag{4.4.16}$$

The above equation represents a convolution of the time series signal, $v(t)$, with a frequency dependant window function, $|f|/\big(b\sqrt{2\pi}\big) \cdot \mathbf{exp}\big(-t^2 f^2/2\big)$, (which is a Gaussian window function). Therefore, as the convolution in the time domain is a multiplication in the frequency domain, the ST can be calculated by multiplying the Fourier transform of the analyzed signal $v(t)$ by the Fourier transform of the window function.

The Fourier transform of the Gaussian function is calculated as:

$$G(f) = e^{-2\pi^2\alpha^2/f^2} \tag{4.4.17}$$

where α is a constant equal to $1/b$ in Equation (4.4.15).

It can be seen Equation (4.4.16) that, due to the term $(\mathbf{exp}(-j2\pi ft))$, the ST of a signal, $V_{ST}(\tau, f)$, is a complex transform. Therefore, this equation can be written as:

$$V_{ST}(\tau, f) = A(\tau, f) \; e^{-j\varphi(\tau, f)} \tag{4.4.18}$$

where, $A(\tau, f)$, is the amplitude of the ST-spectrum, and $\varphi(\tau, f)$ is its phase angle.

In the discrete form, the ST is calculated as:

$$V_{ST}[kT, \frac{n}{N}] = \sum_{m=0}^{N-1} V\left[\frac{m+n}{N}\right] \cdot \mathbf{exp}\left(-\frac{2\pi^2 m^2 \alpha^2}{n^2}\right) \cdot \mathbf{exp}\left(j\frac{2\pi m}{N}k\right) \tag{4.4.19}$$

where,

V is the Fourier transform of the discrete time signal $v[kT]$,

T is the time between two consecutive samples of the signal,

k, m, and n are equal to $0, 1, 2, \ldots N-1$, and

N is the total number of samples in the signal.

4.4.2 Experimental Results of ST

In this section, the performance of the ST with real power quality events are tested using the signals shown in Figure 4.2. In the tests, the variation of the factor, α, was also considered. This allowed to study the effects of the factor α on the Fourier transform of the window function. The results given in Figures 4.22 and 4.23 are for three values of α: 0.1, 1.0, and 3.0.

In Figure 4.22, the ST of the motor starting voltage sag is presented in a 3-D plot. One can see from the plots in this figure that, the ST can detect both types of disturbances despite the wide range of the frequencies contents covered by these disturbances. The figure also shows that, for the sag events, in the case of α less than 1, the frequency resolution around the 50 Hz component is low, (which can be seen in the the case of $\alpha = 0.1$ in Figure 4.22 (top)). However, a better resolution is achieved for $\alpha = 1.0$ and 3.0 (as shown in Figures 4.22 (middle) and 4.22 (bottom) respectively).

In Figure 4.23, it can be observed for the capacitor switching event, on the other hand, the amplitude of the superimposed transient frequencies are inversely proportional to α. Similarly, setting α less than 1.0 results in additional oscillations in the ST domain, while setting it higher than 1.0 results more attenuations in the amplitude of the transient frequency. Therefore, it is suggested that the value of α for power quality analysis should be 1.0.

However, it can be emphasised here that, although the ST can identify the events clearly, it suffers from a relatively long computation time. This is specifically when the incremental step of the frequency is selected to be less than 10 Hz or when the signal consists of a large number of samples, (which is the case of long duration sags where the event covers more than 10 cycles).

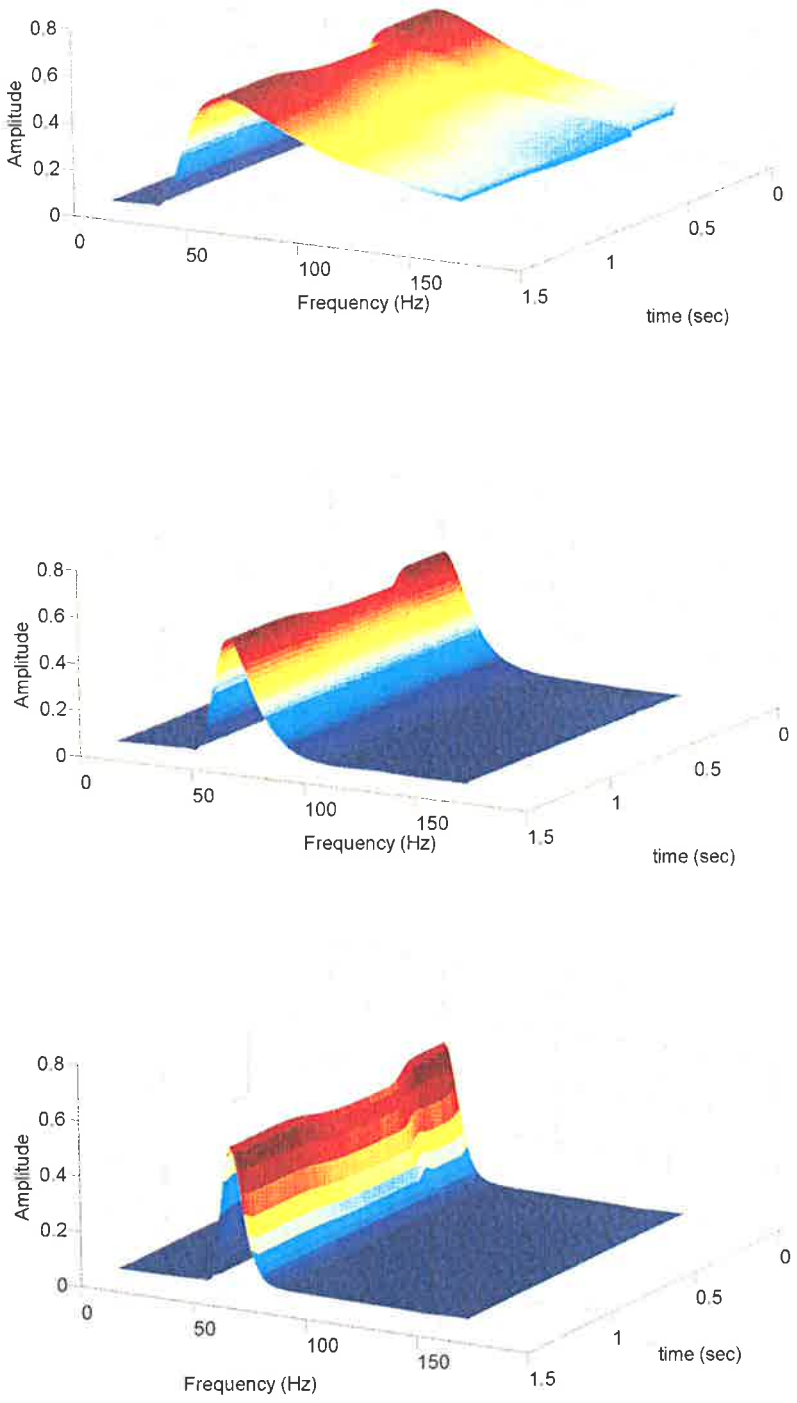

Figure 4.22: The ST of the motor starting sag using three values of α: 0.1 (top), 1.0 (middle), and 3.0 (bottom).

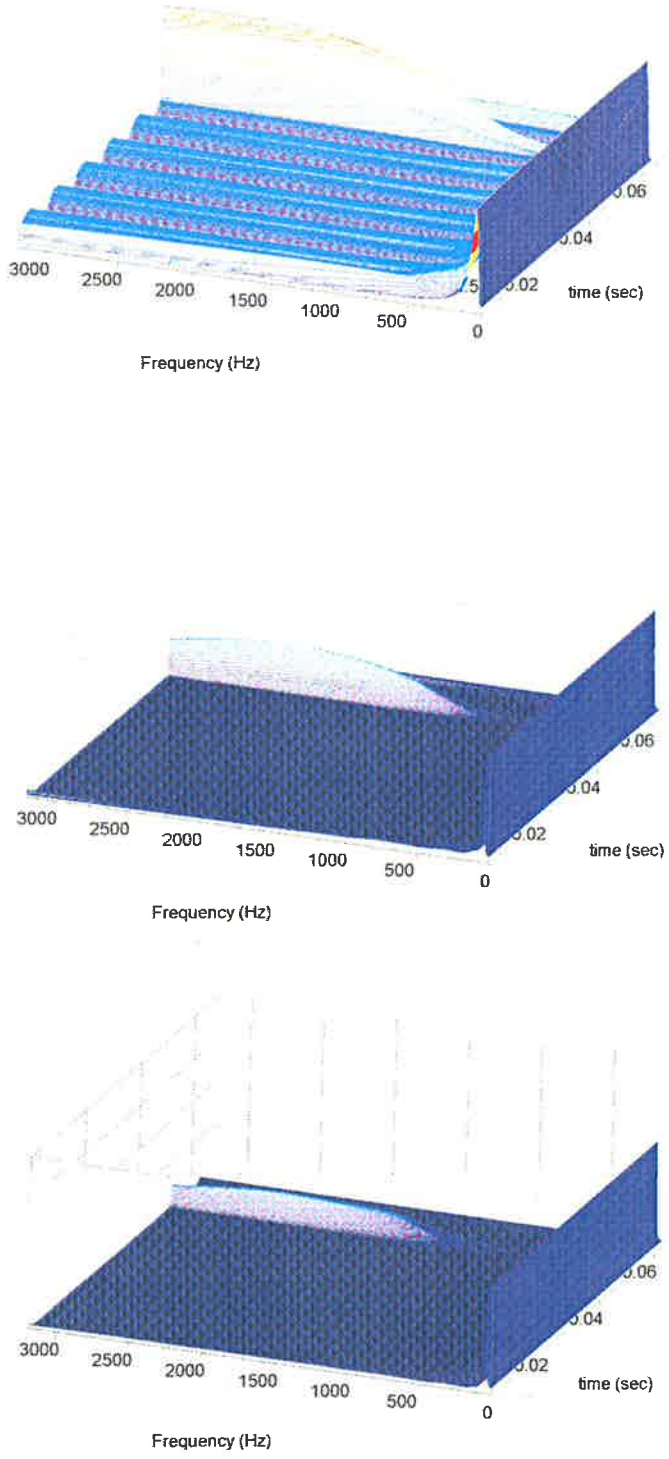

Figure 4.23: The ST of the capacitor switching transient using three values of α: 0.1 (top), 1.0 (middle), and 3.0 (bottom).

4.5 The Hilbert Transform

The Hilbert Transform (HT) has been used widely in the telecommunication research for signal modulation and demodulation, and in various medical image processing applications. In power quality signal analysis, the HT has not been investigated, although it shows an accurate tracking of the changes in the power quality signals. In the following subsections, a brief background of the HT is given and its implementation details and test results are provided for power quality analysis.

4.5.1 Theoretical Background of the HT

The HT is a mathematical process used to generate a complex signals from real signals. It is obtained by convolving the real signal $v(t)$ with the Hilbert function $(1/(\pi\ t))$. That it is [73]:

$$v_{ht}(t) = v(t) * \left(\frac{1}{\pi\ t}\right) = \frac{1}{\pi}\int_{-\infty}^{+\infty} \frac{v(\lambda)}{t-\lambda} \tag{4.5.20}$$

where $v_{ht}(t)$ is the HT of $v(t)$.

As it is known in the convolution theorem, the integration in the last equation is calculated in frequency domain by multiplying the Fourier transform of the real signal, $v(t)$, and the Fourier transform of the Hilbert function, as follows:

$$V_{ht}(\omega) = V(\omega) \cdot H(\omega) \tag{4.5.21}$$

where,
$V_{ht}(\omega)$ is the Fourier transform of $v_{ht}(t)$,
$V(\omega)$ is the Fourier transform of $v(t)$,
$H(\omega)$ is the Fourier transform of the Hilbert function $(1/(\pi\ t))$, and
ω is $2\pi f$, and f is the frequency of the signal.

The Fourier transform of the Hilbert function,$H(\omega)$, is a complex function has an infinite amplitude in the real plane, "δ function", and either +1 or −1 in the Imaginary plane as shown in Figure 4.24. Mathematically it can be defined as:

$$H(\omega) = j \begin{cases} -1 & \omega > 0 \\ +1 & \omega < 0 \end{cases} \tag{4.5.22}$$

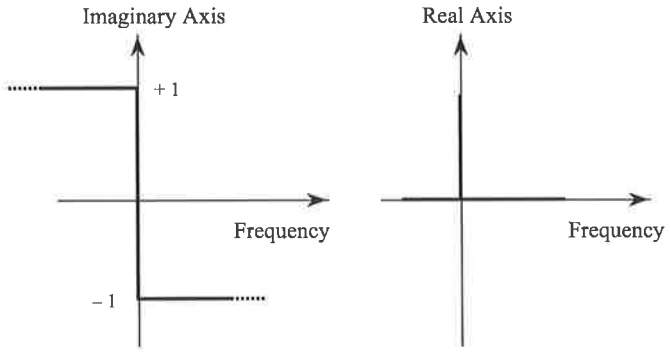

Figure 4.24: Frequency response of the Hilbert function in Imaginary (left) and Real (right) planes.

Therefore, the HT rotates the positive frequency spectral component of the studied signal (the real signal) by $-j$, and the negative frequency spectral component by $+j$. Thus, by taking the inverse Fourier transform of the multiplication in Equation (4.5.21), the resultant is a shifted version of the studied signal by a 90° phase shift.

4.5.2 The Analytical Signal

The analytical signal is a complex signal constructed from the HT of the studied signal (the real signal) and the studied signal itself. I.e. the analytical signal, v_a, of the signal $v(t)$ can be defined as:

$$v_a(t) = v(t) + jv_{ht}(t) \tag{4.5.23}$$

The polar form of $v_a(t)$ is given by:

$$v_a(t) = A(t) \cdot e^{j\varphi} \tag{4.5.24}$$

where, $A(t)$ is the envelope of the studied signal, and is equal to:

$$A(t) = \sqrt{(v(t))^2 + (v_{ht}(t))^2} \tag{4.5.25}$$

and φ is the instantaneous phase of signal and equal to:

$$\varphi(t) = \tan^{-1}\left(\frac{v_{ht}(t)}{v(t)}\right) \tag{4.5.26}$$

From the instantaneous phase of the signal, the instantaneous frequency f_{ins} is calculated as:

$$f_{ins}(t) = \frac{d\varphi(t)}{dt} \tag{4.5.27}$$

4.5.3 Experimental Results of the HT

In order to show the performance of the HT on real power quality events, the envelope of the pervious studied events (the motor sag and the capacitor switching transient) have been calculated as shown in Figures 4.25 and 4.26.

As it can be seen from the figures, the envelope of the both signals tracks accurately the disturbances in the signals. It should be noted that there is some oscillations in the envelope, which are due to the noise in the captured signal. The advantage of the HT over the previous studied signal processing techniques is its simplicity in calculation and hence speed.

4.6 The Clark Transform

The Clarke transformation (CT) is commonly utilized in real-time motor control applications. This is due to the fact that in a three-phase system, the phase quantities are not independent variables. Therefore it is possible to transform a three-phase system to an equivalent orthogonal two-phase representation. In this section this concept has been applied to power quality events, as a new power quality signal pro-

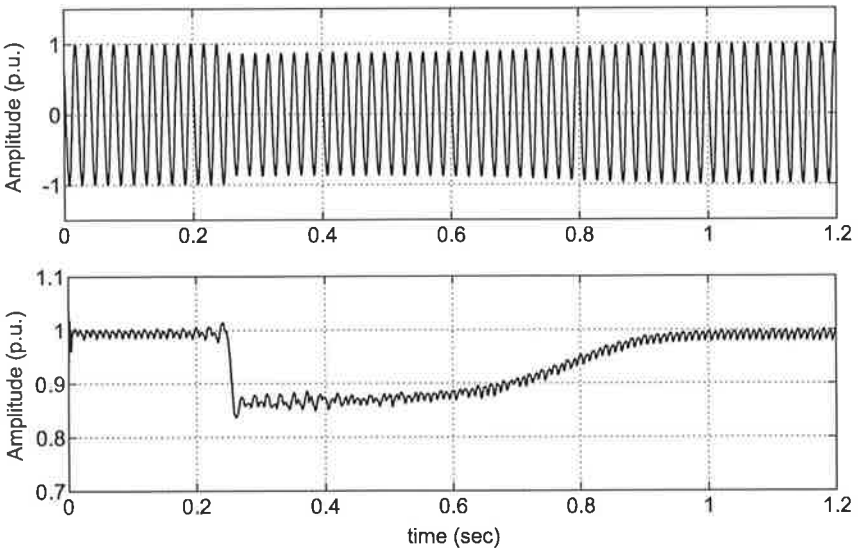

Figure 4.25: Motor starting voltage sag (top), and it envelope using the HT technique (bottom).

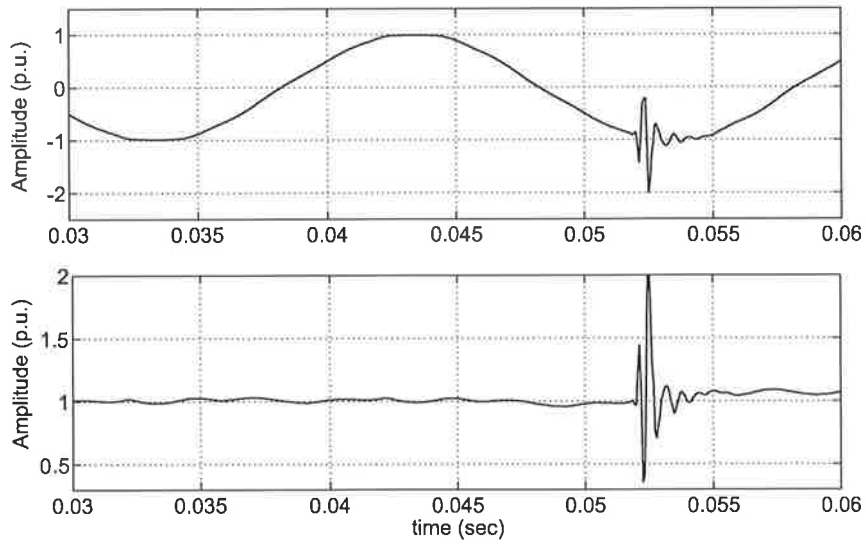

Figure 4.26: Capacitor switching transient (top), and it envelope using the HT technique (bottom).

cessing technique, in order to offer an alternative method which is able to process all three phases of the three-phase systems simultaneously.

4.6.1 Theoretical Background of the CT

The CT is based mainly on the symmetrical components theory in the three phase systems which decomposes the three phase in the system as following:

$$\begin{bmatrix} v_a(t) \\ v_b(t) \\ v_c(t) \end{bmatrix} = k \begin{bmatrix} 1 & 1 & 1 \\ \alpha^2 & \alpha & 1 \\ \alpha & \alpha^2 & 1 \end{bmatrix} \begin{bmatrix} v_+ \\ v_- \\ v_0 \end{bmatrix} \tag{4.6.28}$$

where,

v_a, v_b, and v_c are the three-phase system's signals,

v_+, v_-, and v_0 are the *positive*, *negative*, and *zero* sequence components respectively,

α is a complex operator equal to $\exp(j2\pi/3)$, and

k is a constant.

The terms in Equation (4.6.28) can be written in a more compact matrical form as:

$$\mathbf{v}_{\text{ph}} = \mathbf{S} \cdot \mathbf{v}_{\text{s}} \tag{4.6.29}$$

where,

$\mathbf{v}_{\text{ph}}$ is the instantaneous three-phase signals' vector,

$\mathbf{v}_{\text{s}}$ is the vector of the instantaneous sequence components, and

$\mathbf{S}$ is the sequences transformation matrix.

The sequence components are obtained by inverting Equation (4.6.29) as:

$$\mathbf{v}_{\text{s}} = \mathbf{S}^{-1} \cdot \mathbf{v}_{\text{ph}} \tag{4.6.30}$$

where,

$$\mathbf{S}^{-1} = \frac{1}{3k}\begin{bmatrix} 1 & \alpha & \alpha^2 \\ 1 & \alpha^2 & \alpha \\ 1 & 1 & 1 \end{bmatrix} \tag{4.6.31}$$

All the information in the three-phase system's signals can be preserved when selecting $k = 1/\sqrt{3}$, considering only either the real or imaginary terms of the elements in the Equation (4.6.31) and discarding the imaginary operator j. This concept leads to the Clarke transformation matrix, T_c, as follows:

$$T_c = \sqrt{\frac{2}{3}}\begin{bmatrix} 1 & \mathrm{Re}(\alpha) & \mathrm{Re}(\alpha^2) \\ 0 & \mathrm{Im}(\alpha^2) & \mathrm{Im}(\alpha) \\ \frac{1}{\sqrt{2}} & \frac{1}{\sqrt{2}} & \frac{1}{\sqrt{2}} \end{bmatrix} = \begin{bmatrix} 1 & -\frac{1}{2} & -\frac{1}{2} \\ 0 & \frac{\sqrt{3}}{2} & -\frac{\sqrt{3}}{2} \\ \frac{1}{\sqrt{2}} & \frac{1}{\sqrt{2}} & \frac{1}{\sqrt{2}} \end{bmatrix} \tag{4.6.32}$$

Therefore, due to the specific selection of the elements in Equation (4.6.31) which was done by Clarke [74], the three-phase system cab be represented by two orthogonal phases, in addition to the zero sequence component. Thus, Equation (4.6.30), according to the Clarke transformation, becomes:

$$\begin{bmatrix} v_\alpha(t) \\ v_\beta(t) \\ v_0(t) \end{bmatrix} = \begin{bmatrix} 1 & -\frac{1}{2} & -\frac{1}{2} \\ 0 & \frac{\sqrt{3}}{2} & -\frac{\sqrt{3}}{2} \\ \frac{1}{\sqrt{2}} & \frac{1}{\sqrt{2}} & \frac{1}{\sqrt{2}} \end{bmatrix}\begin{bmatrix} v_a \\ v_b \\ v_c \end{bmatrix} \tag{4.6.33}$$

where,

v_α and v_β are the two orthogonal phases of the three phase system, and

v_0 is the zero sequence component of the three-phase system.

Note that the factor "$\sqrt{2/3}$ " is ignored in the derivation of Equation (4.6.33) where it has no impacts when using this transform for power quality signals analysis.

Therefore, as the two phase vectors, v_α and v_β, are orthogonal, (similar to the case of HT), sufficient information on the power quality events can be obtained by calculating an instantaneous envelope of the three phase system's signals. The three

phase envelope, $A_{3ph}(t)$, is calculated as:

$$A_{3ph}(t) = \sqrt{\left(v_\alpha(t)\right)^2 + \left(v_\beta(t)\right)^2} \tag{4.6.34}$$

4.6.2 Experimental Results of the CT

Similar to the previous discussion, the performance of the CT on the power quality events has been investigated on the three-phase motor starting sag and three-phase capacitor switching transient. In addition, in order to investigate the sensitivity of the proposed technique, more tests have been performed on events with only one phase or two phases of the three phase system are influenced by the event.

In Figure 4.27, the three-phase envelope of motor starting sag affecting all the three phases in the system is shown. The results obtained are similar to that obtained by the HT technique, however, all the three phases are involved in the calculating in this transform. It should be noted here that more ripples were resulted in the envelope, which can be smoothed by filtering the envelope using simple FIR filter. In the figure, the envelope was filtered by averaging every 64 points of the envelope.

In Figure 4.28, the three-phase filtered envelopes are shown for motor starting sags affecting one phase and two phases. One can see from the figure how the three-phase envelope is affected by the disturbances in each phase.

Figures 4.29 and 4.30 compare the three-phase envelopes of transients events when the transient occur on all phases, (Figure 4.27), or when occur on one or two phases of the system (Figure 4.28 (top) and (bottom) respectively). It can be concluded from the figures that the proposed CT able to respond efficiently to the disturbances in all of the phases.

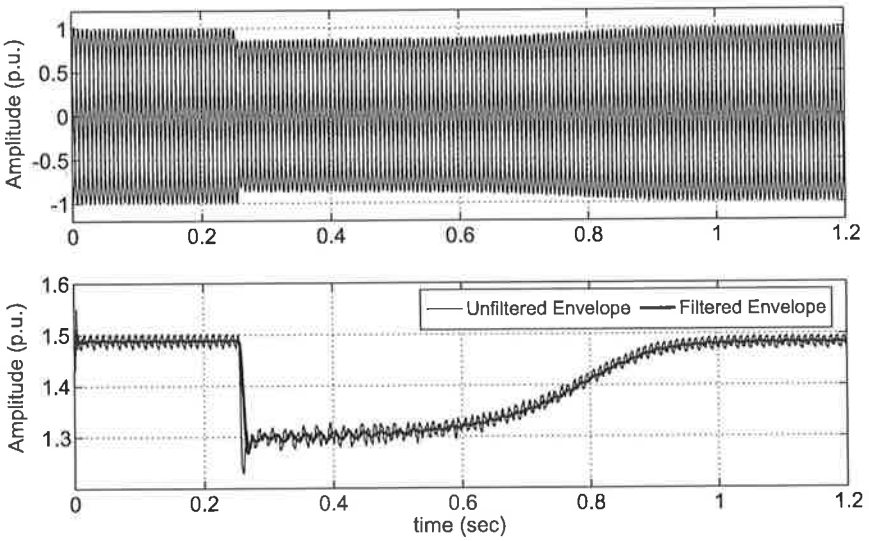

Figure 4.27: Three-phase motor starting sag event (top), and it three-phase envelope using the CT technique (bottom).

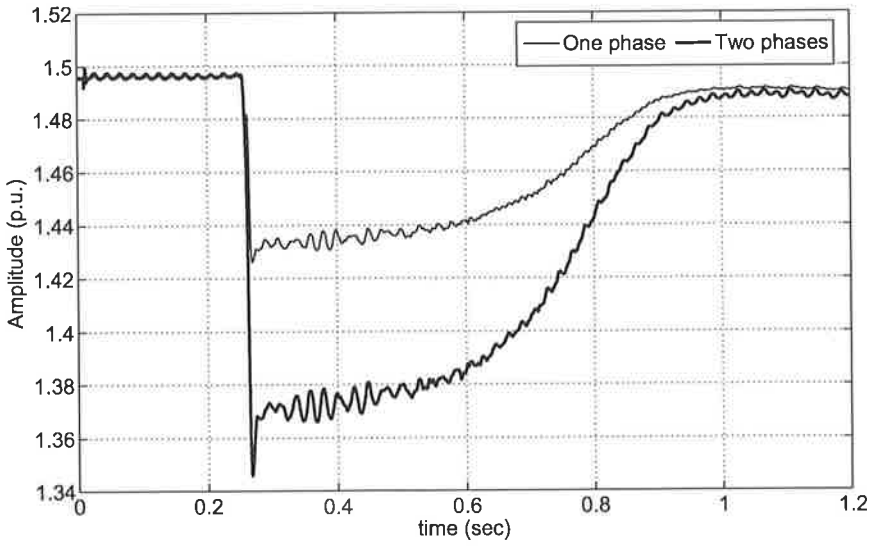

Figure 4.28: Three-phase envelopes of motor starting sag affecting one phase and two phases using the CT technique.

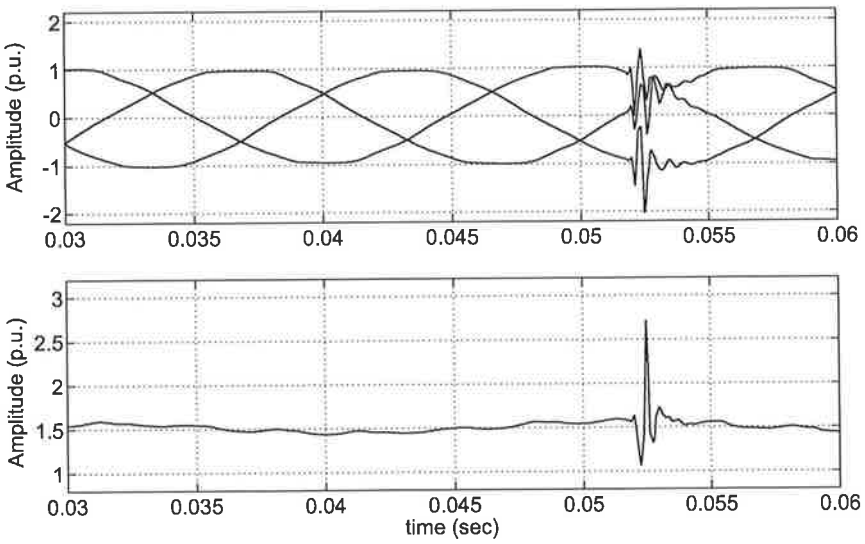

Figure 4.29: Three-phase Capacitor switching transient event(top), and it three-phase envelope using the CT technique (bottom).

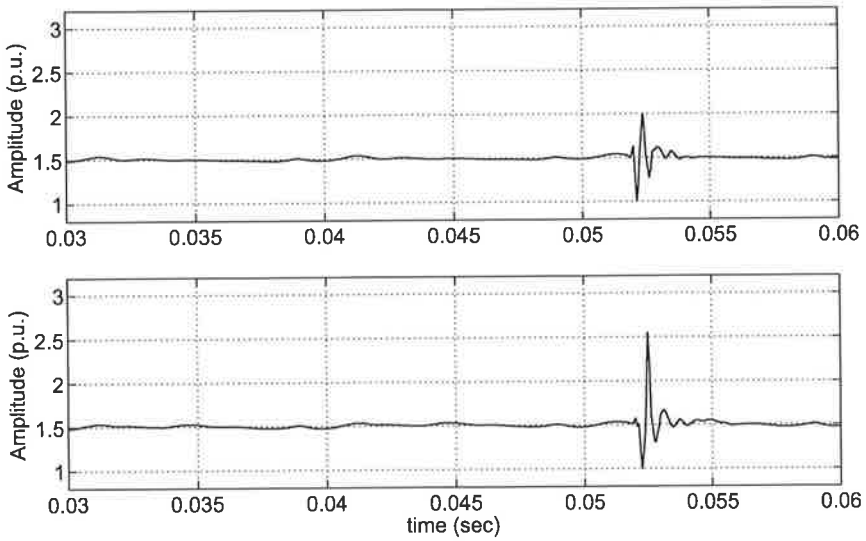

Figure 4.30: Three-phase envelopes of capacitor switching transient affecting one phase, (top), and two phases, (bottom), using the CT technique.

4.7 Conclusion

In the Chapter, different signal processing techniques recently considered in the literature for extracting the features of power quality signals have been examined. This included: the Short-time Fourier Transform, (STFT), Continuous and discrete Wavelet transforms, (including the Multiresolution analysis and Wavelet Packet transform), and the S-Transform, (ST). In addition, the Hilbert Transform, (HT), and Clarke Transform, (CT) were introduced as a new power quality feature extraction techniques. In order to investigate the practical implementation of the studied technique, real power quality signals belong to two different categories according to the IEEE standard have been used in the study. The advantages and disadvantages of implementation of each technique have been discussed.

Among the studied techniques, the STFT and the CWT techniques were found to be the least preferable alternatives for power quality analysis. The main disadvantage of the former technique was the frequency and time resolution trade off due to its fixed window. The main drawback of the CWT technique is its redundancy in using large number of scales which make it more difficult to interpret its results, while its discrete version (DWT) can offer sufficient information about power quality disturbances using only limited number of scales. However, because the Wavelet technique decompose the signals in terms of non-trigonometric functions known as mother wavelets, different mother wavelets can have different impacts on the power quality events gives different results. Therefore, the most appropriate mother wavelet have been examined based on the sensitivity of the energies of the decomposed signals to the disturbances. The study showed that the Daubechies, db4, was the most appropriate mother wavelet for analysing the power quality signals using the Wavelet technique.

In addition, the ST technique was investigated with different values of the Gaussian window factor. It was shown that the setting of this factor to 1.0 is an appropriate selection for analysing the power quality signals using the ST technique. Furthermore, the performance of the newly introduced power quality feature ex-

traction techniques was shown to be sufficient for tracking the disturbances in the signals as compared with the previous techniques which will be investigated further in the upcoming chapters.

Chapter 5

Distinguishing Capability of the Feature Extraction Techniques

5.1 Introduction

THE primary step for improving the power quality in a particular power system is to monitor the voltage and current signals to identify the type of disturbances, and thus, the correct preventative action can be taken. However, due to a large amount of data that can be captured during monitoring and saving power quality data, it is necessary, to separate the types of events in order to identify the causes of the disturbances. Therefore, in order to differentiate the power quality events, it is necessary to define specific characteristics which distinguish each event from others. This can be achieved using an appropriate feature extraction technique.

Unlike the previous conducted studies which were based on examining a single signal processing technique to evaluate its performance for automatic classification of power quality events, this thesis investigates combinations of different features using different techniques (or different features from the same technique). This approach aims to demonstrate the capability of the techniques considered in distinguishing different power quality events. The techniques studied in this chapter are based on the most appropriate techniques for power quality feature extraction examined in Chapter 4.

5.2 Distinguishing Features of Power Quality Events

To be able to examine the distinguishing capability of the feature extraction techniques, it is necessary to interpret the results so that the characteristics of the power quality events can be described in terms of specific features. Therefore, the following subsections propose several features using four techniques: the Wavelet Packet multiresolution, S-Transform, Hilbert transform, and Clarke transform, which will be implemented and examined to investigate their distinguishing capability.

5.2.1 Distinguishing features of Wavelet Packet Transform

The energy of a signal that is based on the Wavelet transform can be defined in terms of its details and approximation energies as:

$$E_{signal} = \sum_{k} |u[k]|^2 + \sum_{m} \sum_{k} |w_m[k]|^2 \tag{5.2.1}$$

where $u[k]$ and $w_m[k]$ are the approximated and detailed versions of the original signal at level m respectively.

The first term in Equation (5.2.1) is the energy of the reconstructed approximated version of the signal, while the second term represents the energy of the reconstructed detailed version of the signal. Therefore, if the raw signal is decomposed into m levels, a vector of the energies of the reconstructed detailed signals at each level of the decomposition can be formed as:

$$E_v[m] = \left[\|w_1\|_2^2 \quad \|w_2\|_2^2 \quad \cdots \quad \|w_m\|_2^2 \right] \tag{5.2.2}$$

where,
$\|w_m\|_2^2$ is the energy of the reconstructed detailed signals at level m, and
$E_v[m]$ is a vector of the energies of the reconstructed detailed signals.

The vector E_v is represented statistically by defining two features, $F1$ and $F2$ that represents the Wavelet Packet technique (WPT) as following:

$$F1 = \frac{1}{M}\sum_{m} E_v[m] \tag{5.2.3}$$

$$F2 = \sqrt{\frac{1}{M}\sum_{m}\left(E_v[m] - \frac{1}{M}\sum_{m} E_v[m]\right)^2} \tag{5.2.4}$$

where,

$F1$, and $F2$ are the mean and standard deviations of E_v respectively, and

M represents the number of decomposed levels

5.2.2 Distinguishing features of S-Transform

The S-Transform of a discrete-time signal $v[k]$, as explained in the Chapter 4, can be rewritten as:

$$V_{ST}[kT, \frac{n}{N}] = \sum_{m=0}^{N-1} V\left[\frac{m+n}{N}\right] \cdot \mathbf{exp}\left(-\frac{2\pi^2 m^2 \alpha^2}{n^2}\right) \cdot \mathbf{exp}\left(j\frac{2\pi m}{N}k\right) \tag{5.2.5}$$

where,

$V\left[m + n/N\right]$ is the Fourier transform of the discrete time signal $v[kT]$,

T is the time between two consecutive samples of the signal,

k, m, and n are equal to $0, 1, 2, \ldots N-1$, and N is the total number of samples in the signal.

As discussed in the previous chapter, the output from the S-Transform, $V_{ST}[kT, \frac{n}{N}]$ is a complex matrix. The rows of this matrix represent the frequency content of the signal, whereas its columns represent the corresponding time. Therefore, the amplitudes of the frequency contents of the signal versus time can be calculated from the S-Transform matrix as [44]:

$$S[k] = \mathbf{max}\left|V_{ST}[k, \frac{n}{N}]\right| \tag{5.2.6}$$

where $S[k]$ is the frequency amplitude vectors.

The proposed features that will be used for investigating the distinguishing capability of the S-Transform technique are based on the vector $S[k]$ by taking its standard deviation and mean value as follows:

$$F3 = \frac{1}{N}\sum_{k} S[k] \tag{5.2.7}$$

$$F4 = \sqrt{\frac{1}{N}\sum_{k}\left(S[k] - \frac{1}{N}\sum_{m} S[k]\right)^2} \tag{5.2.8}$$

where, N is the length of the vector S.

5.2.3 Distinguishing features of the Hilbert Transform

The features that can be used to examining the distinguishing capability of the Hilbert transform are the mean value and the standard deviation of the Hilbert transform envelope of the target discrete-time signal $v[k]$. The envelope, $A[k]$, of the signal was given in Chapter 4 as:

$$A[k] = \sqrt{\Big(v[k]\Big)^2 + \Big(v_{ht}[k]\Big)^2} \tag{5.2.9}$$

where, $v_{ht}[k]$ is the Hilbert transform of the target signal $v[k]$.
Hence two features are defined as:

$$F5 = \frac{1}{N}\sum_{k} A[k] \tag{5.2.10}$$

$$F6 = \sqrt{\frac{1}{N}\sum_{k}\left(A[k] - \frac{1}{N}\sum_{k} A[k]\right)^2} \tag{5.2.11}$$

where, N is the length of the target signal, and $k = 1, 2, \cdots N$.

5.2.4 Distinguishing features of the Clarke Transform

Similar to the Hilbert Transform, however, for a three-phase system, the three-phase envelope for the target discrete-time signal is calculated as:

$$A_{3ph}[k] = \sqrt{\left(v_\alpha[k]\right)^2 + \left(v_\beta[k]\right)^2} \tag{5.2.12}$$

where,

v_α and v_β are the α and β components that can represent a three phase system, and A_{3ph} is the three-phase envelope of the three-phase signals.

Similar to the previous discussions, two distinct features can be defined to examine the Clarke transform, which are selected based on three-phase Clark's envelope. This envelope is represented statistically by calculating its mean value and standard deviation as below:

$$F7 = \frac{1}{N}\sum_k A_{3ph}[k] \tag{5.2.13}$$

$$F8 = \sqrt{\frac{1}{N}\sum_k \left(A_{3ph}[k] - \frac{1}{N}\sum_k A_{3ph}[k]\right)^2} \tag{5.2.14}$$

where, N is the length of the target signal.

It should be noted here that although in the Clarke transform technique the three-phase signals are transformed into two-phase components, individual phase information is still available from the measured instantaneous voltages (or currents) and the angle of the three phase envelope. For example, in the case of a single-phase (or two-phase) disturbance, the distorted phase (or phases) can be estimated in two steps as follows:

- The angle of the three phase envelope, θ_{A3ph} is calculated as:

$$\theta_{A3ph} = \arctan\left(\frac{v_\beta}{v_\alpha}\right) \tag{5.2.15}$$

- Then the three-phase voltages (or currents) signals are estimated by using this angle as:

$$\begin{cases} va_{Est} = V_{amp}\cos(\theta_{A3ph}) \\ vb_{Est} = V_{amp}\cos(\theta_{A3ph} - 2\pi/3) \\ vc_{Est} = V_{amp}\cos(\theta_{A3ph} + 2\pi/3) \end{cases} \tag{5.2.16}$$

where, va_{Est}, vb_{Est}, vc_{Est} are the instantaneous estimated three phases, and V_{amp} is the amplitude of the three phase system.

- Finally, by comparing the instantaneous values of the measured three-phase signals with the estimated values from Equation (5.2.16), the distorted phase(s) can be identified, which is the one(s) furthest from the estimated value.

Table 5.1 summarise the above features which are utilized to determine all possible combinations of pairs for the optimum feature selection in the power quality event classifications.

Table 5.1: Summery description of the proposed features based on four different signal processing techniques.

Feature	Description
$F1$	Mean value of the energies of the reconstructed signals using WPT
$F2$	Standard deviation of the energies of the reconstructed signals using WPT
$F3$	Mean value of the magnitude-time spectrum using S-Transform
$F4$	Standard deviation of the magnitude-time spectrum using S-Transform
$F5$	Mean value of the signal envelope using Hilbert transform
$F6$	Standard deviation of the signal envelope using Hilbert transform
$F7$	Mean value of the 3-phase envelope using Clarke transform
$F8$	Standard deviation of the 3-phase envelope using Clarke transform

In the following section, different power quality events belonging to several classes will be simulated in order to investigate the ability of the signal processing technique to distinguish type of the events.

5.3 Power Quality Events Simulation

The power quality events studied in this chapter have been classified into the following nine classes:

- Pure signal.
- Sags (dips) due to short circuit faults.
- Sags due to motor starting.
- Swells.
- Transients due to capacitor switching.
- Harmonic distortions.
- Sags contaminated with harmonics
- Flicker.
- Interruptions.

In practical power systems, due to the nature and the causes of an event, the characteristics of of the above events vary significantly. Therefore, in this thesis, to be able to study the effects of all possible variations in the power quality events, 500 random events each having different characteristics have been generated for each power quality event.

A set of sample waveforms which are given in Figure 5.1 demonstrates the characteristics of the studied power quality classes as a function of time. For each class, different events were obtained by randomly varying four parameters that characterize each event. These parameters are defined as follows:

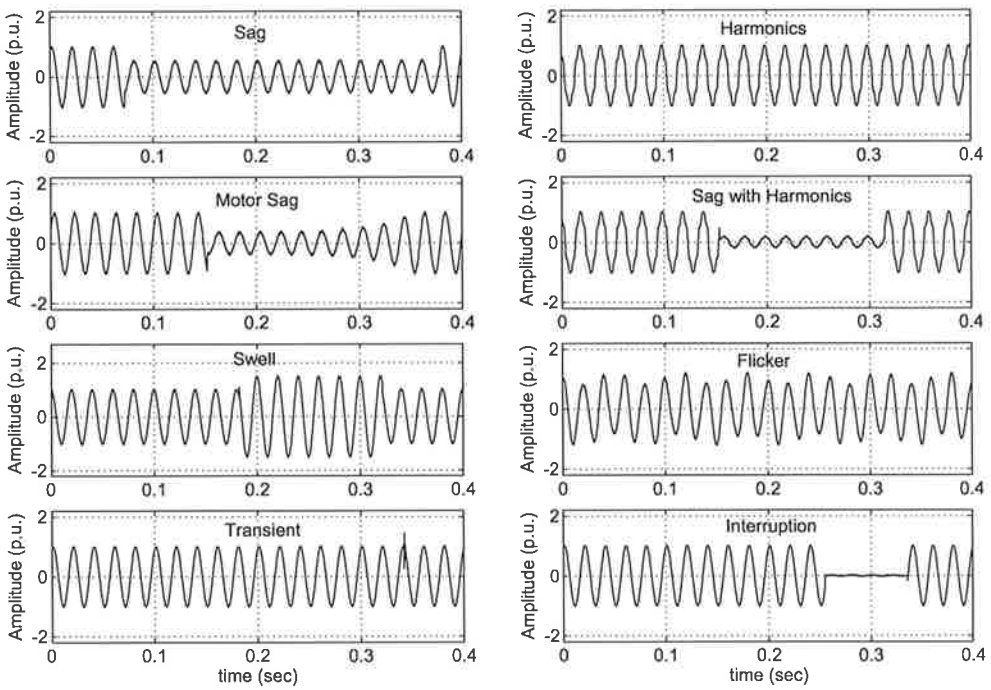

Figure 5.1: A set of sample waveforms showing the profile of the power quality classes studied.

- **The depth of the event**: defined as the changes in the amplitude of a signal.
- **The angle**: represents the phase shift at which the signal is captured.
- **The starting time**: defined as the time at which the event starts.
- **The duration**: defined as the time period of the event.

In the simulated data, it is assumed that the total length of the signals is 20 cycles, and the sampling frequency is chosen to be 16.4 kHz. Although these parameters have been varied randomly, specific constraints were adopted to generate realistic signals reference to the international standards. For example, for the sag events, four parameters were randomly varied as illustrated in Figure 5.2. As can be seen in the figure, the depth of the sag is varied from 10% to 90% of the magnitude of the pure sine waveform. The angle of the signal is varied from 0% to 100% of the entire period (which is a realistic assumption since the captured waveforms in a practical monitoring system could have a phase shift that may vary from 0 to 2π).

In addition, the starting time of the sag is varied from 0% to 80% of the total length of the signal. Moreover, the duration of the sag is varied from 5% to 100% of the total length of the waveform.

As stated above, each of the simulated event accommodated 20 cycles of the signals. Therefore, a duration of 5% corresponds to one cycle of the waveform. In addition, all the events were contaminated with noise level changing randomly from 40 dB to 30 dB.

For the motor sag events, the recovery pattern of the sag was simulated using an exponential function of $A\exp(k^4)$; where A is a constant representing the depth of the motor sag, and k is an index that varied from 0 up to the length of the sag. The sag duration is assumed to be equal or greater than 10 cycles (which is a realistic value for industrial motor drives), and the depth of the sag was varied from 90% to 70% of the signal amplitude.

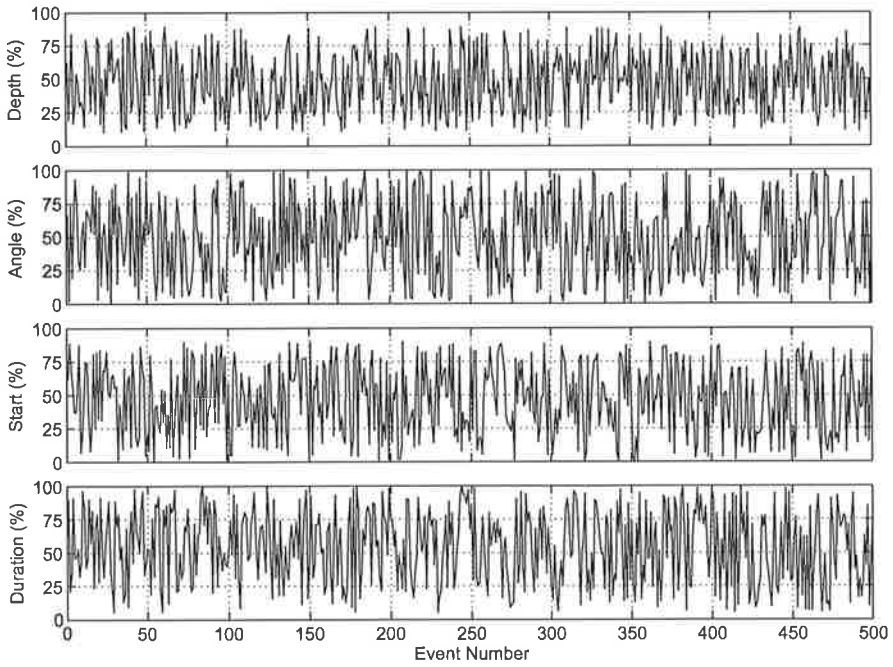

Figure 5.2: Random changes of the parameters characterizing 500 events.

For the interruption and the swell events, the four parameters (depth, angle, starting time and duration) were also varied as described above. However, the amplitude of the pure sine waveform was increased between 10% and 90%.

For the harmonics events, the 2^{nd}, 3^{rd}, 5^{th}, 7^{th}, 9^{th}, and 11^{th} harmonics are used to randomly contaminate the ideal waveforms. During the generation of such events, the total harmonic distortion (THD) of each waveform was kept greater than 5%, as suggested in [61], by applying the following condition:

$$\sqrt{\frac{\sum_i (A_i)}{A_1^2}} \geq 5\%, \qquad i = 2,\ 3,\ 5,\ 7,\ 9,\ 11. \tag{5.3.17}$$

where A_i is the amplitude of the i^{th} harmonic in the signal.
Therefore, if the THD of a waveform was less than 5%, the waveform is regarded as a pure sine waveform.

In the case of the flicker events, the amplitude of the simulated signals was changed periodically to introduce the effect of a flicker. To achieve this, the magnitude of the target waveform was varied as a function of another sine wave as follows:

$$v_{flicker} = (1 + a_f \sin(B\omega t)) \cdot v_{ref} \tag{5.3.18}$$

where,
a_f is a constant that is equal to 0.2,
B is a random variable varying between 0.5 and 0.7.
$\omega = 2\pi f$, and f is the signal frequency, and
v_{ref} is the reference pure signal.
The above equation results an oscillation in the amplitude of the target waveform, which varied randomly from 50% to 70% of the fundamental frequency.

The parameters which were varied randomly in the case of transient events are the oscillation frequency of the transients (varied from 10 times to 15 times of the fundamental frequency) and the amplitude of the overshoot (varied up to 150% of the amplitude of the pure signal).

5.4 Features Scattering of Power Quality Events

The scatter plot provides a useful insight for understanding the correlation between the two features, which may demonstrate the performances of one or more techniques. Therefore, in this section, the proposed features will be scattered together to investigate the distinguishing capability a technique under investigation. The principal idea behind this approach is that the scatter graphs provide "event specific regions" that show the distinguishing capability of a technique.

As mentioned earlier, unlike the previous studies which were based on examining a single technique to evaluate its performance, this study investigates and combines different features using different techniques (or different features using same technique). In the following paragraphs, the scatter graphs are given for a selected number of pairs of features, which aims to demonstrate the distribution of the nine classes considered.

5.4.1 Scattering of features using a single technique

This section investigates the distinguishing capability of using combinations of features from a single technique. The distinguishing capability of the nine studied power quality classes using the proposed features are shown in Figures 5.3 to 5.10.

Figure 5.3 shows the scatter plot of the mean value (F1) and the standard deviation (F2) of the 10 levels reconstructed signals' energies obtained using the Wavelet coefficients. In this study, Daubechies wavelet (db4) is chosen as an appropriate mother Wavelet as discussed in the previous chapter. One can see from the figure that the *swell* events can be distinguished among the events studied. However, it was found that, although, the *sags*, the *motor sags*, the *interruptions*, and the *sags with harmonics* events are separated from the other events, they overlap each other due to their similar characteristics.

The locations of the *harmonics*, the *flicker*, the *transients*, and the *pure signal* events are illustrated more clearly by an enlarged view of the scatter graph shown in Figure 5.4. It can be seen in this figure that the harmonics and the transient events

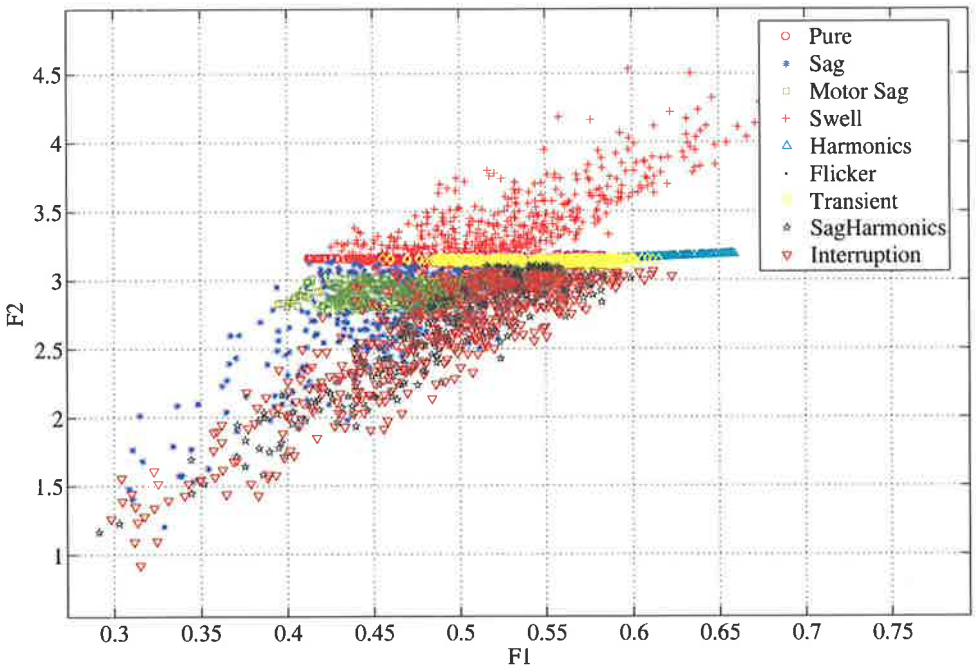

Figure 5.3: Scatter plot of features F1 and F2.

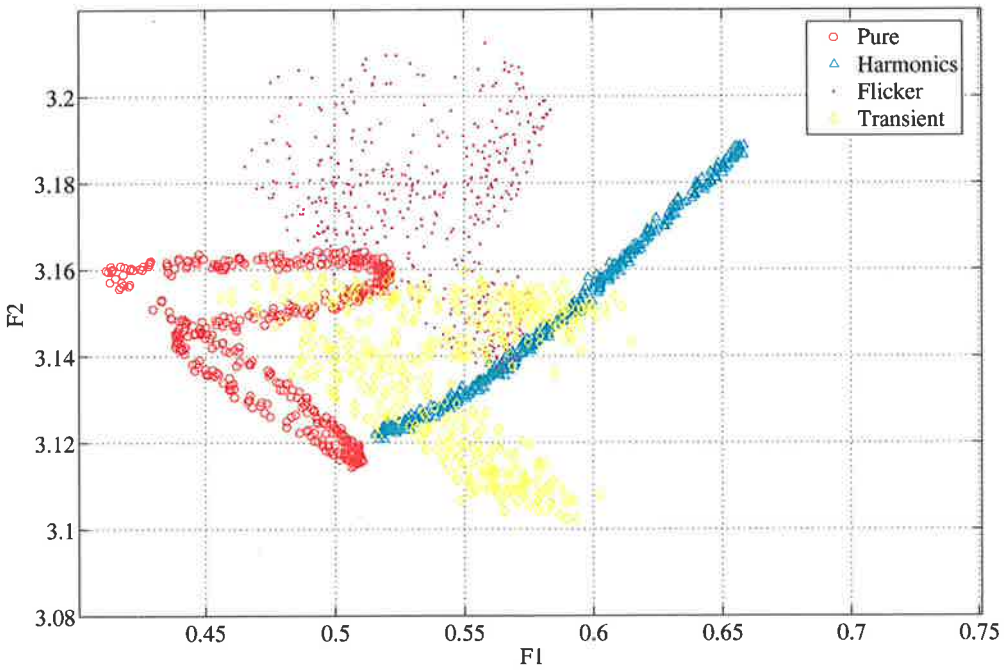

Figure 5.4: Zoomed view of Figure 5.3 to highlight the pure, the harmonic, the flicker, and transient events.

overlap in some regions, which can lead to possible errors in the classification of the events. In addition, it is visible that the *pure signals* spreads over a relatively large area and overlaps with the other "event specific regions". This is because of the fact that the energies of the reconstructed signals are sensitive to the phase angle of the signal. As a result of such overlap, the *harmonic distortions* or the *transients* can be mistakenly classified as the pure signals, or vice versa.

The scatter plot of Figure 5.5, shows the mean value, F3, and the standard deviation, F4, of the S-Transform spectrum. This result reveals a better separation of *harmonics* and *transient* events than the previous features. However, as shown in the figure, the *sag*, the *swell*, and the *interruption* classes still overlap each other.

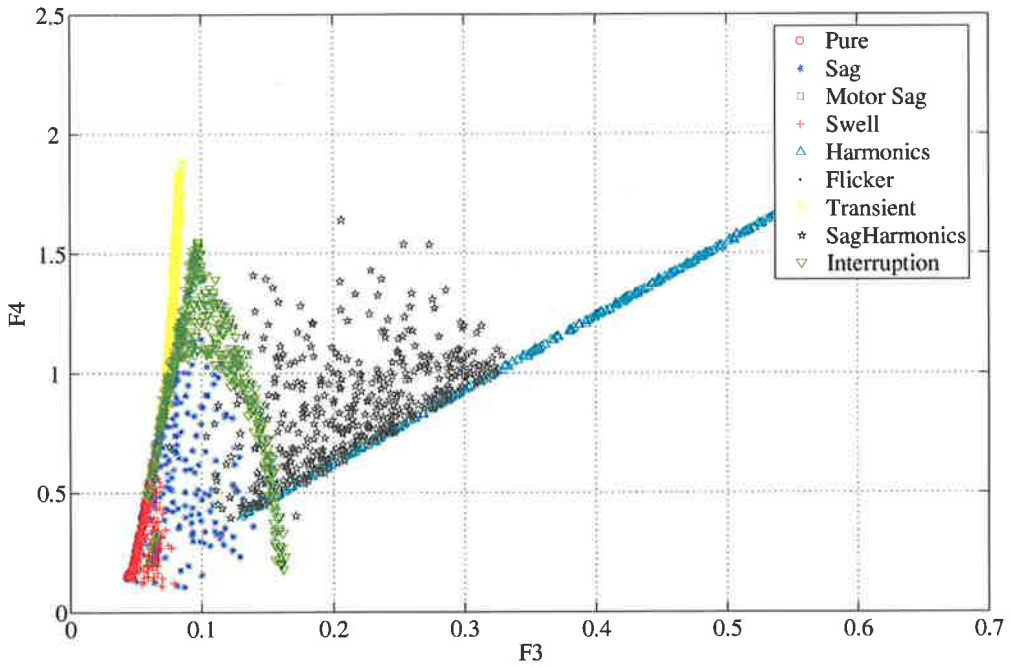

Figure 5.5: Scatter plot of the features F3 and F4.

The results also show that, with these features, the *pure signal*, the *motor sag*, and *flicker* classes occupy a small area in the event specific regions, as compared to the other events, as shown in a zoomed view in Figure 5.6. This figure illustrates

that there is a good distinguishing of the *motor sag* events from the *sag* and *sag with harmonic* classes despite the similarities between these classes. In addition, as expected the *pure signal* class overlapped the *sag* and *swell* events.

The scatter plot of combining the features from the Hilbert Transform (F5 and F6) is illustrated in Figure 5.7. In this scatter plot, unlike the previous results, the *swell*, the *interruption*, the *flicker*, and the *pure* classes can be separated from the other classes. In addition, although the *sag* and the *sag with harmonics* events can mostly be separated from the rest of the classes, they are overlap each other due to the similarity of these events. Furthermore, in spite of the *motor sag* events are being embedded inside the *sag* and the *sag with harmonic* region, they occupy a defined area which distinguishes them from the *sag* and the *sag with harmonic* events. The only two classes in this case which were largely overlapped are the *the sag* and *sag with harmonic* classes, which is attributed to the high similarity of these two classes.

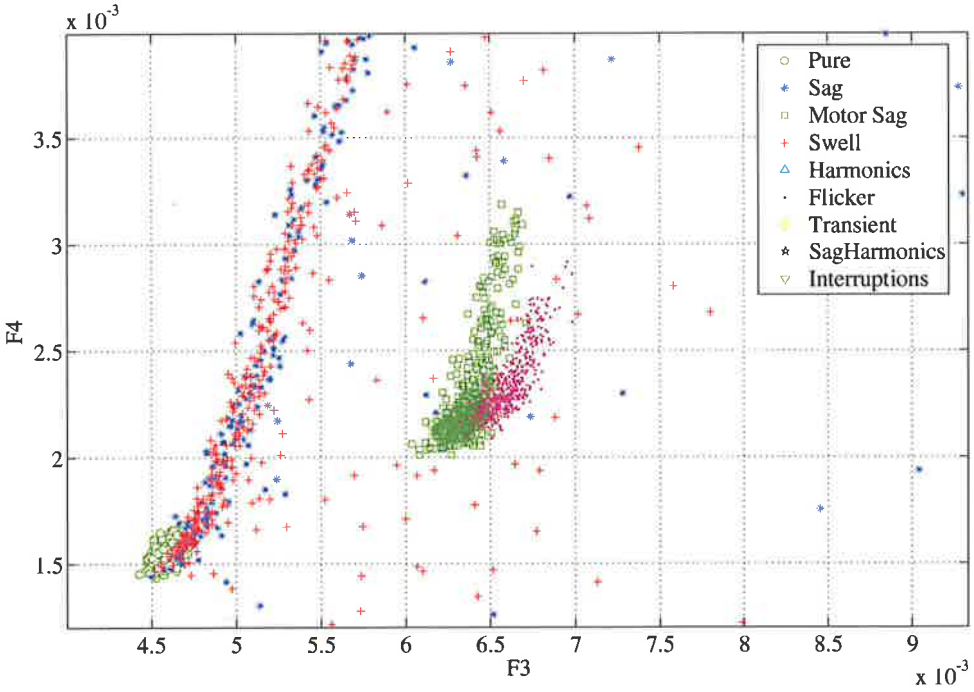

Figure 5.6: Zoomed view of Figure 5.5 to highlight the pure, the motor sag, and the flicker events.

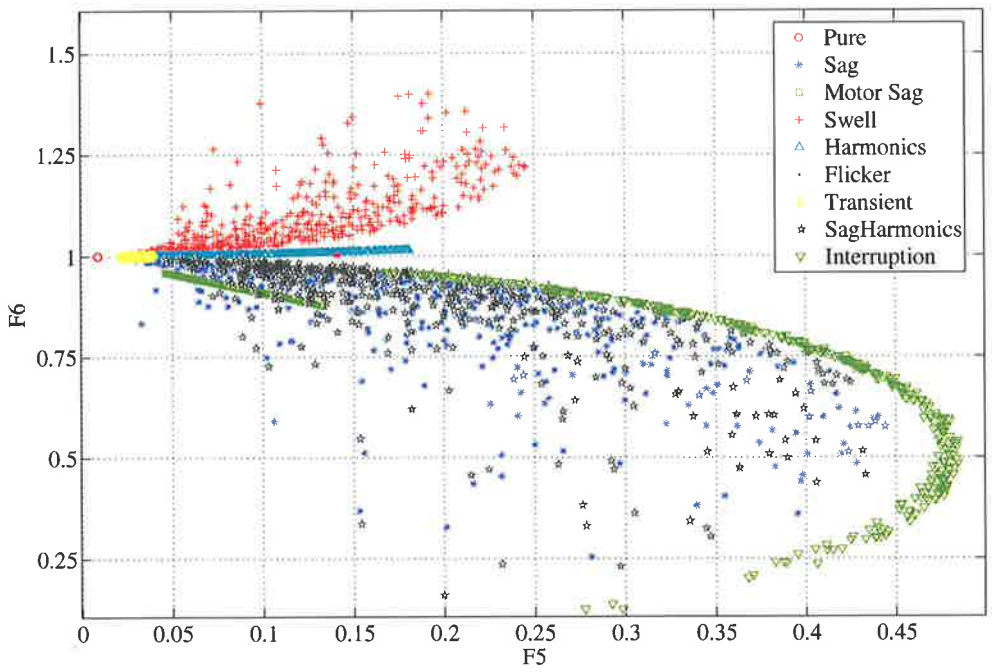

Figure 5.7: The scatter plot of features the F5 and F6.

In the case of the features defined by the Clarke transform, a number of different cases was examined. In the first case, the events were assumed to occur on a single phase. The scatter plot of the features F7, and F8 is shown in Figure 5.8. As can be seen in the figure, the events distribution using these features is similar to the case when using the features from the Hilbert transform. This was expected because of the similarities of the two techniques in the principle of representing the studied signal(s) in terms of two orthogonal phases. However, they differ since the Hilbert transform is applied for single phase systems while the Clarke transform is applicable to three phase systems.

The scatter plots of the cases that assumes the events occur in two and three phases are shown in Figures 5.9 and 5.10 respectively. As can be seen in the figures, the responses of the features to the events in both cases are similar. However, the specific region for the events in each phase were found to occupy different areas.

Although the feature from the two new proposed techniques (the Hilbert transform and the Clarke transform) have shown overall better distinguishing capabilities

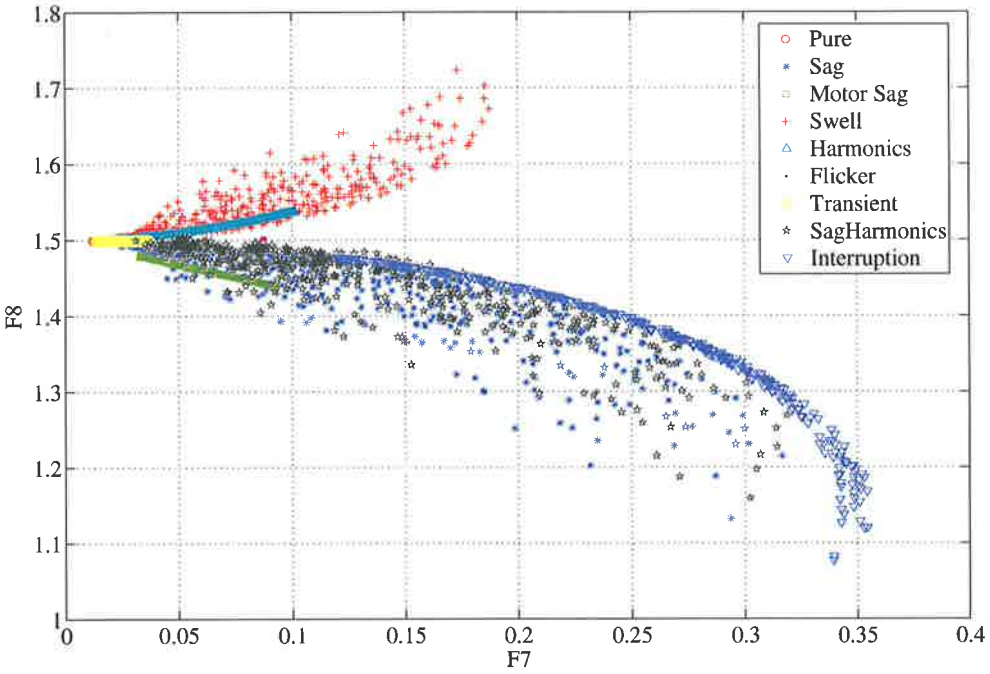

Figure 5.8: The scatter plot of the features F7 and F8 for events occurring on a single phase.

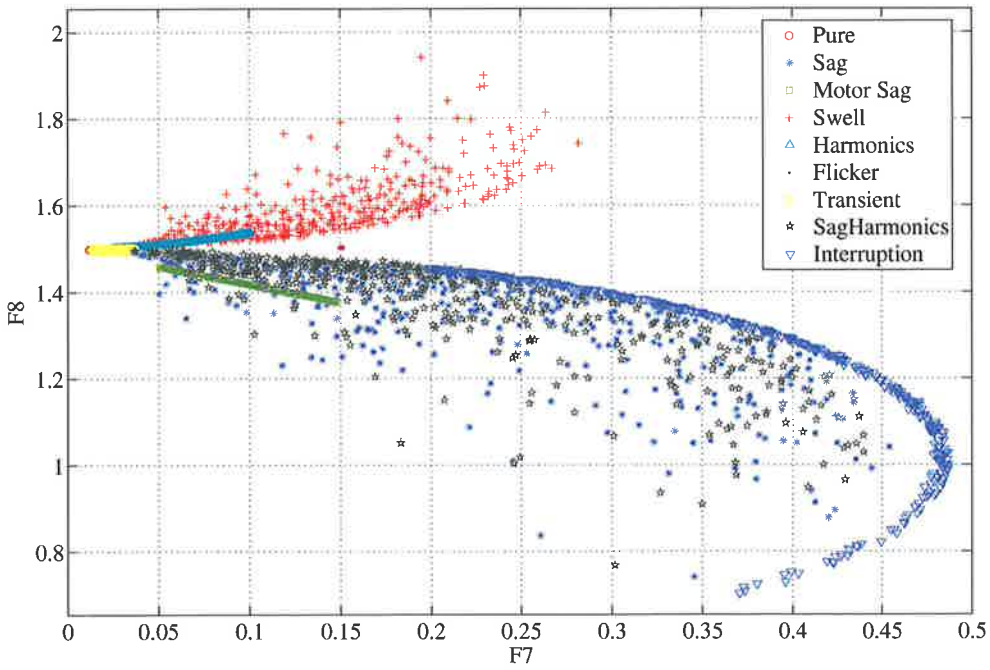

Figure 5.9: The scatter plot of the features F7 and F8 for events occurring on two phases.

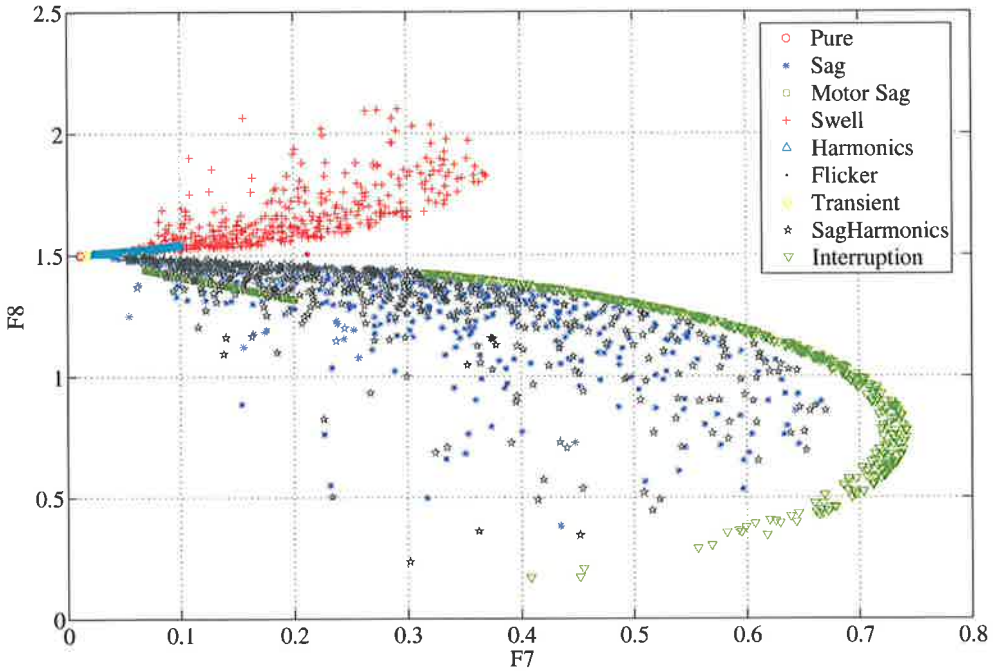

Figure 5.10: The scatter plot of the features F7 and F8 for events occurring on all three phases.

for the studied power quality events than the previously discussed techniques, the results presented in this section reveal that, some classes can be distinguished easily using the previous techniques such as the *sag with harmonics* class utilizing features from the S-Transform.

5.4.2 Scattering of features from different techniques

As it was shown in the previous sections, the combinations of features from single techniques respond differently to each of the classes studied. Therefore, in order to cover the possible combinations of the proposed features, the distinguishing capability of combinations of the features from different techniques will be examined in this section. Thus, out of the eight proposed features, there is 24 possible combinations of features that belong to different techniques. However, the focus in this section will be on some combinations of the features only, which display better capabilities to distinguish.

The scatter plot in Figure 5.11 shows the events specific regions when combining the features F2 and F3 from the Wavelet Packet transform and the S-Transform respectively. Although a slight improvement in distinguishing the *sag with harmonic* events (compared to the features using only Wavelet Packet transform in Figure 5.3) were observed, there is a significant improvement in the *swell events* region (compared to the features from the S-Transform technique only in Figure 5.5). In addition, in this combination of features, the *Transients* and the *Flicker* events were found to occupy only a small region compared to the other events. This compacted distribution make these events distinguished from others.

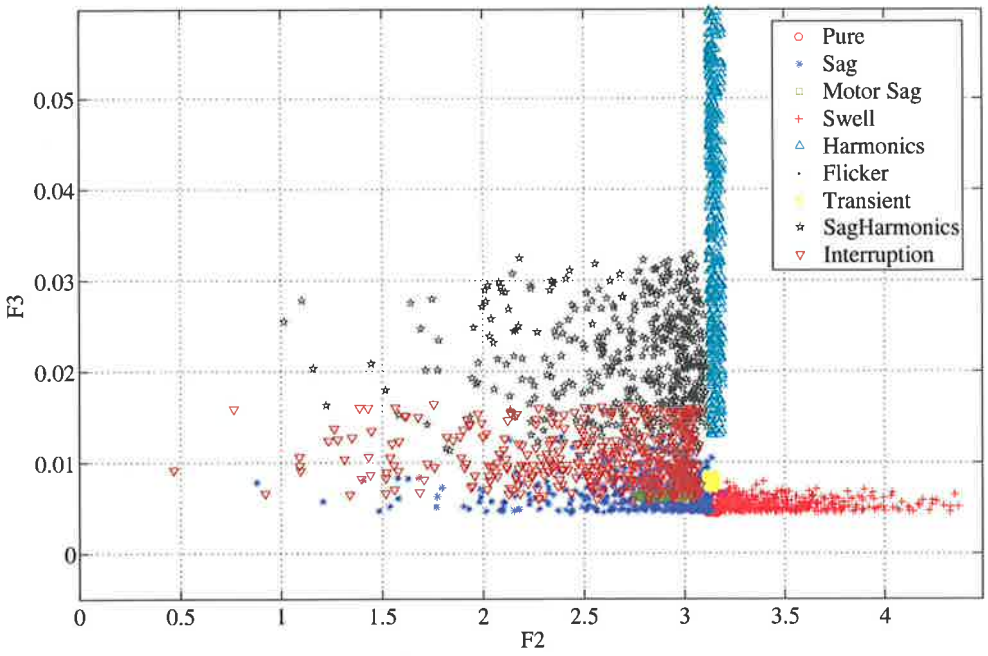

Figure 5.11: The scatter plot of the features F2 and F3.

However, it was observed that, combining the features using the Wavelet Packet transform and the Hilbert transform or the Clarke transform techniques have not resulted any significant improvements to distinguish the studied events. Some of the case studies are presented in Figures 5.12 and 5.13, which show the response of combining the Wavelet Packet transform with the Hilbert transform and the Clarke transform respectively. It should be mentioned here that when considering the features using the Clarke transform, the events were simulated only in one phase.

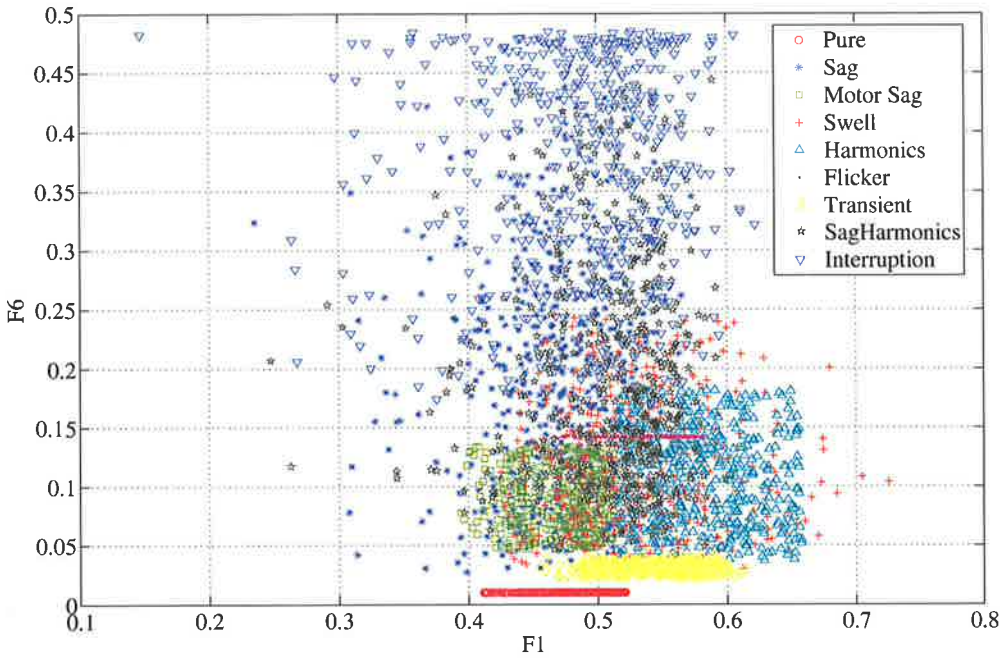

Figure 5.12: The scatter plot of the features F1 and F6.

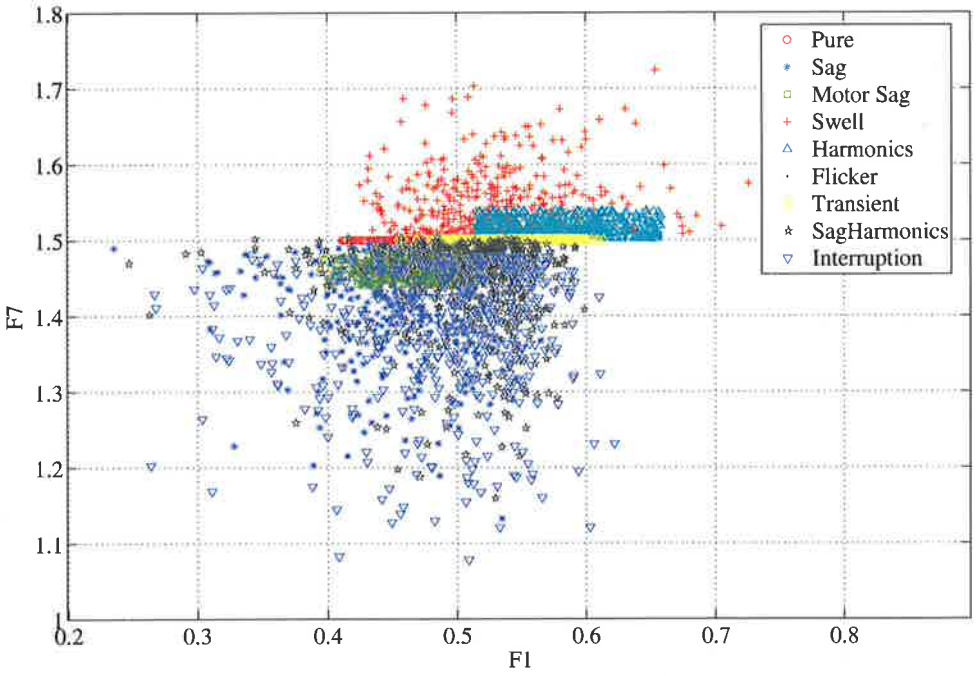

Figure 5.13: The scatter plot of the features F1 and F7.

Figures 5.14 and 5.15 demonstrates some selected cases showing the response of using combinations of the features from the S-Transform technique with the Hilbert transform (Figure 5.14) or the Clarke transform (Figure 5.15). A unique observation from these figures is the ability of the combinations considered which distinguish the *sag* and the *sag with harmonics* events in spite of the similarity between these two classes.

The final case presented in this section considered the features form Hilbert transform and Clarke transform. Although these combinations of features provide distinct regions for dissimilar events, they fail to distinguish between the similar events such as the *sag*, the *sag with harmonics*, or the *motor sag*. A selected case is given in Figure 5.16.

In addition to the results given above, further scatter plots were also produced to investigate all the possible combinations the proposed features described above. The distinguishing capability of the possible pairs of all the features is summarized in Table 5.2.

In this table, each pair of the features used to generate the scatter plots are given in the left column under the label, "Features". The numbers in the cells of the table indicate the events that overlap. The rows with bold fonts denotes the features pairs that belonging to single technique. In addition, the dash sign, "–", in some cells means the regions of these classes are totally separated from the other events.

For example, when combining the features F1 and F2, (shown as "F1 F2" in the table) the *Pure signal* classes region (event class (1)) in the scatter plot overlaps with the regions of the event classes 5, 6, and 8, which are *Transient*, *Harmonics*, and *Flicker* events respectively. Similarly, the numbers in the second cell of the first row, (3, 7, and 9), indicate that these classes' regions (*Transient*, *Sag with harmonic*, and *Interruption*) are overlap with the event class 2 region (The *sag*).

It can be concluded from the table that, the Pure class is the most distinguished class for most of the features, except for the features defined by the Wavelet tech-

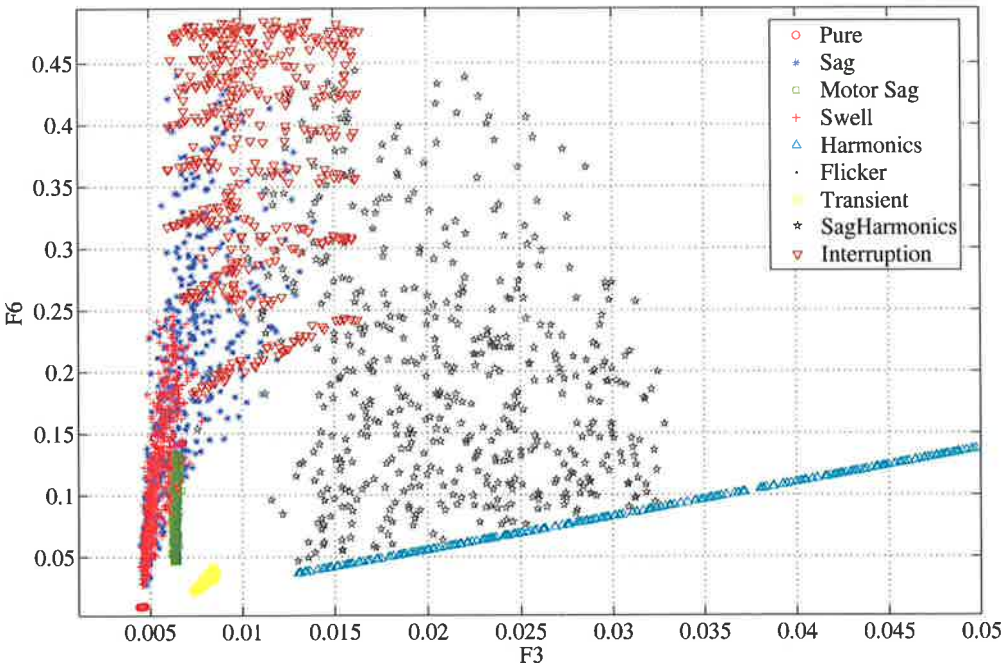

Figure 5.14: The scatter plot of the features F3 and F6.

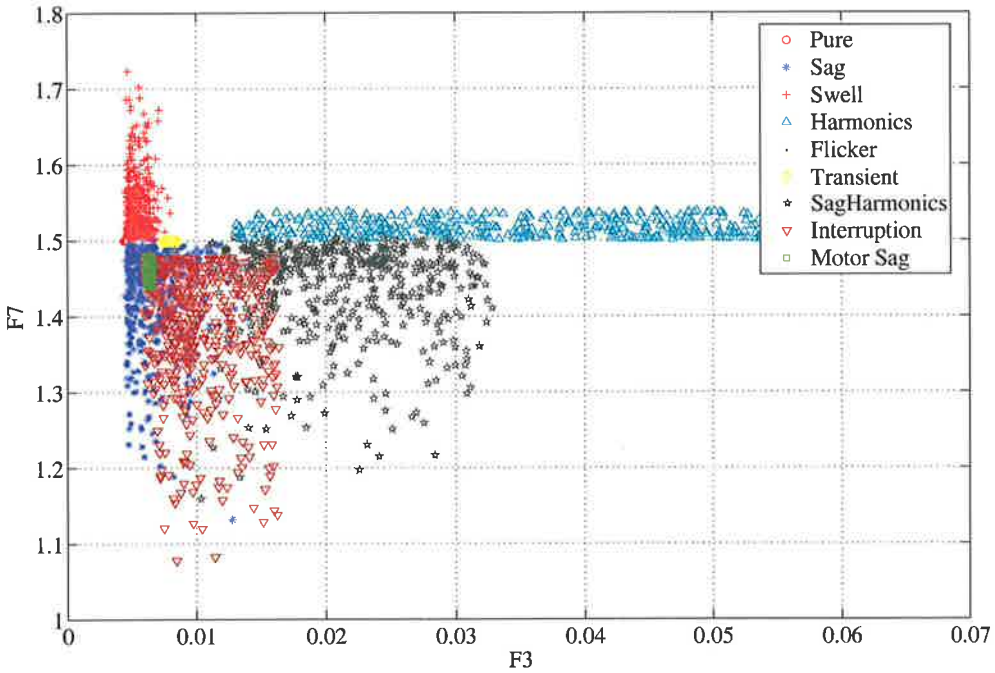

Figure 5.15: The scatter plot of the features F3 and F7.

nique. The reason for this is attributed to the sensitivity of the Wavelet technique to the phase shift of the signal which enlarges the Pure class specific region and consequently, increases the chances of overlapping with other events. On the other hand, the sag related classes, (the *sag*, the *motor sag*, and the *sag with harmonics*), are the least distinguished events. This is primarily due to the high degree of similarities among these classes.

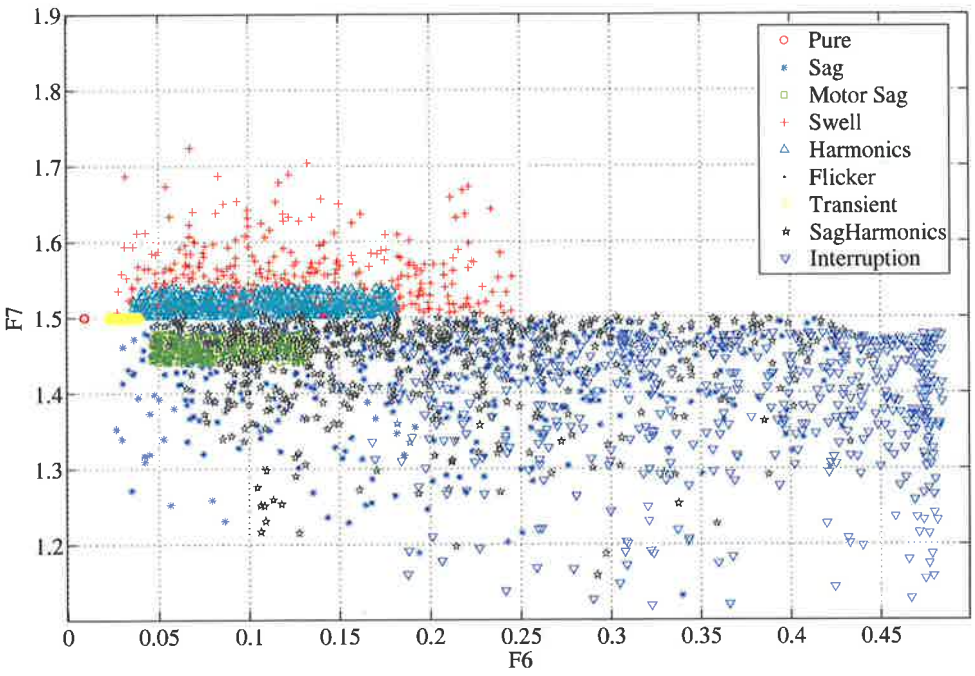

Figure 5.16: The scatter plot of the features F6 and F7.

Table 5.2: Summary of distinguishing capabilities of the combinations of the studied features

Features	Power Events Classes								
	Event class (1) Pure	Event class (2) Sag	Event class (3) Motor Sag	Event class (4) Swell	Event class (5) Transient	Event class (6) Harmonic	Event class (7) Sag+Harmonic	Event class (8) Flicker	Event class (9) Interruption
F1 F2	**5, 6, 8**	**3, 7, 9**	**2, 7, 9**	**8**	**1, 6, 8**	**1, 5, 8**	**2, 3, 9**	**1, 4, 5, 6,**	**2, 3, 7**
F1 F3	2, 4,	Overlap ALL	2, 8, 4	1, 2, 8, 3	2, 9	2, 7, 9	2, 6	2, 4	2, 5, 6
F1 F4	2, 4	Overlap ALL	2, 4, 8, 9	1, 2, 3, 8	2, 6, 7, 9	2, 5, 7, 9	2, 5, 6, 9	2, 4	2, 5, 6, 7
F1 F5	5, 6, 8	3, 7, 9	2, 7, 9	--	1, 6, 8	1, 5, 8	2, 3, 9	1, 5, 6	2, 3, 7
F1 F6	--	3, 4, 5, 6, 7, 8, 9	2, 4, 7	2, 3, 5, 6, 7, 8, 9	2, 4, 6	2, 4, 5, 7, 8	2, 3, 4, 6, 8, 9	2, 4, 6, 7	2, 4, 7
F1 F7	5, 7	3, 7, 9	2, 7, 9	6	1, 7	4, 8	1, 2, 3, 5, 9	6	2, 3, 7
F1 F8	5, 7	3, 7, 9	2, 7, 9	6	1, 7	4, 8	1, 2, 3, 5, 9	6	2, 3, 7
F2 F3	2, 4	2, 3, 9	2, 9	1	--	7,9	6,9	--	2, 3, 6, 7
F2 F4	2	1, 3, 7, 9	2, 9	6, 8	6	4, 5	2, 9	4	2, 3, 7
F2 F5	5, 6, 8	3, 7, 9	2, 7, 9	--	1, 6, 8	1, 5 ,8	2, 3, 9	1, 5, 6	2, 3, 7
F2 F6	--	3, 5, 6, 7, 9	2, 7	--	2, 6	2, 5	2, 3, 9	--	2, 7
F2 F7	5, 6, 8	3, 7, 9	2, 7, 9	--	1, 6, 8	1, 5, 8	2, 3, 9	1, 5, 6	2, 3, 7
F2 F8	5	3, 7, 9	2, 7	--	1, 6	5, 7, 8	2, 3, 6, 9	5	2, 4, 7
F3 F4	**2, 4**	**1, 3, 4, 5, 7, 8, 9**	**2, 4, 8**	**1, 2, 3, 9**	**2, 9**	**7**	**2, 6, 9**	**2, 3**	**2, 5, 7**
F3 F5	--	3, 7, 9	2, 9	--	--	--	2, 9	--	2, 3, 7
F3 F6	--	3, 4, 8, 9	2, 4	2, 3, 8, 9	--	--	9	2, 4	2, 4, 7
F3 F7	--	3, 7, 9	2, 9	--	--	--	2, 9	--	2, 3, 7
F3 F8	--	3, 4, 5, 8, 9	2, 4, 8	2, 3, 8	2	7	6, 9	2, 3, 4	2, 6
F4 F5	--	3, 7, 9	2, 9	--	6	5	2, 9	--	2, 3, 7
F4 F6	--	3, 4, 7, 8, 9	2, 4	2, 3, 7, 8, 9	--	--	2, 4, 9	2, 4	2, 4, 7
F4 F7	--	3, 7, 9	2, 9	6, 8	7	4	2, 5, 9	4	2 ,3, 7
F4 F8	--	3, 4, 6, 7, 8, 9	2, 4, 8	2, 3, 6, 7, 8, 9	6	2, 4, 5, 7	2, 4, 6, 9	2, 3, 4	2, 3, 7
F5 F6	**--**	**3, 7, 9**	**2, 7**	**--**	**6**	**5**	**2, 3, 9**	**--**	**2, 7**
F5 F7	5	3, 7, 9	2, 7, 9	6	1, 8	4, 8	2, 3, 9	5 ,6	2, 3, 7
F5 F8	5	3, 7, 9	2, 7	6	1, 6	4, 5, 8	2, 3, 9	6	2, 7
F6 F7	--	3, 7, 9	2, 7	6	6	4, 5, 8	2, 3, 9	6	2, 7
F6 F8	--	All Except 1	All Except 1	All Except 1	All Except 1	All Except 1	All Except 1	All Except 1	All Except 1
F7 F8	**--**	**3, 7, 9**	**2, 7**	**6**	**--**	**4**	**2, 3, 9**	**--**	**2, 7**

5.5 Conclusion

As the performance of the automatic clustering systems, (which will be discussed in Chapter 6), depends mainly on how distinctive the selected features are, this chapter investigates the distinguishing capability of the Wavelet transform and the S-Transform techniques. In addition, the Hilbert transform and the Clarke transform were introduced as new power quality signal processing techniques for single phase and three phase systems respectively. The detailed investigations were performed by interpreting the results using these techniques in terms of eight proposed features presented in this chapter. In these investigations, scatter plots were used to demonstrate how the proposed features can be used to distinguish among nine classes of power quality events.

Furthermore, in order to assess their capabilities to distinguish between different types of power quality events using the features proposed, it was passible to examine the ideal combination features either from single technique or from different techniques. When using only a single signal processing technique, it was found that the feature defined by the Hilbert transform and the Clarke transforms have a better distinguishing capability than the other techniques. This was clear from the least numbers of overlapping events in each class. However, it was observed for the sag related classes, combining two techniques gives a better distinguishing results. For example, the sag with harmonics class is best distinguished when selecting the pairs of features (F3 and F6), or (F3 and F7), and for the *motor sag* events, the pairs F3 and F6 have the best distinguishing results.

Chapter 6

Automatic Clustering of Power Quality Events

6.1 Introduction

THE clustering of the power quality events monitored during the tests is the principal step to analyse the causes of these events. However, due to a large number of data that may be collected in a power system, manual inspection of the events is not a practical option. Therefore, it is desirable to have an automatic analysis tool which can be integrated into the monitoring system and can be utilized to handle a large database for automatic clustering.

The principle block diagram of the automatic monitoring process can be illustrated in Figure 6.1. As shown in the figure, the distortions that represent the power quality events, can be captured using voltage and/or current signals. Then, the features that distinguish the captured signals are extracted using a suitable signal-processing technique in the 'Feature Extraction' block. Finally, the disturbances are separated automatically by applying a suitable decision-making technique(s) on the extracted features. At this stage, the decisions of the automatic monitoring systems can be further specified based on the underlying events, rather than the type only. However such approach requires a large amount of data that belong to known sources.

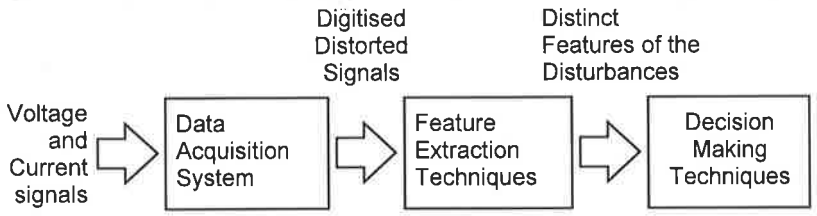

Figure 6.1: The principle block diagram of an automatic recognition system.

Therefore, this chapter investigates the automatic clustering of power quality events. The k-Nearest Neighbour technique is suggested in this study as a decision-making technique based on the features discussed in the previous chapter. The optimum selection of the number of neighbours to minimize the classification errors is also investigated.

6.2 Nearest Neighbour Recognition Technique

Although the Nearest Neighbour (NN) technique requires a large memory size to store the training data, this technique can be considered as a good candidate in automatic recognition of power quality events. This is primely due to the recent developments in the semiconductor memory technologies and reduced cost.

The main advantage of the NN technique is that it is a nonparametric technique which is simple, yet, effective in many cases [78], where no prior statistical knowledge about the data is required. The classification decisions in the NN technique are made based on a set of training features that represent all of the expected classes of power quality events. Therefore, any unknown pattern, x, is compared with all cases of the training features of data. This is done by calculating the distances between the unknown pattern and all other features, and then the unknown pattern is assigned to a class with a minimum distance. This can be written as below [75].

$$x \in W_i \quad \textbf{iff} \quad d(t_j, x) = \min\Big(d(t_j, x)\Big) \tag{6.2.1}$$

where,

W_i is the pattern class, the operator, **iff**, is a mathematical abbreviation for "if and only if", t_j is the training data sample within the class W_i, and d is the distance between the unknown pattern x, and t_j. The distance d is calculated as:

$$d(t_j, x) = \left[\sum_{j}^{N} (t_j - x)^2 \right]^{1/2} \tag{6.2.2}$$

where, N is the total number of the samples within the class W_i.

It can be noted here that the k-Nearest Neighbour (k-NN) technique is similar to the NN technique, except that the k-NN algorithm finds the first k minimum distances d, and the decision is made based on the class which has the majority of minimum distances. However, to apply the k-NN, an appropriate number of neighbours should be chosen prior to the classification, since the accuracy of the classification depends on this number.

In order to demonstrate the performance of the k-NN classifiers, the so called "confusion matrix" can be constructed using a set of test data as given below [76]:

$$\text{confusion matrix} = \begin{pmatrix} a_{11} & \cdots & a_{1n} \\ \vdots & \ddots & \vdots \\ a_{n1} & \cdots & a_{nn} \end{pmatrix}$$

where the diagonal entries a_{ii} of the confusion matrix denote the number of elements from the test data whose true class is i, and n is the total number of classes.

In this structure of the confusion matrix, the diagonal entries represent the correct classes, while the off-diagonal entries represent the misclassified classes. Therefore, the classification error and the accuracy can be calculated using the confusion matrix as follows [35].

$$N_{correct} = \sum_{i=1}^{N} a_{ii} \tag{6.2.3}$$

$$N_{error} = \sum_{i=1}^{N} \sum_{j=1}^{N} a_{ij} \qquad \forall \ i \neq j \tag{6.2.4}$$

$$Error = \frac{N_{error}}{N} \times 100\ \% \tag{6.2.5}$$

$$Accuracy = \frac{N_{correct}}{N} \times 100\ \% \tag{6.2.6}$$

where, $N_{correct}$ and N_{error} are the number of correctly classified and misclassified events respectively, N is the total number of tested events, and j and i represent the class indexes.

6.3 Optimum Number of Neighbours in the k-NN Technique

The k-NN technique was used in this study as a decision making technique for clustering power quality events automatically. The technique was tested with the most appropriate signal processing techniques as discussed in Chapter 4. Therefore, four classifiers were constructed for the investigation: the k-NN Wavelet Packet Transform, k-NN S-Transform, k-NN Hilbert Transform, and k-NN Clarke Transform classifiers. The last two classifiers are proposed in this study as new classifiers for single-phase and three-phase systems respectively.

In addition, to ensure the highest possible accuracy, the k-NN classifiers have been investigated by changing the number of neighbours for the decision, (k), from 1 to 50 neighbours. Therefore, the results given below demonstrate the optimal numbers of neighbours for given features that can minimise the classification error. In this study, all the classifiers were tested on a total of 4500 events which were divided into nine different classes as described in the pervious chapter, (pure sinewaves, sags, motor starting sags, swells, transients, harmonics, sag with harmonics, flicker, and interruptions). In addition, another set of the same number of events belonging to the known classes of events were generated and their features were calculated and used as training or reference data for the studied classifiers.

6.3.1 k-NN Wavelet Packet Classifier

The decisions in the k-NN Wavelet Packet classifier are based on combining the features F1 and F2 (the mean value and the standard deviations of the energies of the reconstructed signals) as described in the previous chapter. The performance of the k-NN Wavelet Packet classifier based on classifying 4500 events assuming different number of neighbours is demonstrated in Figure 6.2 and Table 6.1.

In Figure 6.2, the average of the classification errors were plotted against the number of neighbours utilized for the classification decisions. This figure indicates that a minimum average error of 25.58%, (see Figure 5.3 which shows why this error is high), which is obtained when the classification decision is made based on 6 neighbours. However, because the even number of neighbours may not indicate a confident classification. Therefore, the best number of neighbours is considered 5, which also indicates an error around the similar value, 25.64%. The confusion matrix at the best number of neighbours (5 neighbours) is shown in Table 6.1.

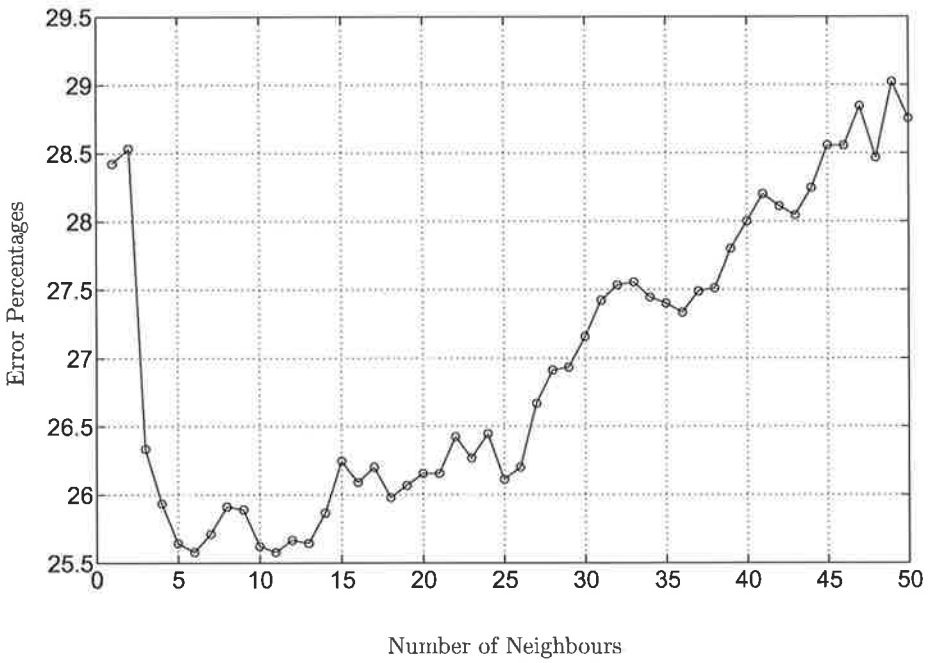

Figure 6.2: Average classification errors of k-NN Wavelet Packet (%) using the features F1 and F2.

Table 6.1: Confusion Matrix of k-NN Wavelet Packet Classifier

	Pure	Sag	Motor Sag	Swell	Harm-onics	Flicker	Trans-ient	Sag + Harm	Interr-uption
Pure	**478**	0	0	0	1	0	21	0	0
Sag	1	**190**	107	0	0	0	1	131	70
Motor Sag	0	82	**390**	0	0	0	0	27	1
Swell	0	0	0	**472**	0	28	0	0	0
Harmonics	12	0	0	0	**459**	0	29	0	0
Flicker	0	0	0	4	0	**496**	0	0	0
Transient	34	0	0	0	66	0	**400**	0	0
Sag + Harmonics	0	119	89	0	0	0	4	**200**	88
Interruption	0	88	40	0	0	0	0	111	**261**

In Table 6.1, the column headings represent the true classes of the power quality signals, and the row headings represent the classification results of the classes. For example, the number 478 in the first column and row indicates that among the 500 cases of pure sinewave signals, the k-NN classifier could classify 478 cases correctly. Although the classification error may be considered high in Figure 6.2, as indicated above, this is an average error including all the nine events, which could be reduced significantly, if similar events, such as sag, motor sag, and sag with harmonics, are excluded in the calculations of the classifier average error.

6.3.2 k-NN S-Transform Classifier

In the k-NN S-Transform Classifier, the training data are constructed to be based on the features F3 and F4 (the mean value and the standard deviation of the S-Transform spectrum). The average classification error for this classifier at different number of neighbours is presented in Figure 6.3. As the results show, the minimum average error in this case is 17.78% which occurred when the decision was based on 5 neighbours.

Similarly, the corresponding confusion matrix results for this classifier based on 5 neighbours are given in Table 6.2. Although the average error is still considered high, it can be noted that the k-NN S-Transform classifier has better classification results than the previous k-NN Wavelet Packet Classifier. For example, in this classifier, the classification of the sags due to faults, the motor starting sags and the sags with harmonics have been improved significantly, whereas the classification error of classifying the swell event has increased.

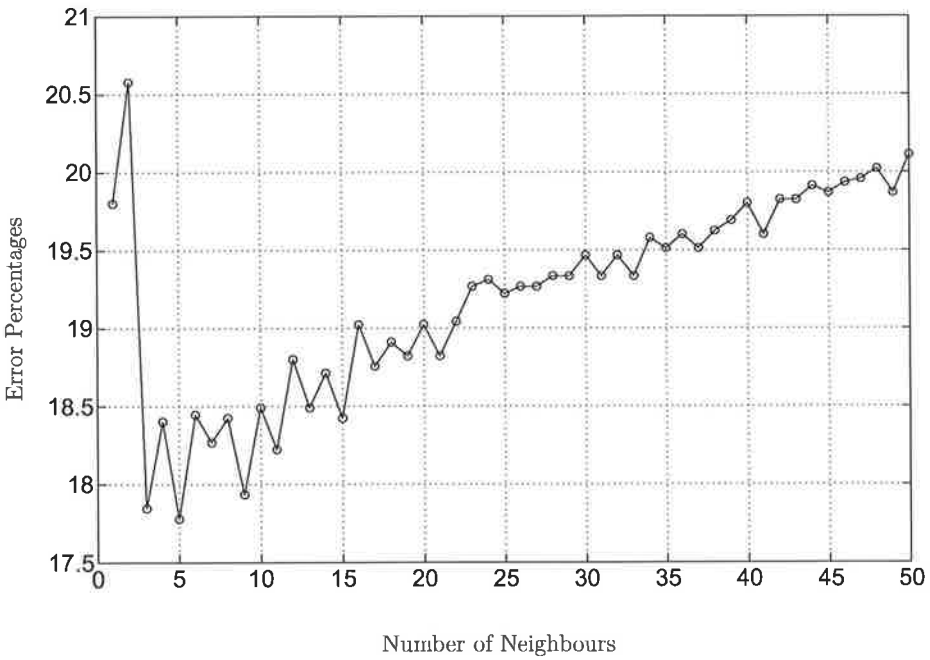

Figure 6.3: Average classification errors of k-NN S Transform (%) using the features F3 and F4.

Table 6.2: Confusion Matrix of k-NN S-Transform Classifier

	Pure	Sag	Motor Sag	Swell	Harm-onics	Flicker	Trans-ient	Sag + Harm	Interr-uption
Pure	**486**	2	0	12	0	0	0	0	0
Sag	16	**235**	3	159	0	1	18	11	57
Motor Sag	0	0	**456**	0	0	44	0	0	0
Swell	34	139	10	**308**	0	5	0	0	4
Harmonics	0	0	0	0	**476**	0	0	24	0
Flicker	0	0	41	0	0	**459**	0	0	0
Transient	0	11	0	0	0	0	**484**	0	5
Sag + Harmonics	0	8	0	0	80	0	0	**371**	41
Interruption	0	32	0	7	1	0	26	9	**425**

6.3.3 k-NN Hilbert Transform Classifier

Figure 6.4 is given to illustrate the classification error of the k-NN Hilbert Transform Classifier based on the features of F5 and F6 (the mean value and the standard of signal envelope) at different numbers of neighbours. In this classifier, a better overall classification accuracy is achieved as compared to the pervious classifiers, where the minimum average classification error is reduced to 10.8%. The number of neighbours which generated the minimum accuracy error was 1 neighbour.

The results of the confusion matrix for 1 neighbour are shown in Table 6.3. It can be concluded from this table that most of the classification errors in the k-NN Hilbert Transform are due to the pure sag events and the sag with harmonics, while the errors in classifying the motor sag events were slightly increased. Moreover, the error in the swell events was reduced considerably as compared to the k-NN S-Transformer Classifier.

Figure 6.4: Average classification errors of k-NN Hilbert Transform (%) using the features F5 and F6.

Table 6.3: Confusion Matrix of k-NN Hilbert Transform Classifier

	Pure	Sag	Motor Sag	Swell	Harm-onics	Flicker	Trans-ient	Sag + Harm	Interr-uption
Pure	**500**	0	0	0	0	0	0	0	0
Sag	0	**264**	15	0	0	0	0	214	7
Motor Sag	0	6	**494**	0	0	0	0	0	0
Swell	0	0	0	**500**	0	0	0	0	0
Harmonics	0	0	0	0	**494**	0	6	0	0
Flicker	0	0	0	0	0	**500**	0	0	0
Transient	0	0	0	0	6	0	**494**	0	0
Sag + Harmonics	0	191	9	0	0	0	0	**274**	26
Interruption	0	0	0	0	0	0	0	6	**494**

6.3.4 k-NN Clarke Transform Classifier

The proposed k-NN Clarke Transform classifier is constructed based on the features F7, and F8 (mean value and standard deviations of signal three-phase envelope). It should be emphasised here that, since the Clarke Transform is a three-phase technique, three-phase systems were also considered in the tests.

The average classification error of the k-NN Clarke Transform Classifier versus number of neighbours is shown in Figure 6.5. As can be seen from the figure, the minimum average error for this classifier is 11.5% which was based on one neighbour. It is clear from the trend of the graph that increasing the selected number of neighbours results in higher classification error.

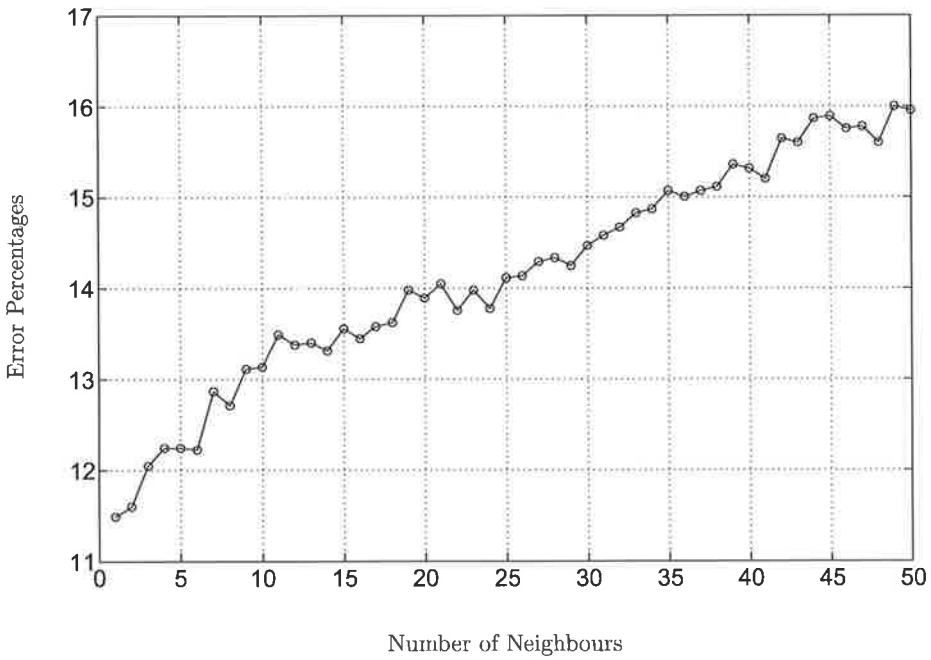

Figure 6.5: Average classification errors of k-NN Clarke Transform (%) using the features F7 and F8.

The confusion matrix with the optimal number of neighbours (one neighbour) is given in Table 6.4. Although the average error with the optimal number of neighbours, in this classifier is slightly higher as compared to the performance of the k-NN Hilbert Transform classifier, a better classification for the motor starting sag events was achieved. It can be seen from the table that the main source of the average error is due to misclassifying the sags and the sag with harmonics events, where almost half of these events were wrongly classified.

Table 6.4: Confusion Matrix of k-NN Clarke Transform Classifier

	Pure	Sag	Motor Sag	Swell	Harm-onics	Flicker	Trans-ient	Sag + Harm	Interr-uption
Pure	**500**	0	0	0	0	0	0	0	0
Sag	0	**250**	11	0	0	0	0	239	0
Motor Sag	0	1	**499**	0	0	0	0	0	0
Swell	0	0	0	**485**	15	0	0	0	0
Harmonics	0	0	0	2	**498**	0	0	0	0
Flicker	0	0	0	0	0	**500**	0	0	0
Transient	0	0	0	0	0	0	**500**	0	0
Sag + Harmonics	0	231	12	0	0	0	0	**252**	5
Interruption	0	0	0	0	0	0	0	1	**499**

6.4 Practical Implementation of k-NN Classifiers

In order to test the two proposed classifiers (k-NN Hilbert Transform and k-NN Clarke Transform classifiers) on real power quality events, Pelican-Point power generation station, in South Australia, has been monitored using the monitoring system described in chapter 3. The monitoring system was installed to monitor the voltage supply of a 160 kW, 3-phase cooling pump. The schematic diagram for the busbar metering panel in the station is presented in Figure 6.6, where the voltage sensors were installed on E1, E2, and E3 lines which are the motor feeders.

In addition, due to the inability to capture all the possible power quality classes at the selected site, previously collected real time data have been also included for testing the classifier. The tested classes of events are sag due to faults on single phase or three phases, sags due to motor starting, transients, and interruptions. Samples of these events are given in Figures 6.7 and 6.8. The performance of both classifiers on all tested real data was encouraging where all tested events were correctly classified.

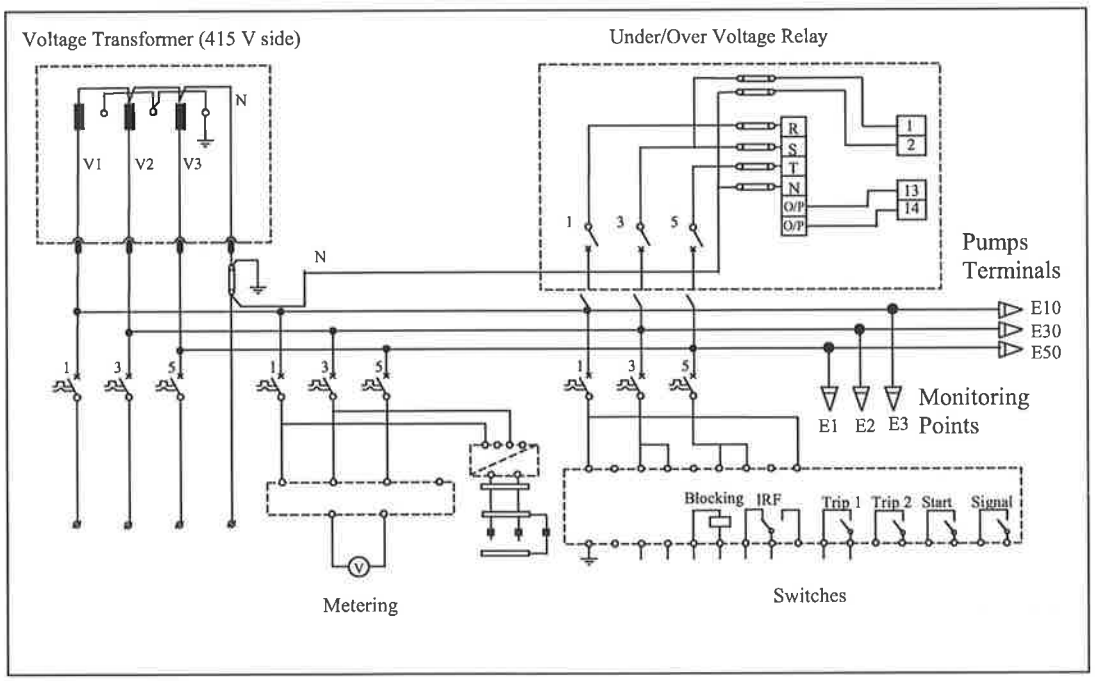

Figure 6.6: Basic wiring diagram of the monitored site in Pelican Point Power Station in South Australia.

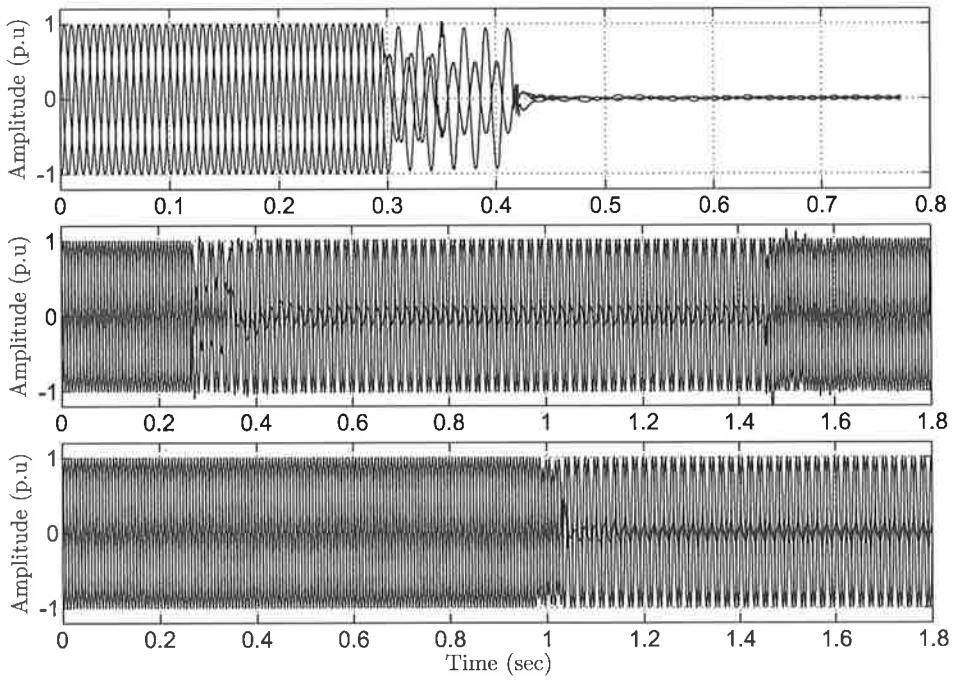

Figure 6.7: Monitored sample of real-time signals: interruption (top), and two sag events at different times (middle and bottom).

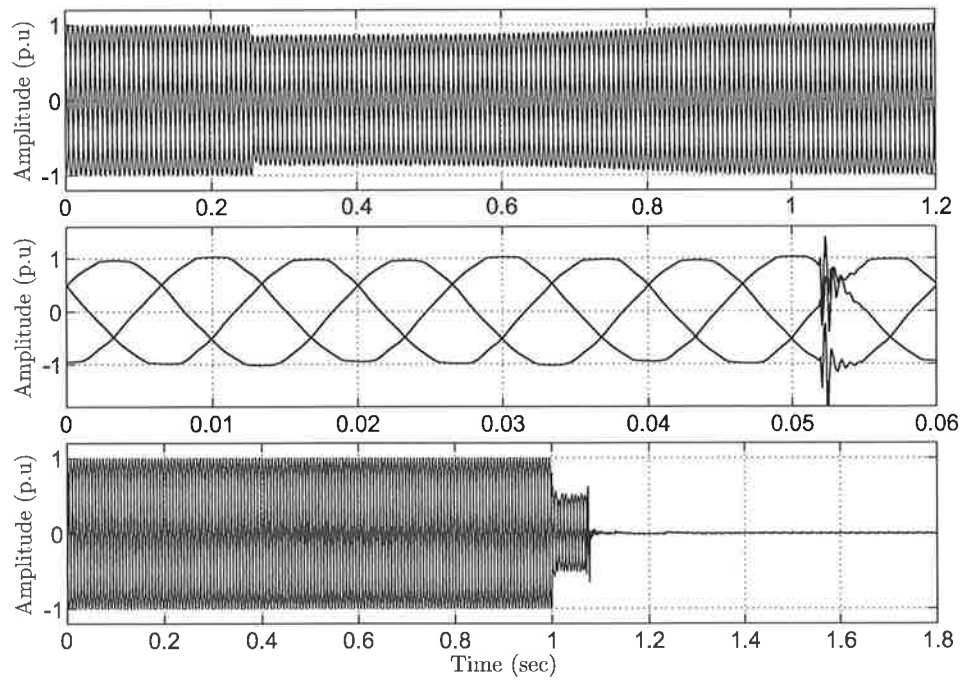

Figure 6.8: Monitored sample of real-time signals: motor sag (top), transient (middle), and interruption (bottom).

6.5 Analysing the Classified Events

Once the captured data is classified, further information about the event is usually required, which can be used for analysing the source of the events. This section shows the use of the three-phase signal envelope obtained from the Clarke transform for extracting the events characteristics such as the start (and the end), the duration and depth (or height) of the event automatically.

As will be shown in the next figures, the start, the end, and hence the duration of the events can be readily specified using the three phase envelope of the distorted signal. However, the depth (or height) of the event is not directly related to the three-phase envelope. The following figure (Figure 6.9) shows the relation between the depth of the sag events in each phase and the depth of the three-phase envelope of the signal. According to the figure, if the disturbance occurs on only one phase, the minimum value of the three phase envelope will be **1.0635** pu which is equivalent to interruption on a single phase. Similarly, in case of two phases are affected, the minimum three phase envelope will be **0.637** pu when any two phases of the three-phase system are entirely interrupted.

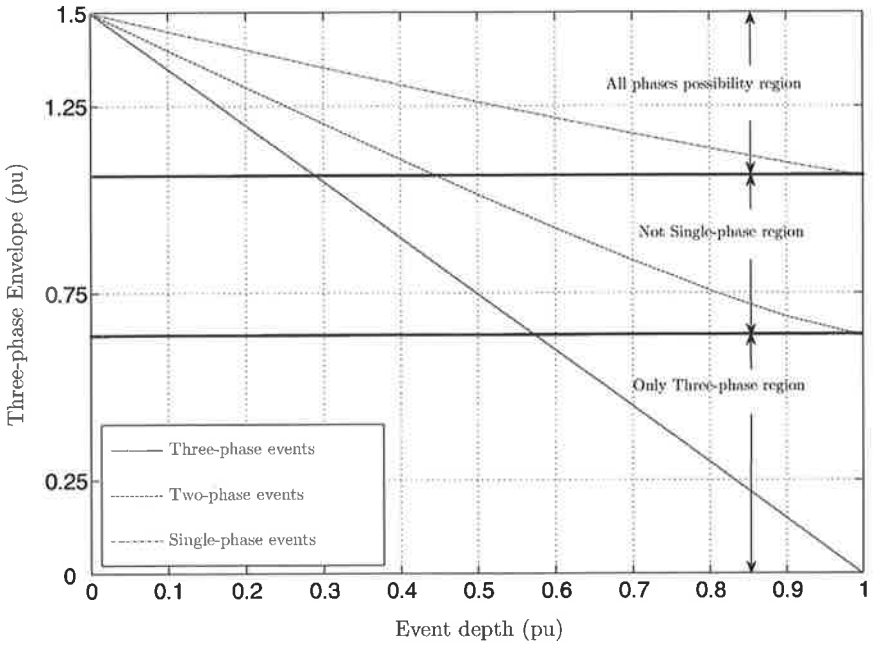

Figure 6.9: Effects of three-phase envelope on the depth of the sag events.

Therefore, three regions can be defined from the curves in the figure that can be used for distinguishing between the events on the three phases. In the first region, if the value of the three-phase envelope is less than 0.637 pu, then all the three-phases are affected by the disturbance. The second region is when the three-phase envelope is between 1.0635 pu and 0.637 pu. In this case the event could be either on two phases or three phases, but not on one phase. The third region is where the disturbance could be in either one, two, or three phases. The same discussion applies to the height of the event as shown in Figure 6.10.

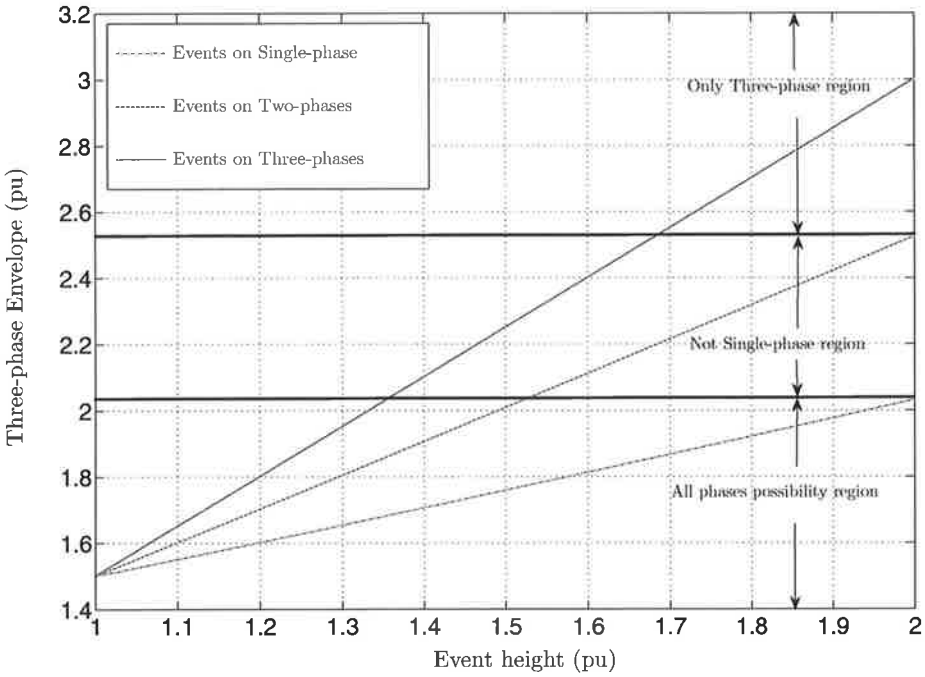

Figure 6.10: Effects of three-phase envelope on the height of the swell events.

The above discussion can be illustrated more in the following two case studies. The first case study, which shown in Figure 6.11(top), is a three phase voltage sag on the three phases. This signal was classified as an sag event by the Clarke-k-NN classifier. The sag starts at 0.53 s and ends at 1.63 s. The minimum depth of the three-phase envelope is 0.163 pu. Since the depth of the three-phase envelope is below 0.637 pu (which lies in the bottom region in Figure 6.9), it can be concluded

from the three-phase envelope directly that events are occurred on all phases. In addition, as the three-phase envelope was dropped to 0.163 pu during the sag period, the depth of the sag can be specified directly for the three-phase envelope as 0.9 pu by referring to three phase curve in Figure 6.9.

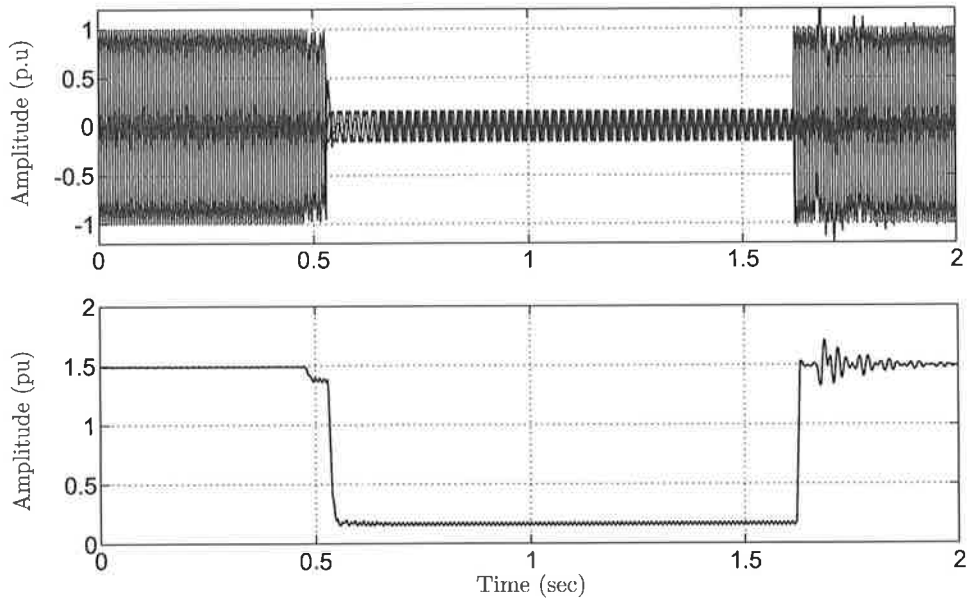

Figure 6.11: Real-time voltage sag (top), and its three-phase envelope (bottom).

The second case study in Figure 6.12 (top) represents a deep sag on one phase. This signal was classified correctly as a sag event using the k-NN Clarke transform classifier. The three-phase envelope of this signal is shown in Figure 6.12 (bottom). The starting and ending times of the event are directly identified by the envelope as 0.27 s, and 1.45 s respectively. In this case, the three-phase envelope is dropped to 1.02 pu which lies in the all-phases possibility region (between 1.5 and 1.0 pu) as shown in Figure 6.10. This means that, according to Figure 6.10, the disturbance could be one of three cases; 0.18 pu deep three phases sag, 0.3 pu deep two phases sag, or 0.8 pu single phase sag. In this case, the three-phase envelope alone is insufficient to specify the exact phase(s) that is (are) affected by the disturbance.

However, the instantaneous value of the three phase voltages during the event period can be used to identify the exact disturbed phase as discussed previously in section 5.2.4.

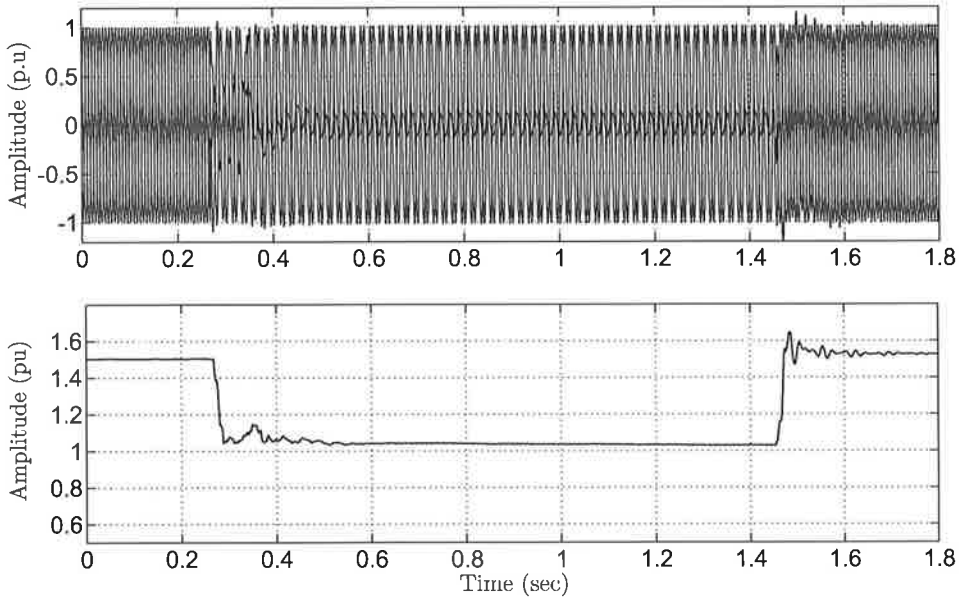

Figure 6.12: Real-time single phase sag event (top), and its three-phase envelope (bottom).

6.6 Conclusion

In the chapter, two new feature extraction techniques were examined with the k-NN technique to construct two classifiers for power quality data clustering. The k-NN Hilbert transform classifier was developed for the single phase analysis of the power systems, while the k-NN Clark transform was offered for three phase systems. The performance of these two techniques were also compared with the Wavelet Packet Transform and S-Transform techniques, using the k-Nearest Neighbour pattern recognition technique.

It was concluded that, the k-Nearest Neighbour based technique can offer an effective automatic classification of power quality events. However, it is required to identify the best number of neighbours for classifying the events accurately. Therefore, as demonstrated, to ensure a highest accuracy in each classifier, the number of neighbours was varied. This provided an error versus number of neighbour pattern where a clear conclusion could be drawn based on the increasing or decreasing profile of the average error. The results were demonstrated for a number of neighbours varying between 1 to 50 neighbours. It was observed that, above 50 neighbours, the profile of the average error follows the same pattern, which means no accuracy improvement would be expected for higher number of neighbours. In the study, a total of 4500 events were considered in testing each classifier, which were obtained from nine different types of events, each containing 500 different classes. In addition, the proposed classifiers were tested on a number of real-time signals, and the classification results were encouraging.

From the results of each classifier, it was demonstrated that the proposed two new classifiers (k-NN Hilbert Transform and k-NN Clarke Transform) were found to be very effective classifiers compared with the k-NN S Transform and k-NN Wavelet Packet Transform classifiers, except in the case of the sag with harmonic events, where the k-NN S Transform offers better solution. The classification accuracy of each individual class of event using the techniques studied are summarized in Table 6.5. For example, 100% of accuracy in the table indicates that the confidence about the classification of an event using a given technique is 100%. The table also includes the best number neighbour for each classifier, which is always less than 5 neighbours. The numbers in bold, in the table, indicate the highest accuracy that was achieved for a given event and a classifier.

As it was expected, the classification accuracy of pure sag events and sag with harmonics were low, mainly due to the similarity of these two events. However, a significant improvement have been achieved with the two proposed classifiers (k-NN Hilbert Transform and k-NN Clarke Transform) in distinguishing the pure sag events as compared to the other classifiers. As it can be seen from table 6.5, although in

case of the sag with harmonics events the k-NN S Transform has performed better than others, its performance with swell events was the lowest.

Therefore, as an overall performance, the two new proposed classifiers, for single phase and three phase systems, have provided improvements in classifying the power quality events considered, except the sag with harmonic events. It should be mentioned that more accurate results can be obtained if considering more than one of the examined classifier studied in this chapter. In this case, the decision on each class will be based on the majority decision of each classifier. However, this will costs more memory, where in this case more memory for the training data of each classifier will be required.

Table 6.5: k-NN Performance with Different Feature Extraction Techniques

Class	Classification Accuracy in %			
	k-NN Wavelet Packet	k-NN S Transform	k-NN Hilbert Transform	k-NN Clarke Transform
Pure	95.6	97.2	**100**	**100**
Sag	38	47	**52.8**	50
Motor Sag	78	91.2	98.8	**99.8**
Swell	94.4	61.6	**100**	97
Harmonics	91.8	95.2	98.8	**99.6**
Flicker	99.2	91.8	**100**	**100**
Transient	80	96.8	98.8	**100**
Sag with Harmonics	40	**74.2**	54.8	50.4
Interruption	52.2	85	98.8	**99.8**
Number of Neighbors	5	5	1	1

In addition it was demonstrated that once the captured data is classified, further information about depth (or height) of the event can be extracted automatically from the three-phase envelope of the signal. This was demonstrated by using the envelope versus depth (height) curves.

Chapter 7

Conclusions and Future Work

7.1 Conclusions

THE work presented in this thesis investigates the application of digital signal processing techniques in the power quality automating classification field, and thus, an optimized automatic monitoring system with an improved accuracy is proposed. The proposed monitoring system involved three main steps; detecting the power quality events, extracting the distinctive features that characterise each event, and clustering automatically the similar events into a pre-defined categories. The main conclusions in each step are summarised in the following subsections.

7.1.1 Detection of power quality events

It was shown in the study that, because power quality disturbances can affect the voltage signals in power systems in different ways, the existing detection strategies are not suitable for monitoring all power quality events. Therefore, in this study, an alternative detection technique is proposed which is based on monitoring all of the three-phase signals in power systems simultaneously and has high sensitivity to both short and long duration events. A developed monitor system that implements the proposed detection technique was tested on real time signals.

7.1.2 Extraction of Power Quality Features

Based on the recent literature on feature extraction techniques, four techniques widely implemented are: the Short Time Fourier Transform (STFT), the Continuous Wavelet Transform (CWT), the Wavelet Multiresolution Technique (MRA) (or the more generalised form of the technique, the Wavelet Packet Transform, (WPT)), and the S-Transform (ST). In this study, the practical implementations of these techniques are investigated using real power quality signals belong to different categories according to the IEEE standard [59]. The advantages and disadvantages of each technique have been discussed.

Among the studied techniques, the STFT and CWT were found to be the least preferable alternatives for power quality analysis. The main disadvantage of the STFT technique was the frequency and time resolution trade off due to its fixed window size. The main drawback of the CWT technique was its redundancy in using a large number of scales which make it more difficult to interpret its results, while its discrete version (MRA) can offer sufficient information to identify power quality disturbances using only a limited number of scales.

In addition, the Hilbert Transform, (HT), and Clarke Transform, (CT), are introduced as new power quality techniques and compared with the previous power quality techniques. The HT technique is used for analysing single phase signals, whereas the CT technique is used for analysing three-phase signals. In both techniques changes in the calculated envelope signal(s) is used to monitor disturbances in the signals.

In order to be able to examine the distinguishing capability of the different feature extraction techniques, several features have been proposed based on the WPT, ST, HT, and CT. The ability of the proposed features to distinguish between nine types of power quality events was tested. The test data set included types of sag events such as sag due to faults, sag due to starting induction motors, and sag with harmonics. Scatter plots were used to demonstrate how the proposed features could be used in combinations, (either from a single technique or different techniques),

to distinguish between the nine classes. When using features from a single signal processing technique, it was found that the features defined by the HT and CT have a better distinguishing capability than the other techniques. This was clear from the least numbers of overlapping events in each class. However, it was observed that for the sag related classes, (i.e. sag due to faults, sag due to motor starting, and sag with harmonics classes), combining features from ST technique with the proposed techniques gives better results.

7.1.3 Automatic Clustering of Power Quality Events

The k-Nearest Neighbour pattern recognition technique, (k-NN), was used in this study as a decision-making technique. Although the k-NN technique requires a large capacity of memory to store the training data, due to the recent developments in semiconductor memory technologies, it is a good candidate in automatic recognition of power quality events. The main advantage of the k-NN technique is that it is nonparametric technique which is simple, yet, effective in many cases, as no prior statistical knowledge about the data is required. The k-NN was used with the proposed features from the HT and CT techniques to construct two new classifiers for single-phase systems and three-phase systems respectively. As the number of neighbors affects the accuracy of the decisions, the optimum number of neighbors in each classifier was determined.

The performance of the proposed classifiers was compared with k-NN classifiers that use WPT and ST techniques. From the results of each classifier, it was demonstrated that the proposed two new classifiers (k-NN HT and k-NN CT) were found to be very effective classifiers compared with the k-NN ST and k-NN WPT classifiers, except in the case of the sag with harmonic events, where the k-NN ST offers a better solution. Based on tests on 4500 simulated cases, the overall accuracy of the k-NN CT was 88.5% and k-NN HT was 89.2% as compared with 74.4% and 82.2% for k-NN WPT and k-NN ST classifiers respectively. It should be noted that the accuracy is calculated based on all nine studied power quality classes, and could be increased significantly if the detailed classes were excluded from the calculations.

7.2 Future Work

One advantage of the proposed classifiers (for single phase system and three-phase system) is their ability to be readily used in classifying other classes of power quality events. In this study, nine classes of power quality events have been considered. However, more work can be done to enhance the ability to determine the underlying cause of the disturbances. To achieve this, a sufficiently large database of measurements which has been classified by cause is required. For example, for harmonic distortion, the order and amplitude of the harmonics can indicate the source of the harmonics. In addition, a knowledge of the operating characteristics of the system that is being monitored (e.g. protection system, voltage control methods, load characteristics) can be incorporated into the knowledge-base of the classifier to improve the decisions making process.

Furthermore, other information that can be of interest is the determination of the location of the power quality events in power system. One way to achieve this is by using the measured voltage and current signals to calculate the power flow in the power system which may used to identify the location of the events.

Appendix A

Calculation Tables for Choosing an appropriate Mother Wavelet

The following tables (Tables A.1 to A.4), shows the percentage difference between the calculated energies at 32 decomposition levels of tested signals described in section 4.3.6.2, (Signals A, B, C, and D) to their reference pure signals. These values are used as an indicator on how the mother wavelet can distinguish between the pure and the distorted signals. In the tables 11 mother wavelets are included in the comparison. The last column shows the mother wavelet which gives the maximum difference in the energies.

Table A.1: Energy values of 32 reconstructed signals form Signal A using WPT

db2	db4	db6	db8	db10	db12	db40	coif1	coef5	sym2	sym8	Total Max	Name MAX
0.43805	0.434	0.43419	0.43493	0.43317	0.43537	0.4347	0.43407	0.43476	0.43805	0.43288	0.43805	db2
0.36387	2.6312	8.49	3.023	3.9679	2.2299	3.6282	0.070615	1.6655	0.36387	3.4062	8.49	db6
0.26975	5.0489	3.9683	8.7929	4.9577	8.6104	2.9658	0.24322	3.988	0.26975	2.1963	8.7929	db8
6.2351	3.5875	4.8959	4.5313	2.0556	1.2752	6.6688	5.3496	1.9194	6.2351	2.6054	6.6688	db40
0.12842	3.6418	18.874	6.4615	24.898	7.1605	8.1211	0.93212	17.477	0.12842	12.452	24.898	db10
3.7282	4.5652	5.1644	5.8678	9.2666	6.4883	7.9624	28.523	12.336	3.7282	4.7042	28.523	coif1
21.422	3.6953	6.4807	5.4242	2.7807	1.5194	4.2817	24.592	5.8818	21.422	1.1224	24.592	coif1
11.362	2.37	0.91911	3.7787	5.2489	2.655	2.3116	4.5482	3.0181	11.362	0.43074	11.362	db2
0.9962	5.8356	57.649	48.37	22.104	14.995	23.484	0.9821	22.105	0.9962	26.499	57.649	db6
8.0526	12.659	8.6418	9.8747	6.6964	7.3849	18.204	4.2232	16.163	8.0526	13.275	18.204	db40
18.793	13.415	42.703	15.662	12.399	16.257	21.796	7.275	26.103	18.793	11.516	42.703	db6
10.701	11.713	14.506	12.032	12.428	16.163	18.616	6.68	30.722	10.701	10.134	30.722	coif5
36.304	6.7233	24.965	12.634	12.738	7.7442	21.934	28.603	7.1345	36.304	10.922	36.304	db2
14.829	2.5566	21.959	5.656	19.023	9.1175	13.681	6.1708	4.1314	14.829	10.18	21.959	db6
19.243	8.3197	11.752	9.4926	13.506	7.4145	9.6323	3.6581	12.263	19.243	6.0073	19.243	db2
3.9955	11.629	22.095	13.993	20.775	8.6085	15.599	1.8927	9.7451	3.9955	17.088	22.095	db6
0.41915	85.67	75.467	791.24	420.41	565.27	493.59	1.4591	155.68	0.41915	712.07	791.24	db8
1.2997	61.832	42.529	172.86	192.61	155.83	127.31	3.4851	113.07	1.2997	103.09	192.61	db10
4.2777	56.077	105.66	69.72	64.277	53.875	69.939	15.941	67.691	4.2777	67.766	105.66	db6
1.4074	95.124	61.158	339.04	174.27	105.97	72.655	19.725	90.93	1.4074	71.197	339.04	db8
7.0031	78.44	21.471	41.083	25.76	15.108	45.437	21.166	36.573	7.0031	14.117	78.44	db4
7.1732	70.735	15.542	30.81	34.321	27.966	30.68	8.1601	62.004	7.1732	18.274	70.735	db4
7.4667	51.654	52.972	34.83	67.897	47.323	64.033	7.6893	92.7	7.4667	59.819	92.7	coif5
1.9455	64.859	35.953	78.793	36.005	22.705	34.712	2.005	36.427	1.9455	23.899	78.793	db8
8.1105	125.45	26.529	9.8392	34.61	121.02	12.233	19.05	17.53	8.1105	18.672	125.45	db4
10.686	185.5	12.47	6.1968	17.595	78.325	13.321	14.664	11.083	10.686	11.493	185.5	db4
41.23	127.28	15.759	9.0575	22.067	29.381	11.336	8.2198	21.52	41.23	9.2799	127.28	db4
12.116	176.76	14.44	11.3	31.473	40.434	12.083	4.558	24.618	12.116	5.5803	176.76	db4
10.955	44.712	10.894	33.256	56.213	29.576	32.759	31.029	24.067	10.955	15.023	56.213	db10
6.9493	72.805	16.679	29.763	39.299	30.65	18.6	11.432	23.69	6.9493	19.03	72.805	db4
15.542	143.99	14.191	4.4148	26.227	19.976	18.191	16.753	11.985	15.542	14.476	143.99	db4
11.034	98.895	3.8167	8.0219	63.505	15.412	20.453	3.4074	21.322	11.034	6.8173	98.895	db4

Table A.2: Energy values of 32 reconstructed signals form Signal B using WPT

db2	db4	db6	db8	db10	db12	db40	coif1	coef5	sym2	sym8	Total Max	Name MAX
0.25399	0.23549	0.21301	0.24839	0.21337	0.23478	0.22548	0.20188	0.24232	0.25399	0.20974	0.25399	db2
3.3905	15.489	30.012	19.375	18.631	11.111	18.547	1.3005	11.405	3.3905	18.259	30.012	db6
2.458	20.571	13.557	21.246	14.201	22.918	13.449	1.3497	19.128	2.458	9.6147	22.918	db12
25.789	28.017	18.55	15.388	12.993	7.7757	24.664	17.354	4.6065	25.789	17.067	28.017	db4
2.4205	3.8073	10.654	9.222	19.862	4.6702	6.0858	2.5489	13.978	2.4205	10.566	19.862	db10
16.597	11.188	10.455	9.6346	12.65	12.836	13.155	51.297	19.001	16.597	9.4201	51.297	coif1
36.132	10.926	24.532	27.468	18.637	9.7056	10.057	43.062	15.395	36.132	5.1634	43.062	coif1
35.082	7.2409	4.9825	14.969	25.631	9.0289	10.249	25.876	7.82	35.082	2.9495	35.082	db2
2.9489	3.4888	20.94	11.006	9.781	10.187	7.2304	3.0129	7.7717	2.9489	7.9078	20.94	db6
18.468	9.9111	5.6143	4.4636	2.3046	2.7264	5.3885	12.279	7.7928	18.468	6.2774	18.468	db2
54.229	16.873	23.761	2.9863	4.8478	2.8729	4.5915	12.788	4.9273	54.229	3.1376	54.229	db2
36.352	5.0441	4.9324	2.649	2.3506	3.3502	3.8683	14.99	6.9685	36.352	1.405	36.352	db2
27.156	3.9627	23.882	4.9576	12.112	6.3175	15.924	18.248	3.9899	27.156	8.491	27.156	db2
10.96	4.8546	26.254	4.0927	8.4616	6.4379	6.4774	7.3112	3.3028	10.96	7.4498	26.254	db6
18.417	8.1452	5.2462	1.9191	3.066	0.64587	1.3612	9.7286	2.8845	18.417	3.1026	18.417	db2
7.2613	8.4962	8.0915	7.7728	8.5564	2.7816	2.6949	4.1721	2.188	7.2613	6.2247	8.5564	db10
0.83274	83.418	73.854	740.94	400.19	546.66	475.48	2.6167	145.56	0.83274	675.87	740.94	db8
3.8228	62.687	40.006	158.36	167.11	137.2	125.87	8.8254	108.41	3.8228	92.539	167.11	db10
9.1203	53.909	90.124	73.165	64.835	48.421	65.611	27.172	76.754	9.1203	63.665	90.124	db6
4.6677	79.69	51.516	299.07	180.01	98.348	64.001	29.49	78.548	4.6677	67.651	299.07	db8
8.5925	63.936	21.289	36.446	21.505	11.649	37.346	17.998	37.84	8.5925	11.679	63.936	db4
3.4033	58.612	17.075	30.067	33.301	21.605	28.824	7.5415	53.895	3.4033	12.575	58.612	db4
9.03	48.554	63.544	33.045	57.469	50.66	62.822	10.89	89.591	9.03	61.965	89.591	coif5
4.0331	43.686	29.627	74.546	30.159	20.638	30.548	4.8911	24.977	4.0331	19.697	74.546	db8
3.5238	34.816	10.077	6.2098	11.012	30.854	5.8561	9.3944	6.8557	3.5238	9.5525	34.816	db4
7.2885	103.09	6.3359	4.1385	11.99	44.82	8.0202	4.9436	5.7776	7.2885	5.2409	103.09	db4
22.438	90.437	16.506	9.6418	18.861	24.289	11.111	6.7075	22.811	22.438	9.2537	90.437	db4
6.4822	74.062	6.5009	9.1125	19.92	21.833	12.262	3.0101	14.446	6.4822	3.7782	74.062	db4
7.1605	37.15	7.0889	27.22	50.71	25.918	29.275	27.531	17.949	7.1605	16.774	50.71	db10
5.7095	37.35	11.187	17.583	22.068	22.178	11.823	7.9863	15.253	5.7095	12.954	37.35	db4
8.6702	58.552	6.3055	5.2719	22.042	15.391	22.747	4.9176	8.5249	8.6702	8.3472	58.552	db4
4.6729	55.912	2.5667	3.4671	38.61	12.26	12.897	2.2489	15.133	4.6729	5.4758	55.912	db4

Table A.3: Energy values of 32 reconstructed signals form Signal C using WPT

db2	db4	db6	db8	db10	db12	db40	coif1	coef5	sym2	sym8	Total Max	Name MAX
0.035594	0.036865	0.03478	0.035137	0.035383	0.035178	0.03524	0.032264	0.035379	0.035594	0.035053	0.036865	db4
0.034214	0.10202	0.16887	0.046309	0.67975	0.22805	0.39913	0.080401	0.34554	0.034214	0.086121	0.67975	db10
0.085063	0.68021	2.5855	4.831	3.5193	4.0733	1.9759	0.1026	2.7923	0.085063	1.0958	4.831	db8
0.38573	1.3641	1.293	2.6153	0.95277	0.54343	3.2066	0.080021	0.87319	0.38573	0.67089	3.2066	db40
0.082078	1.3464	5.5653	4.4024	9.7656	2.2727	2.6479	0.13828	5.6076	0.082078	5.2263	9.7656	db10
0.13673	0.56378	1.6082	2.407	3.904	2.0002	2.6293	0.59391	4.1454	0.13673	1.5182	4.1454	coif5
7.951	4.9306	10.168	9.6185	4.6415	2.2873	3.8012	7.4721	4.5921	7.951	1.9346	10.168	db6
6.8655	0.59979	0.75514	1.5304	2.7427	1.2103	1.0084	2.0624	1.091	6.8655	0.078013	6.8655	db2
0.020088	0.36089	4.5735	3.3237	1.7485	1.4757	1.4769	0.016904	1.7016	0.020088	1.7865	4.5735	db6
0.069285	0.9264	0.82898	0.78553	0.28246	0.41463	1.1795	0.023861	1.6775	0.069285	1.5243	1.6775	coif5
4.5619	6.3918	10.477	1.8112	1.9915	1.6658	1.5877	4.7854	3.3523	4.5619	1.387	10.477	db6
3.8796	1.0501	0.68343	0.453	0.53004	0.60344	0.82795	2.4614	1.8205	3.8796	0.2899	3.8796	db2
13.675	1.959	16.522	4.0337	5.4475	2.9806	9.7837	8.0057	2.3663	13.675	4.4858	16.522	db6
3.8994	1.0812	7.2101	0.61169	3.1241	1.3947	1.2542	2.209	0.77947	3.8994	2.3385	7.2101	db6
8.9249	2.7295	3.7628	0.89664	1.9345	0.64613	0.9889	2.4806	1.4001	8.9249	0.98015	8.9249	db2
0.7493	1.1292	1.7598	2.0287	1.4525	0.38897	0.75037	0.11834	0.28352	0.7493	0.89441	2.0287	db8
0.042988	12.681	11.446	123.37	64.337	89.916	77.293	0.012936	23.334	0.042988	115.35	123.37	db8
0.023608	9.5386	6.001	26.979	30.068	23.004	20.621	0.050022	18.089	0.023608	15.071	30.068	db10
1.1311	8.1321	14.551	9.8582	9.433	7.3313	9.3901	6.2264	10.278	1.1311	9.7138	14.551	db6
0.077497	13.945	9.1906	53.216	29.331	16.555	10.993	5.5125	13.908	0.077497	11.032	53.216	db8
2.7125	15.275	3.1245	5.9728	3.4829	1.4636	5.1331	5.7842	5.0348	2.7125	1.5511	15.275	db4
1.087	12.729	1.9345	3.9306	4.4745	3.1266	3.8911	1.8822	7.4066	1.087	1.8859	12.729	db4
4.8171	8.9301	8.5632	4.9536	9.0691	6.7094	9.6178	2.6528	13.456	4.8171	8.2449	13.456	coif5
0.2211	7.9324	4.4087	11.591	4.5399	2.7625	4.4675	0.31866	4.5204	0.2211	2.8262	11.591	db8
0.415	10.696	1.9001	0.59674	2.1703	9.4373	0.59261	1.5432	1.0167	0.415	1.4465	10.696	db4
1.362	25.237	0.65357	0.36035	2.034	9.1893	0.99895	1.0829	0.5522	1.362	0.69029	25.237	db4
7.2544	19.468	2.1964	1.0931	2.6723	3.6017	0.90865	1.3975	2.6941	7.2544	0.83677	19.468	db4
0.62699	16.681	1.1	1.145	3.1813	3.5201	1.5451	0.22717	2.8682	0.62699	0.24566	16.681	db4
2.0941	10.433	1.079	4.4026	7.7554	3.9487	5.1522	9.7468	3.1472	2.0941	2.1385	10.433	db4
1.3719	8.3768	1.5352	2.8874	4.0646	3.7624	1.9052	2.0814	2.5189	1.3719	1.7402	8.3768	db4
1.9085	17.574	1.0707	0.43545	3.8309	2.208	3.12	1.3587	1.0262	1.9085	1.4181	17.574	db4
0.38692	9.6208	0.22341	0.33246	6.6371	1.6272	1.8091	0.10829	2.4961	0.38692	0.66902	9.6208	db4

Table A.4: Energy values of 32 reconstructed signals form Signal D using WPT

db2	db4	db6	db8	db10	db12	db40	coif1	coef5	sym2	sym8	Total Max	Name MAX
0.01808	0.017949	0.017922	0.018034	0.017905	0.017991	0.017982	0.017867	0.017997	0.01808	0.017898	0.01808	db2
0.09642	0.51065	1.5824	0.69052	0.99969	0.32137	0.80662	0.11797	0.28992	0.09642	0.94263	1.5824	db6
0.33106	4.68	4.1925	12.183	9.3261	9.5038	2.1571	0.35507	2.2637	0.33106	4.8839	12.183	db8
11.062	1.6651	2.5452	0.97583	0.76968	0.66208	2.0722	4.8631	0.61759	11.062	1.9614	11.062	db2
16.088	13.757	207.99	110.32	84.675	87.764	103.48	3.4172	59.13	16.088	45.237	207.99	db6
77.697	12.997	95.598	84.594	78.434	85.376	103.87	66.089	168.66	77.697	38.527	168.66	coif5
26.624	5.3667	12.861	14.546	13.064	3.5886	8.8958	25.845	15.935	26.624	2.1203	26.624	db2
314.73	13.166	13.175	34.837	59.583	32.696	30.296	10.5	19.157	314.73	3.8365	314.73	db2
14.367	38.179	595.14	617.12	98.602	147.62	199.91	17.866	197.95	14.367	207.18	617.12	db8
36.95	138.24	169.4	568.2	125.35	98.966	168.62	67.68	275.95	36.95	232.72	568.2	db8
247.57	49.901	1818.5	129.2	287.94	136.95	157.92	36.8	163.26	247.57	141.36	1818.5	db6
394.6	47.824	71.836	88.628	178.22	332.14	186.78	17.864	182.88	394.6	110.91	394.6	db2
105.9	85.874	362.8	79.667	268.56	52.956	109.62	273.76	107.35	105.9	461.36	461.36	sym8
39.539	111.37	590.92	78.193	189.31	140.36	125.18	171.31	198.82	39.539	138.96	590.92	db6
89.258	113.41	56.221	86.018	229.78	98.81	135.18	60.774	170.47	89.258	232.17	232.17	sym8
93.112	107.81	84.534	162.6	319.22	147.96	193.99	8.1513	83.732	93.112	281.68	319.22	db10
22.564	3974.5	2999.9	23578	18691	19575	9833.1	30.152	4559.1	22.564	12731	23578	db8
12.933	1173	1817.8	5500.1	6759.9	7549.8	1598.9	78.5	1531.9	12.933	3000.8	7549.8	db12
47.743	380.42	2252.6	2673.5	987.65	702.8	1018.1	53.379	764.86	47.743	1808.1	2673.5	db8
81.936	1728.5	2123	5067.5	2545.3	1364.7	1049.9	329.89	1063.9	81.936	906.32	5067.5	db8
39.464	832.65	163.11	1205.5	95.99	57.362	478.08	28.094	445.86	39.464	87.658	1205.5	db8
73.584	1115.7	127.18	1122.3	279.51	293.69	351.28	76.467	939.89	73.584	174.79	1122.3	db8
62.295	913.28	880.89	861.43	941.01	330.05	1615.6	82.712	1647.4	62.295	455.79	1647.4	coif5
36.211	754.91	409.7	824.07	424.79	202.33	366.37	38.555	617.83	36.211	192.84	824.07	db8
84.349	1032.6	130.78	142.03	496.86	717.5	129.35	142.2	49.94	84.349	9.6462	1032.6	db4
156.8	2650.9	147.78	111.21	514.9	1121.3	157.62	68.282	36.787	156.8	14.125	2650.9	db4
423.9	633.47	29.333	93.24	303.53	259.36	94.506	30.665	288.88	423.9	17.421	633.47	db4
148.42	692.67	137.73	176.09	531.31	267.27	205.55	48.857	202.1	148.42	11.025	692.67	db4
128.25	124.12	20.143	588.42	728.44	329.33	269.02	279.33	55.208	128.25	386.77	728.44	db10
490.11	248.01	45.469	284.64	475.94	312.02	145.54	125.44	207.2	490.11	132.03	490.11	db2
377.89	1534.5	60.985	70.493	393.07	211.35	262.68	68.154	58.979	377.89	102.76	1534.5	db4
121.62	1001.2	19.303	44.847	406.99	138.04	117.85	22.364	159.35	121.62	63.008	1001.2	db4

List of Publications

[P1] Gargoom, A.M.; Ertugrul, N.; and Soong, W.L. 'Comparative Study of using Different Mother Wavelets on Power Quality Monitoring', Australian Universities Power Engineering Conference, AUPEC04, 26-29 September, 2004, Brisbane, Australia.

[P2] Gargoom, A.M.; Ertugrul, N.; and Soong, W.L.; 'A Comparative Study on Effective Signal Processing Tools For Power Quality Monitoring', the 11th European Conference on Power Electronics and Applications (EPE), Dresden, Germany, EPE 2005.

[P3] Gargoom, A.M.; Ertugrul, N.; and Soong, W.L.; 'A comparative study on effective signal processing tools for optimum feature selection in automatic power quality events clustering', Industry Applications Conference, 2005. Fortieth IAS Annual Meeting. Volume 1, 2-6 Oct. 2005 Page(s): 52 - 58.

[P4] Gargoom, A.M.; Ertugrul, N.; and Soong, W.L.; 'Automatic recognition of power quality events', In review for: IEEE Transaction on Power Delivery, March, 2006.

[P5] Gargoom, A.M.; Ertugrul, N.; and Soong, W.L.; 'Automatic Classification and characterisation of power quality events', In review for: IEEE Transaction on Power Delivery, August, 2006.

Bibliography

[1] Douglas, J., 'Solving problems of power quality', in EPRI journal, Vol. 18, no.8, Dec. 1998, Page(s): 6-15.

[2] Clemmensen, Jane M., 'Estimating the cost of Power Quality', IEEE Spectrum, June 1998, Page(s): 40-41.

[3] Gaouda, A. M., 'Wavelet automated recognition system for power quality monitoring', PhD thesis, Waterloo, Canada, 2001.

[4] Thallam, R.S.; and Eckroad, S., 'Multimode battery energy storage system for custom power applications', IEEE Power Engineering Society 1999 Winter Meeting, Vol. 2, 31 Jan-4 Feb 1999, Page(s): 1147 - 1150.

[5] Cho, J.W.; Kim, H.J.; Bae, J.H.; Sim, K.D.; and Seong, K.C., 'Fabrication and test of a 3MJ SMES magnet', IEEE Transactions on Applied Superconductivity, Vol. 14, No. 2, June 2004, Page(s): 743 - 745.

[6] Awad, H.; Svensson, J.; and Bollen, M. H. J., 'Static series compensator for voltage dips mitigation', IEEE Power Tech Conference Proceedings, Bologna, 2003, Vol. 3, 23 - 26 June 2003, Page(s): 8.

[7] Chen, G.; Chen, Y.; Sanchez, L.F.; and Smedley, K.M., 'Unified power quality conditioner for distribution system without reference calculations', The 4th International Power Electronics and Motion Control Conference, 2004. IPEMC2004. Vol. 3, 14 - 16 Aug. 2004, Page(s): 1201 - 1206.

[8] Moschakis, M.N.; and Hatziargyriou, N.D., 'A detailed model for a thyristor-based static transfer switch', IEEE Transactions on Power Delivery, Vol. 18, No. 4, Oct. 2003, Page(s):1442 - 1449.

[9] Jong-Young Park; Jong-Keun Park; Kwang-Myoung Son; and Byoung-Moon Han, 'Coordination of an SVC and external reactor/capacitor banks using fuzzy multi-objective optimization', IEEE Power Engineering Society Summer Meeting, 2001, Vol. 3, 15-19 July 2001, Page(s): 1483 - 1488.

[10] Faiz, J.; and Siahkolah, B., 'Sag mitigation by an electronic tapchanger: specifications and comparisons with other custom power tools', IEE Proceedings on Generation, Transmission, and Distribution -Vol. 152, Issue 5, 9, Sept. 2005, Page(s): 697 - 704.

[11] Brumsickle W.E.; Schneider R.S.; and Luckjiff G.A., 'Dynamic Sag Correctors:Cost-Effective Industrial Power Line Conditioning', IEEE Trans on IA, vol. 37 , No. 1, Jan / Feb. 2001, Page(s): 212 - 216.

[12] Hunter, I., 'Power quality issues, a distribution company perspective', Power Engineering Journal, Vol. 15, No. 2, April 2001, Page(s): 75 - 80.

[13] Bollen M. H. J., 'Understanding power quality problems: voltage sags and interruptions', IEEE Press, New York, 1999.

[14] Liu, Y.Z., 'A wavelet based model for on-line tracking of power system harmonics using Kalman filtering', IEEE Power Engineering Society Summer Meeting, Vol. 2, 15 - 19 July 2001, Page(s): 1237 - 1242.

[15] Hong-Tzer Yang; and Chiung-Chou Liao, 'A de-noising scheme for enhancing wavelet-based power quality monitoring system', IEEE Transactions on Power Delivery, Vol. 16, Issue 3, July 2001, Page(s): 353 - 360.

[16] Jurado, F. and Saenz, José R., 'Comparison between discrete STFT and wavelets for the analysis of power quality events', Electric Power Systems Research, Vol. 62, Issue 3, 28 July 2002, Page(s): 183 - 190.

[17] Flores, R.A, 'State of the art in the classification of power quality events, an overview' in Proc. 10th International Conference on Harmonics and Quality of Power, 2002, Vol. 1, Page(s): 17-20.

[18] Azam, M.S.; Fang Tu; Pattipati, K.R.; and Karanam, R., 'A dependency model-based approach for identifying and evaluating power quality problems', IEEE Transactions on Power Delivery, Vol. 19, No. 3, July 2004, Page(s): 1154 - 1166.

[19] Gu, Y.H.; and Bollen, M.H.J., 'Time-frequency and time-scale domain analysis of voltage disturbances', IEEE Transactions on Power Delivery, Vol. 15 Issue: 4, Oct. 2000, Page(s): 1279 - 1284.

[20] Angrisani, L.; Daponte, P.; and D'Apuzzo, M., 'A virtual digital signal processing instrument for measuring superimposed power line disturbances', Measurement, Vol. 24, No. 1, Oct. 1998, Page(s): 9-19.

[21] Angrisani, L.; D'Apuzzo, M, and Testa, A., 'A measurement method based on the wavelet transform for power quality analysis', IEEE Transaction on Power Delivery, Vol. 13, No. 4, October 1998, Page(s): 990 - 998.

[22] Angrisani, L.; Daponte, P.; and D'Apuzzo, M., 'Wavelet network-based detection and classification of transients'; IEEE Transactions on Instrumentation and Measurement, Vol. 50, No. 5, October. 2001, Page(s): 1425 - 1435.

[23] Poisson, O.; Rioual, P.; and Meunier, M., 'New signal processing tools applied to power quality analysis', IEEE Transactions on Power Delivery, Vol. 14, No. 2, April 1999, Page(s): 561 - 566.

[24] Poisson, O.; Rioual, P.; and Meunier, M., 'Detection and measurement of power quality disturbances using wavelet transform', IEEE Transaction on Power Delivery, July 2000, Vol. 15, Issue 3, Page(s): 1039 - 1044.

[25] Jurado, F.; Acero, N.; and Ogayar, B., 'Application of signal processing tools for power quality analysis', Canadian Conference on Electrical and Computer Engineering, May 2002. IEEE CCECE 2002, Vol. 1, Page(s): 82 - 87.

[26] Jiansheng Huang; Negnevitsky, M.; and Nguyen, D.T., 'A neural-fuzzy classifier for recognition of power quality disturbances', IEEE Transactions on Power Delivery, Vol. 17, No. 2, April 2002, Page(s): 609 - 616.

[27] Santoso, S.; Powers, E. J.; and Grady, W. M., 'Electric power quality disturbance detection using wavelet transform analysis', 1994, Proceedings of the IEEE-SP International Symposium on Time-Frequency and Time-Scale Analysis, 25 - 28 Oct. 1994, Page(s): 166 -169.

[28] Santoso, S.; Powers, E. J.; Grady, W.M.; and Hofmann, P., 'Power quality assessment via wavelet transform analysis'.; Power Delivery, IEEE Transactions on Vol. 11, No. 2, April 1996, Page(s): 924 - 930.

[29] Santoso, S.; Grady, W. M.; Powers, E. J.; Lamoree, J.; and Bhatt, S. C., 'Characterization of distribution power quality events with Fourier and wavelet transforms', IEEE Transactions on Power Delivery, Vol. 15 Issue: 1, Jan. 2000, Page(s): 247 - 254.

[30] Gaouda, A.M., Salama, M.M.A, Sultan, M.R., and Chikhani, A.Y., 'Power quality detection and classification using wavelet-multiresolution signal decomposition', IEEE Transactions on Power Delivery, Vol. 14, Issue: 4 July 1999, Page(s): 1469 - 1476.

[31] Gaouda, A.M.; Kanoun, S.H.; Salama, M.M.A.; and Chikhani, A.Y., 'Wavelet-based intelligent system for monitoring non-stationary disturbances', Proceedings of International Conference on Electric Utility Deregulation and Restructuring and Power Technologies, 2000. DRPT 2000. 4-7 April 2000, Page(s): 84 - 89.

[32] Gaouda, A.M.; El-Saadany, E.F.; Salama, M.M.A.; Sood, V.K.; and Chikhani, A.Y., 'Disturbance monitoring in HVDC systems using wavelet multi-resolution analysis', 2000, Proceeding of the International Conference on Electric Utility Deregulation and Restructuring and Power Technologies, DRPT 2000, 4 - 7 April 2000, Page(s): 678 - 684.

[33] Gaouda, A.M.; Salama, M.M.A.; Sultan, M.R.; and Chikhani, A.Y., 'Application of multiresolution signal decomposition for monitoring short-duration variations in distribution systems', IEEE Transactions on Power Delivery, Vol. 15, No. 2, April 2000, Page(s): 478 - 485.

[34] Gaouda, A.M.; Kanoun, S.H.; Salama, M.M.A.; and Chikhani, A.Y., 'Wavelet-based signal processing for disturbance classification and measurement', IEE Proceedings- Generation, Transmission and Distribution, Vol. 149, No. 3, May 2002, Page(s): 310 - 318.

[35] Gaouda, A.M.; Kanoun, S.H.; Salama, M.M.A.; and Chikhani, A.Y., 'Pattern recognition applications for power system disturbance classification', IEEE Transactions on Power Delivery, Vol. 17, No. 3, July 2002, Page(s): 677 - 683.

[36] Gaouda, A.M.; El-Saadany, E.F.; Salama, M.M.A.; Sood, V.K.; and Chikhani, A.Y., 'Monitoring HVDC systems using wavelet multi-resolution analysis', IEEE Transactions on Power Systems, Vol.: 16, No.: 4, November. 2001, Page(s): 662 -670.

[37] Gaouda, A.M, 'Data clustering and storing for wide-area power quality monitoring', Electric Power Systems Research, Vol. 70, No. 1, June 2004, Page(s): 56 - 63.

[38] Zhu, T.X.; Tso, S.K.; and Lo, K.L., 'Wavelet-based fuzzy reasoning approach to power-quality disturbance recognition', IEEE Transactions on Power Delivery, Vol. 19, No. 4, Oct. 2004, Page(s): 1928 - 1935.

[39] Zwe-Lee Gaing, 'Wavelet-based neural network for power disturbance recognition and classification', IEEE Transactions on Power Delivery, Vol. 19, No. 4, October. 2004, Page(s): 1560 - 1568.

[40] Santoso, S.; Powers, E.J.; Grady, W.M.; and Parsons, A.C., 'Power quality disturbance waveform recognition using wavelet-based neural classifier. Part-I. Theoretical foundation', IEEE Transactions on Power Delivery, Vol. 15 No.: 1 , Jan. 2000, Page(s): 222 -228.

[41] Santoso, S.; Powers, E.J.; Grady, W.M.; and Parsons, A.C., 'Power quality disturbance waveform recognition using wavelet-based neural classifier. Part-2. Theoretical foundation', IEEE Transactions on Power Delivery, Vol. 15 No. 1, Jan. 2000, Page(s): 229 -235.

[42] Dash, P.K.; Panigrahi, B.K.; and Panda, G, 'Power quality analysis using S-transform', IEEE Transactions on Power Delivery, Vol. 18, No. 2, April 2003, Page(s): 406 - 411.

[43] Lee, I.W.C.; and Dash, P.K., 'S-transform-based intelligent system for classification of power quality disturbance signals', IEEE Transactions on Industrial Electronics, Vol. 50, Issue 4, Aug. 2003, Page(s): 800 - 805.

[44] Chilukuri, M.V.; and Dash, P.K., 'Multiresolution S-transform-based fuzzy recognition system for power quality events', IEEE Trans. on Power Delivery, Vol. 19, No. 1, Jan. 2004, Page(s): 323 - 330.

[45] Dash, P.K.; Panigrahi, B.K.; Sahoo, D.K.; and Panda, G., 'Power quality disturbance data compression, detection, and classification using integrated spline wavelet and S-transform', IEEE Transactions on Power Delivery, Vol. 18, Issue 2, April 2003, Page(s): 595 - 600.

[46] Lee, I.W.C.; and Dash, P.K., 'An S-transform based neural pattern classifier for non-stationary signals' 6th International Conference on Signal Processing, 2002 Vol. 2, 26-30 Aug. 2002, Page(s): 1047 - 1050.

[47] Dash, P.K.; Chilukuri, M.V.; and Panigrahi, B.K., 'Power quality analysis and classification using a generalized phase corrected wavelet transform', International Conference on Power Electronics, Machines and Drives, 2002., 4-7 June 2002, Page(s): 610 - 615.

[48] Daniels, R., 'Power quality monitoring using neural networks' in Proc. 1st International Forum Applications Neural Networks Power System, 1991, Page(s). 195-197.

[49] Ghosh, A. K. and Lubkeman, D. L., 'Classification of power system disturbance waveforms using a neural network approach', IEEE Transaction on Power Delivery, Vol. 10, Feb. 1995, Page(s): 109-115.

[50] Ghosh, A. K. and Lubkeman, D. L., 'The classification of power system disturbance waveforms using a neural network approach', in Proc. IEEE Power Eng. Soc. Transmission, Distribution Conf., 1994, Page(s): 323-329.

[51] Dash, P. K.; Panda, S. K.; Liew, A. C.; Mishra, B.; and Jena, R. K., 'New approach to monitoring electric power quality' Electric. Power System. Research., vol. 46, No. 1, 1998, Page(s): 11 - 20.

[52] Wijayakulasooriya, J.V.; Putrus, G.A.; and Minns, P.D., 'Electric power quality disturbance classification using self-adapting artificial neural networks', IEE Proceedings- Generation, Transmission and Distribution, Vol. 149, No. 1, Jan. 2002, Page(s): 98 - 101.

[53] Powers, Jaehak Chung, E. J.; Grady, W. M., and Bhatt, S. C., 'Power disturbance classifier using a rule-based method and wavelet packet-based hidden Markov model', IEEE Transaction on Power Delivery, Jan. 2002, Vol. 17, No. 1, Page(s): 233 - 241.

[54] Kochukuttan, H.; and Chandrasekaran, A., 'Development of a fuzzy expert system for power quality applications', Proceedings of the Twenty-Ninth Southeastern Symposium on System Theory, 9-11 March 1997, Page(s): 239 - 243.

[55] Liang Cai; and Hongkun, Chen.,'Fuzzy studies on power quality. I. Index and evaluation', 10th International Conference on Harmonics and Quality of Power, 2002, Vol. 2, 2002, Page(s): 414 - 418.

[56] Anis Ibrahim, W. R., and Morcos, M. M., 'An adaptive fuzzy technique for learning power-quality signature waveforms', IEEE Power Engineering Review, Vol. 21, No. 1, Jan. 2001, Page(s): 56 - 58.

[57] Dash, P.K.; Mishra, S.; Salama, M.A.; and Liew, A.C., 'Classification of power system disturbances using a fuzzy expert system and a Fourier linear combiner',

IEEE Transactions on Power Delivery, Vol. 15 Issue: 2, April 2000, Page(s): 472 - 477.

[58] Gaouda, A.M.; Kanoun, S.H.; and Salama, M.M.A., 'On-line disturbance classification using nearest neighbor rule', International . J. Electric Power System Research, Vol. 57, No.1, Jan. 2001, Page(s): 1 - 8.

[59] IEEE Std. 1159-1995, 'IEEE recommended practice for monitoring electric power quality', 1995.

[60] IEEE Std 446-1995 [The Orange Book], 'IEEE recommended practice for emergency and standby power systems for industrial and commercial applications', 1995.

[61] IEEE Std 519-1992, 'IEEE recommended practices and requirements for harmonic control in electrical power systems', 1992.

[62] IEEE Std. 141-1993, 'IEEE recommended practice for power distribution in industrial plants', 1993.

[63] Skvarenina, T. L., 'The Power Electronics Handbook', West Lafayette, Indiana, CRC Press, 2002.

[64] Short, T.A., 'Electric Power Distribution Handbook'. Boca Raton, FL, USA, CRC Press, 2004.

[65] McGranaghan, M.F.; Zavadil, R.M.; Hensley, G.; Singh, T.; and Samotyj, M., 'Impact of utility switched capacitors on customer systems-magnification at low voltage capacitors', IEEE Transactions on Power Delivery, Vol. 7, No. 2, April 1992, Page(s): 862 - 868.

[66] Ribeiro, P. F., 'Wavelet Transform: An advanced tool for analyzing nonstationary harmonic distortion in power systems', IEEE Proceeding of International Conference on Harmonics in Power Systems, 1994, Page(s): 365 -369.

[67] Chul H. K.; and Aggarwal, R., 'Wavelet transforms in power systems. II. Examples of application to actual power system transients', Power Engineering Journal, Vol. 15, No: 4 , Aug. 2001, Page(s): 193 - 202.

[68] Pillay, P.; and Bhattacharjee, A., 'Application of wavelets to model short-term power system disturbances', IEEE Transactions on Power Systems, Vol. 11, No. 4, Nov. 1996, Page(s): 2031 - 2037.

[69] Chan, Y. T., 'Wavelet Basics', Springer, 1995.

[70] IEEE 1159.2 working group website: http://grouper.ieee.org//groups/1159/2/testwave.html, retrieved on October, 2003.

[71] Stockwell, R.G.; Mansinha, L.; and Lowe, R.P., 'Localization of the complex spectrum: the S transform' , IEEE Transactions on Signal Processing , Vol. 44, No. 4, April 1996, Page(s): 998 - 1001.

[72] Pinnegar, C.R., Mansinha, L., 'The S-transform with windows of arbitrary and varying shape', Geophysics, Vol. 68, No. 1, January-February 2003, Page(s): 381 - 385.

[73] Poularikas, Alexander D., 'The Transforms and Applications Hand-book', Boca Raton: CRC Press LLC, 2000.

[74] Ferrero, A., and Superti-Furga, G., 'New approach to the definition of power components in three-phase systems under nonsinusoidal conditions', IEEE Transaction on instrumentation and measurement, Vol. 40, No. 3, June, 1991, Page(s): 568 - 577.

[75] Micheli-Tzanakou, Evangelia; and Tzanakou E. M., 'Supervised and Unsupervised Pattern Recognition', CRC Press, 2000.

[76] Kuncheva, Ludmila I., 'Combining Pattern Classifiers: Methods and Algorithms', Wiley-IEEE, 2004.

[77] Kyei, J.; Ayyanar, R.; Heydt, G.; Thallam, R.; and Blevins, J., 'The design of power acceptability curves', IEEE Transactions on Power Delivery, Vol. 17, No. 3, July 2002, Page(s): 828 - 833.

[78] Entorf, H. C.; Garijo, F. J.; and Riquelme, J. C., 'Advances in Artificial Intelligence', IBERAMIA 2002, Page(s). 23.

[79] Gu, Irene Yu-Hua; and Styvaktakis, E., 'Bridge the gap: signal processing for power quality applications', Electric Power Systems Research, Vol. 66, Issue 1, July 2003, Page(s): 83 - 96.

[80] Elmitwally, A.; Farghal, S.; Kandil, M.; Abdelkader, S.; and Elkateb, M.; 'Proposed wavelet-neurofuzzy combined system for power quality violations detection and diagnosis', IEE Proceedings-Generation, Transmission and Distribution, Vol. 148, Issue 1, Jan. 2001, Page(s): 15 - 20.